https://doi.org/10.15388/vu.thesis.909
https://orcid.org/0000-0003-3804-0510

VILNIUS UNIVERSITY
STATE RESEARCH INSTITUTE CENTER FOR PHYSICAL SCIENCES AND TECHNOLOGY

Kamilė Jonynaitė

Pulsed Electric Field Effects Across Biological Scales: From Photosynthetic System Functioning to Microbial Community Dynamics in *Chlorella vulgaris* Systems

DOCTORAL DISSERTATION

Natural Sciences,
Physics (N 002)

VILNIUS 2026

The dissertation was prepared between 2020 and 2026 at State Research Institute Center for Physical Sciences and Technology. The research was supported by the German Federal Environmental Foundation (DBU).

Academic Supervisor:
Dr. Arūnas Stirkė (Center for Physical Science and Technology, Natural Sciences, Physics, N 002)

This doctoral dissertation will be defended in a public meeting of the Dissertation Defence Panel:

Chairman – Prof. Habil. Dr. Leonas Valkūnas (Center for Physical Science and Technology, Natural Sciences, Physics, N 002).
Members:
Dr. Lena Golubewa (Center for Physical Science and Technology, Natural Sciences, Physics, N 002),
Prof. Dr. Eglė Lastauskienė (Vilnius University, Natural Sciences, Biology, N 010),
Dr. Revilija Mozuraitytė (SINTEF Ocean, Norway, Natural Sciences, Chemistry, N 003),
Dr. Paulius Ruzgys (Vytautas Magnus University, Natural Sciences, Biophysics, N 011).

The dissertation shall be defended at a public meeting of the Dissertation Defence Panel at 13:00 on 30 April 2026 in meeting room D401 of the Center for Physical Science and Technology.
Address: Sauletekio al. 3, Room D401, Vilnius, Lithuania
Tel. +370 645 15 550; e-mail: office@ftmc.lt

https://doi.org/10.15388/vu.thesis.909
https://orcid.org/0000-0003-3804-0510

VILNIAUS UNIVERSITETAS
VALSTYBINIS MOKSLINIŲ TYRIMŲ INSTITUTAS FIZINIŲ IR TECHNOLOGIJOS MOKSLŲ CENTRAS

Kamilė Jonynaitė

Impulsinio elektrinio lauko poveikis skirtingose biologinėse skalėse: nuo fotosintetinės sistemos funkcijos iki mikrobinės bendrijos dinamikos *Chlorella vulgaris* sistemose

DAKTARO DISERTACIJA

Gamtos mokslai,
Fizika (N 002)

VILNIUS 2026

Disertacija rengta 2020–2026 metais Valstybiniame mokslinių tyrimų institute Fizinių ir technologijos mokslų centre.
Mokslinius tyrimus rėmė Vokietijos federalinis aplinkosaugos fondas (DBU).

Mokslinis vadovas:
Dr. Arūnas Stirkė (Fizinių ir technologijos mokslų centras, gamtos mokslai, fizika, N 002).

Gynimo taryba:
Pirmininkas – prof. habil. dr. Leonas Valkūnas (Valstybinis mokslinių tyrimų institutas Fizinių ir technologijos mokslų centras, gamtos mokslai, fizika, N 002).
Nariai:
dr. Lena Golubewa (Valstybinis mokslinių tyrimų institutas Fizinių ir technologijos, gamtos mokslai, fizika, N 002),
prof. dr. Eglė Lastauskienė (Vilniaus universitetas, gamtos mokslai, biologija, N 010),
dr. Revilija Mozuraitytė (SINTEF Ocean, Norvegija, gamtos mokslai, chemija, N 003),
dr. Paulius Ruzgys (Vytauto Didžiojo universitetas, gamtos mokslai, biofizika, N 011).

Disertacija ginama viešame Gynimo tarybos posėdyje 2026 m. balandžio mėn. 30 d. 13 val. Fizinių mokslų ir technologijų centro D401 kab.
Adresas: Saulėtekio pr., 3, D401 kab., Vilnius, Lietuva
Tel. +370 645 15 550; paštas: office@ftmc.lt

LIST OF ABBREVIATIONS

Abs	Absorbance
BG+AA	BG-11 supplemented with acetic acid
BG-11	Blue-Green medium 11
BSA	Bovine serum albumin
C	Membrane capacitance
CDIF	Cell death-inducing factor
DBM	Dry biomass (basis used for %DBM)
DNA	Deoxyribonucleic acid
E	Electric field strength
FDA	Fluorescein diacetate
F_v/F_m	Maximum photochemical quantum yield of photosystem II
GAD	Gliding arc discharge
HPH	High-pressure homogenization
H_2O_2	Hydrogen peroxide
LHCII	Light-harvesting complex II
µsPEF	Microsecond pulsed electric field
NO_2^-	Nitrite
NO_3^-	Nitrate
nsPEF	Nanosecond pulsed electric field
OD	Optical density
PAS	Plasma-activated solution / supernatant
PEF	Pulsed electric field
PSI	Photosystem I
PSII	Photosystem II
R	Membrane resistance
RONS	Reactive oxygen and nitrogen species
ROS	Reactive oxygen species
SDS-PAGE	Sodium dodecyl sulfate-polyacrylamide gel electrophoresis
SYTOX Green	Nucleic-acid stain used for plasma membrane permeabilization assessment

SYTO® 9	Nucleic-acid stain used for total cell counting / viability assays
TAP	Tris-acetate-phosphate medium
TPF	1,3,5-triphenylformazan
TTC	Triphenyltetrazolium chloride
YO-PRO-1®	Nucleic-acid stain for membrane permeabilization assessment

TABLE OF CONTENT

INTRODUCTION OF DISSERTATION

Pulsed electric field (PEF) technology applies short, intense electrical pulses to biological materials. When cells are exposed to an external electric field, ions redistribute along the membrane surface. This charges the membrane like a capacitor and generates an induced transmembrane potential that adds to the resting potential. When this induced voltage exceeds a critical threshold (often reported in the ~0.2-1.0 V range depending on conditions), water molecule penetration induces lipid bilayer structural rearrangement that can expand into hydrophilic pores [1,2]. These pores permit passage of otherwise excluded molecules, producing membrane permeabilization. Depending on pore number, size, and cellular repair capacity, permeabilization can be transient (reversible) or progress toward irreversible dysfunction and death [3,4].

This controllable permeabilization has enabled broad PEF implementation across fields. In food processing, PEF has become an established industrial tool, routinely applied for large-scale operations (e.g., potato processing) [5]. In medicine, pulsed field ablation and electrochemotherapy have reached clinical implementation, supported by standardized treatment protocols and regulatory approval [6,7]. In biotechnology, PEF is used for molecular delivery and to enhance recovery of intracellular products from microorganisms [8]. Despite this broad adoption, understanding of the underlying mechanisms has progressed at very different rates across fields.

Mechanistic understanding has advanced furthest in medical applications, where the need for predictable outcomes and safety justification has driven detailed work on membrane charging, intracellular targeting, and cell death pathways. Food processing followed a different trajectory. While a solid theoretical basis for electroporation exists, recent reviews continue to note that the mechanisms responsible for microbial inactivation are not fully understood [9,10]. Biotechnology applications, including microalgae processing, remain even more strongly empirical. Treatment parameters are often optimized experimentally, with limited attention to the specific cellular structures affected or the pathways leading from electrical exposure to biological outcome [11]. This imbalance has practical consequences. Without a mechanistic framework, it is difficult to predict organism-specific responses, to design treatments targeting defined cellular components, or to rationally combine PEF with complementary technologies.

Microalgae occupy a distinctive position within this landscape. Beyond their established role as biotechnological production platforms, they are increasingly developed as food and feed ingredients and as sources of

functional compounds (e.g., protein fractions, natural pigments, and omega-3 lipids), placing microalgal biomass in a processing context where PEF is already valued as a mild, scalable food technology [8,12]. Two decades of research have demonstrated what PEF treatment can achieve in microalgae: enhanced extraction of intracellular, food-relevant compounds, pilot-scale continuous processing, and cascade approaches enabling recovery of multiple products from a single biomass stream [13–18]. Post-treatment incubation is frequently reported to increase extraction yields further and is commonly attributed to enzymatic autolysis following cell death, although the enzymes and processes involved remain poorly defined [19–21]. This delay implies that the electrical pulse often initiates a biological execution process that unfolds over time, yet the steps controlling that execution remain poorly resolved. Despite these advances, the physiological responses of microalgal cells to PEF remain insufficiently understood, particularly with respect to intracellular damage and post-treatment degradation dynamics.

Beyond application relevance, microalgae represent a challenging and, at the same time, informative biological system for studying electric field effects. They combine eukaryotic cellular organization with rigid cell walls, large membrane-bound organelles, and cultivation under conditions that range from axenic monocultures to complex microbial communities[22,23]. Their dominant chloroplast occupies a substantial fraction of cell volume and contains elaborate thylakoid membrane networks [22,24] with high protein density and a lipid composition distinct from both plasma membranes and mitochondria [25,26]. These features create electrical boundary conditions that differ fundamentally from those of mammalian cells, where most mechanistic electroporation paradigms were developed. As such, microalgae are not simply another application target; they provide a stringent test of how well existing electrophysiological concepts generalize to photosynthetic systems.

This dissertation examines PEF effects across three organizational scales of microalgal systems: the photosynthetic apparatus, the individual cell, and mixed microbial populations. These are not independent topics, but different observational scales of the same physical interaction between electric fields and living matter. At each scale, current frameworks leave key questions unresolved.

At the organellar scale, PEF effects on the photosynthetic machinery remain poorly characterized, even though chloroplast activity is central to cellular energy supply and redox homeostasis and can therefore shape downstream recovery, viability, and post-treatment degradation dynamics [27]. Reported observations after PEF exposure include reduced

photosynthetic performance [28], structural alterations of thylakoid organization [29], and changes in chloroplast-associated gene expression [30]. Taken together, these findings indicate that the photosynthetic apparatus is affected, yet they do not resolve whether dysfunction arises from direct electrical interaction with chloroplast membranes or indirectly from plasma membrane permeabilization and subsequent cytosolic imbalance. Chapter 1 therefore uses chlorophyll optical assays, including time-resolved fluorescence lifetime measurements, as non-invasive probes to link PEF-induced photosynthetic impairment with membrane permeabilization dynamics in *Chlorella vulgaris*.

At the cellular scale, PEF-induced permeabilization is well documented [1], but the pore formation itself is not a purely electrical event. Pulse delivery generates reactive oxygen and nitrogen species through electrochemical reactions in the surrounding liquid [31]. These species can increase membrane permeability independently of the transmembrane potential [32–34]. Whether this oxidative component actively shapes downstream biological execution, or simply accompanies it, cannot be determined under standard PEF conditions, where electrical and oxidative inputs cannot be varied independently. Cold atmospheric plasma offers a means to address this directly. As a controllable external ROS source, it allows oxidative load to be systematically varied while the electrical input remains fixed [35,36]. Chapter 2 applies gliding arc discharge plasma prior to a fixed PEF exposure in *C. vulgaris*, testing whether the oxidative context established before pore formation determines how the electrical input is biologically executed: macromolecular release, metabolic fate, and cell death pathway engagement.

At the community scale, PEF effects are typically studied in monocultures, despite the fact that industrial microalgal cultivation generally operates under non-axenic conditions [37]. Electroporation theory predicts differential susceptibility based on cell size and architecture, with smaller bacterial cells requiring higher field strengths than larger eukaryotic cells [38,39]. However, this prediction has rarely been examined within mixed populations [39,40], where physiological state and post-treatment dynamics may alter outcomes. Chapter 3 investigates how microalgae-bacteria co-cultures respond to PEF, testing whether differential susceptibility depends on growth phase and whether this enables selective treatment outcomes.

Aim of the thesis

To investigate PEF effects in microalgal systems across organellar, cellular, and community scales, extending established electrophysiological paradigms to photosynthetic organisms and mixed microbial populations.

Tasks of the thesis

1. Organellar scale: To characterize PEF-induced alterations in chloroplast function in *C. vulgaris* using fluorescence-based assays and to assess their relationship to plasma membrane permeabilization.
2. Cellular scale: To determine whether oxidative context established by gliding arc discharge plasma prior to pore formation shapes the biological execution of a fixed PEF input in *C. vulgaris*.
3. Community scale: To investigate how physiological state and community context affect PEF responses in microalgae-bacteria co-cultures, and to evaluate whether differential susceptibility enables selective extraction of proteins.

Statements for defense

1. PEF shortens chlorophyll fluorescence lifetime at 685 nm in *C. vulgaris* in a pulse duration-dependent manner without altering absorption spectra, indicating that photosynthetic apparatus impairment arises from enhanced non-radiative energy dissipation rather than pigment degradation.
2. Sequential plasma pretreatment (250 V power supply) followed by PEF decouples membrane permeabilization from macromolecule release, suppresses caspase-like activity, and induces a non-apoptotic, non-necrotic cell-death phenotype that differs from classical PEF-induced programmed cell death and requires direct plasma exposure.
3. PEF treatment (40 kV/cm, 1 μs, 4-100 J/mL) produces consistent algal inactivation (>95%) in *C. vulgaris* while *Delftia* sp. susceptibility is growth phase-dependent, enabling selective extraction of algal proteins from co-cultures without additional protein bands observed with mechanical disruption.

Scientific novelty of this PhD thesis

This dissertation advances mechanistic understanding of pulsed electric field (PEF) effects in microalgal systems by examining electrical field interactions across multiple organizational scales.

At the organellar scale, the work provides the first systematic characterization of PEF-induced alterations in photosynthetic apparatus function in microalgae. Time-resolved chlorophyll fluorescence lifetime measurements show that PEF shortens fluorescence lifetime at 685 nm without altering absorption spectra, indicating modified energy dissipation pathways rather than pigment degradation. By comparing these effects across pulse durations and relating them to plasma membrane permeabilization, the study demonstrates that photosynthetic impairment does not scale directly

with membrane permeabilization, highlighting that these responses represent related but non-equivalent outcomes of electrical treatment. This establishes fluorescence lifetime analysis as a sensitive, non-destructive method for probing electrical effects on the photosynthetic apparatus beyond bulk membrane damage.

At the cellular scale, the dissertation presents the first characterization of sequential plasma-PEF treatment effects in microalgae. It identifies voltage-dependent response regimes that require direct plasma exposure and reveals caspase-independent, non-classical cell death patterns at high treatment intensities. These findings demonstrate that combined plasma-PEF treatment elicits cellular responses in microalgae that differ from classical PEF-induced responses and cannot be explained by plasma membrane permeabilization alone.

At the community scale, the work documents PEF effects in microalgae-bacteria co-cultures, showing that bacterial susceptibility is strongly dependent on growth phase while algal cells undergo consistent disruption. This differential response enables selective extraction of algal proteins from mixed cultures and demonstrates that electrical susceptibility at the population level is governed by physiological state rather than intrinsic species properties alone.

Taken together, the results demonstrate that electrical field susceptibility in photosynthetic systems is not determined solely by plasma membrane permeabilization. Instead, responses to PEF depend on the physiological state of the system, including photosynthetic functionality and growth phase. These findings further suggest that cellular response context, shaped by physiological and redox conditions, can influence how a fixed electrical input is translated into biological outcome. Together, they establish a necessary context for further mechanistic determination of PEF effects in complex photosynthetic systems.

CHAPTER 1. Pulsed Electric Field-Induced Alterations in Photosynthetic Apparatus Function

1.1 Introduction

Pulsed electric field (PEF) effects depend on multiple interacting parameters, including field strength, pulse duration, pulse number, and waveform, each influencing which cellular structures are affected and to what extent [1,4]. Among these parameters, pulse duration plays a central role in determining how electrical energy distributes across the nested membrane architecture of a biological cell. A useful starting point is to treat the cell as an equivalent electrical circuit, where each membrane layer acts as a capacitor and the surrounding aqueous compartments act as resistors (Fig. 1). This analogy is physically grounded: the lipid bilayer is a thin (~4-5 nm), low-dielectric insulating layer sandwiched between ion-conducting aqueous phases, precisely the geometry of a parallel-plate capacitor, while the dissolved ions in the cytoplasm and extracellular medium provide the resistive pathways. Under this model, the transmembrane voltage across the plasma membrane develops over a characteristic charging time constant, $\tau = R \times C$, determined by the effective membrane resistance (R) and capacitance (C). For cells, this time constant typically lies in the sub-microsecond to microsecond range [1,41]. Pulses substantially longer than this τ allow the outer RC-element to charge fully, promoting pore formation and permeabilization while simultaneously shielding the inner compartments from the applied field [2,4,42]. Any effects on organelles under these conditions arise as secondary consequences of membrane disruption rather than direct electrical interaction with intracellular structures [1,5].

When pulse duration approaches or falls below τ, this shielding effect breaks down. The plasma membrane cannot fully polarize during the pulse, and the applied field penetrates to inner membrane structures, where organelle membranes may accumulate transmembrane potentials transiently exceeding that of the plasma membrane [1,43–45]. In mammalian cells, this shift in the primary target from plasma membrane to intracellular compartments has measurable biological consequences. Nanosecond PEF (nsPEF) exposure induces mitochondrial depolarization, calcium release from intracellular stores, and caspase-dependent apoptosis [43,44,46]. In yeast, similar treatments activate metacaspases and trigger programmed death pathways [47]. Although intracellular effects of nanosecond PEF have been documented for several organelles, observations made for mitochondria and the endoplasmic reticulum cannot be directly generalized to all intracellular

compartments. The chloroplast of *C. vulgaris* is a case in point: it differs from these organelles not only in structure and lipid composition, but in carrying functionally active electrochemical gradients during illumination, features that may produce a fundamentally different response to electrical exposure.

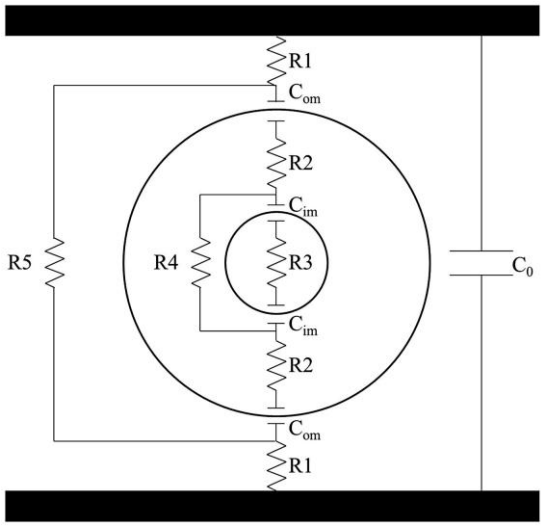

Figure 1 Equivalent electrical circuit model of a biological cell positioned between two electrodes. Cell membranes are represented as capacitors (C) and extra- and intracellular fluids as resistors (R), where the outer membrane (om) and inner membrane (im) components reflect the nested geometry of plasma membrane and organellar barriers. For pulse durations substantially exceeding the membrane charging time constant τ, the outer RC-element charges fully, shielding intracellular compartments. For nanosecond pulses falling below τ, the outer membrane remains incompletely charged, allowing the applied field to reach inner membrane structures. Adapted from Haberkorn et al. (2021) under CC BY 4.0.

The single, cup-shaped chloroplast occupies 40-60% of total cellular volume and contains an elaborate thylakoid membrane network whose total surface area exceeds that of the plasma membrane by 10-100-fold depending on cell size and metabolic state [22,24]. This alone makes the thylakoid system a quantitatively dominant membrane target within the cell interior. What may matter more, however, is that thylakoid membranes are not electrically passive. During illumination, light-driven proton translocation generates transmembrane pH gradients of 1.5-2.3 units and proton-motive forces of 150–170 mV that sustain ATP synthesis [27]. These pre-existing electrochemical gradients distinguish thylakoids from metabolically inert organellar barriers such as the endoplasmic reticulum, where documented nsPEF effects provide the closest available precedent. Whether an externally applied field interacts with an already-polarized, proton-translocating

membrane in the same way it interacts with a relatively quiescent one is not known.

The lipid and protein composition of thylakoid membranes further sets them apart from both the plasma membrane and other organellar membranes, with consequences that are not straightforward to predict. Thylakoids contain 70-78% galactolipids, primarily monogalactosyldiacylglycerol and digalactosyldiacylglycerol, rather than the phospholipids that dominate the plasma membrane [25]. The hydrated galactose headgroups of these lipids produce ionic conductance 5-26-fold higher than phospholipid bilayers [26,48], which may alter charge dissipation rates or pore formation thresholds during pulse application. The acyl chains are also highly polyunsaturated, with α-linolenic acid (18:3) predominating [49,50]. Polyunsaturated lipid domains appear to be preferential sites for pore nucleation, porating approximately five times faster than saturated regions in molecular dynamics simulations of mammalian membranes [3], which might suggest enhanced thylakoid susceptibility. At the same time, thylakoid membranes are densely packed with protein, with photosystem complexes and ATP synthase constituting 40-50% of total membrane mass [51]. This crowding creates spatially heterogeneous environments where protein-lipid interfaces could serve as nucleation sites or, alternatively, where dense protein arrangements constrain pore expansion. Whether the galactolipid composition, high polyunsaturation, and extreme protein density act in concert to increase or decrease net thylakoid susceptibility to electrical permeabilization, relative to the plasma membrane, remains an open question.

Evidence that photosynthetic performance responds to PEF exposure in microalgae does exist. Straessner et al. (2013) reported energy-dependent declines in F_v/F_m, the maximum dark-adapted photochemical quantum yield of photosystem II (PSII), where $F_v = F_m - F_0$, F_0 is minimal fluorescence and F_m is maximal fluorescence measured during a saturating pulse, in *Auxenochlorella protothecoides* following nanosecond pulse treatments [28]. In addition, structural alterations assessed by microscopy have also been reported in *Chlamydomonas reinhardtii* after PEF exposure [23], and gene expression responses linked to chloroplast-associated metabolism have been observed following nsPEF treatment in *Haematococcus pluvialis* [30]. Taken together, these observations indicate that photosynthetic performance and chloroplast-associated physiology can be perturbed by PEF exposure in microalgae. However, the origin of this impairment remains unclear, as altered photosynthetic behavior may arise from either direct PEF effects on chloroplast membranes or secondary consequences of plasma membrane permeabilization and cytosolic disruption.

Chlorophyll fluorescence provides a sensitive probe of photosynthetic organization and function. At room temperature, fluorescence emission originates predominantly from PSII, and changes in fluorescence characteristics reflect alterations in energy transfer within the photosynthetic apparatus [52]. Conventional fluorescence parameters such as F_v/F_m provide a useful measure of overall photosynthetic efficiency. However, a decrease in F_v/F_m alone does not distinguish whether reduced efficiency arises from pigment loss, reaction center damage, or altered energy dissipation. Fluorescence lifetime measurements address this ambiguity by reporting how excited chlorophyll states are deactivated. Shortened lifetimes indicate faster non-radiative energy dissipation and can occur even when pigment content and absorption properties remain unchanged [52,53]. However, the application of fluorescence lifetime analysis to interpret photosynthetic responses to PEF exposure in microalgae remains limited.

Aim of this chapter: To characterize PEF-induced alterations in photosynthetic apparatus function in *C. vulgaris* using time-resolved chlorophyll fluorescence lifetime analysis, and to examine their relationship to plasma membrane permeabilization across different pulse regimes.

Objectives:

1. To characterize PEF-induced changes in photosynthetic function in *C. vulgaris* using time-resolved chlorophyll fluorescence lifetime analysis.
2. To compare photosynthetic responses across nanosecond and microsecond pulse regimes and assess their dependence on pulse duration.
3. To examine how PEF-induced photosynthetic alterations relate to plasma membrane permeabilization under different exposure conditions.

1.2 Materials and methods

Algae Cultivation

C. vulgaris was cultivated in bubble column photobioreactors using BG-11 medium (1.9 mS/cm conductivity, pH 7.3). Photobioreactors were inoculated with stationary phase culture to achieve initial optical density of 0.1 at 750 nm. Cultures were maintained at 21-22°C under illumination (photon flux density 90 µmol/m²/s) with 16/8 h light/dark cycle for 7 days. For PEF experiments, cultures were concentrated to 5 g/L dry weight by centrifugation (4000 rpm, 15 min). Concentration was quantified spectrophotometrically at 750 nm using a calibration curve relating absorbance (Abs) to dry biomass.

Pulsed Electric Field Treatment

Concentrated microalgal suspension (5 g/L) was treated with rectangular electric field pulses. Two different pulse generators were employed:

Microsecond pulses (10 µs; 19 kV/cm; 1 Hz): Transistor-based electroporator with commercial 100 µL electroporation cuvettes (1 mm electrode gap). Field strength calculated from real voltage, current, and electrode distance [54]. These parameters were adopted from dose-response experiments in Paper II of this thesis. That work identified this combination as producing irreversible plasma membrane permeabilization in *C. vulgaris* across a range of tested field strengths. Energy level was varied by adjusting pulse number: a single pulse yielded 8 J/mL, ten pulses yielded 80 J/mL. Both permeabilization extent and fluorescence lifetime showed clear energy dependence. The 80 J/mL condition produced larger responses in both parameters and was used for all subsequent experiments.

For nanosecond pulses, total delivered energy was held constant at 80 J/mL to match the microsecond reference condition, while pulse duration and field strength were varied according to the output capabilities of the available instrumentation. Pulses were generated using a coaxial transmission line pulse generator with 40 µL custom cuvettes (0.7 mm gap), with field strength calculated from incident and reflected voltages [47]. Three pulse durations were tested (10 ns, 60 ns, 90 ns) across a field strength range of 19-86 kV/cm, at repetition rates of 5 Hz for 10 ns and 2 Hz for 60-90 ns pulses. This approach constituted a parameter screen rather than a targeted parametric study, with the aim of identifying whether any nanosecond condition produced photosystem alterations comparable to those observed under microsecond treatment at equivalent energy input.

PEF-treated samples were subsequently analyzed by plasma membrane permeabilization assessment, UV-Vis absorption spectroscopy fluorescence emission spectroscopy and time-resolved fluorescence lifetime measurements at 5 min, 2 h, or 24 h post-treatment.

Plasma Membrane Permeabilization and Extracellular Nucleic Acids Assessment

Membrane permeabilization was quantified using SYTOX Green (final concentration 2 µM), a membrane-impermeant nucleic acid dye. Following PEF treatment, 200 µL of microalgal suspension (OD_{750} = 1) was incubated with SYTOX Green for 5 minutes in the dark at room temperature. After incubation samples were centrifuged (10,000 × g, 1 minute) to separate cells and supernatant. Fluorescence was measured in both resuspended pellet (cell-associated SYTOX signal) and in the supernatant (extracellular SYTOX-accessible nucleic acids) using a luminescence spectrometer (excitation 490

nm, emission 510-540 nm) with 250 µL quartz cuvettes. Permeabilization was calculated from the cell-associated (pellet) SYTOX signal and expressed as percentage relative to fully disrupted positive control (ultrasonicated cells), with untreated cells as a negative control.

UV-Vis absorption spectroscopy

Absorption spectrum was recorded using a JASCO V-670 spectrophotometer over the range 400-900 nm. Measurements were performed on the same *C. vulgaris* suspensions used for fluorescence analysis (OD_{750} = 0.2) in 1 mL polystyrene cuvettes. Untreated suspensions measured under identical conditions served as reference for comparison with PEF-treated samples.

Fluorescence Emission Spectroscopy and Lifetime Measurements

Fluorescence measurements were performed on intact *C. vulgaris* cell suspensions without chloroplast isolation or pigment extraction, preserving the native organizational context of the photosynthetic apparatus in its physiological cellular environment. All measurements were performed using an Edinburgh F920 spectrofluorometer equipped with a 470 nm picosecond diode laser (pulse width τ = 71.6 ps, period T = 200 ns). Measurements used 1 mL polystyrene cuvettes with microalgal suspension adjusted to OD_{750} = 0.2.

To suppress excitation leakage and stray light, optical filters were applied in both excitation and detection paths. A 500 nm short-pass filter was placed directly after the laser output to transmit the 470 nm excitation while suppressing longer-wavelength leakage from the source. A 495 nm long-pass filter was installed in the detection path to block scattered excitation below 495 nm while transmitting chlorophyll fluorescence in the red region.

Emission spectra were recorded in the range from 600-800 nm (1 nm steps, 0.5 ns dwell time, 5 nm monochromator slit width). Fluorescence intensity at 685 nm, corresponding to the characteristic emission of chlorophyll a in PSII, was extracted from full spectra for quantitative analysis.

Fluorescence decay kinetics were measured at 685 nm emission wavelength. Decay curves were fitted to a single-exponential decay function; fitting procedure and statistical treatment are described in the Statistical Analysis section.

Statistical Analysis

Experimental data were processed and statistically analyzed using Microsoft Excel, OriginPro and Python. All experiments were performed independently at least three times, and for each selected PEF parameter set of at least six treated samples were measured. Results are reported as mean ± standard error (SE). Fluorescence decay constants (τ) were determined by

fitting the time-resolved fluorescence signals with a single-exponential decay function:

$$y = y_0 + Ae^{-\frac{t}{\tau}}$$

Fitting was performed on the decay portion of the signal, starting from peak intensity to exclude the instrument response during signal rise. Chlorophyll fluorescence decays in intact cells are inherently multi-exponential, reflecting heterogeneity within the photosynthetic apparatus. But single-exponential fitting was applied as a first-order approximation to assess whether PEF treatment produced detectable changes in fluorescence decay kinetics across conditions. The reported τ values should therefore be interpreted as apparent fluorescence lifetimes representing population-level decay behaviour rather than formally resolved lifetime components [55].

Plasma membrane permeabilization assessed using the SYTOX Green fluorophore was converted to percentage values relative to the positive control (microalgae fully disrupted by ultrasonication). Normality of data distributions was evaluated using the Shapiro-Wilk test, and homogeneity of variances was assessed with the Brown-Forsythe test. Because the assumptions of normality and/or equal variances were violated for some groups, differences between groups were tested using the non-parametric Kruskal-Wallis test, followed by Dunn's post-hoc test. For pairwise comparisons between control and PEF-treated samples at different timepoints (5 min, 2 h, and 24 h post-treatment), the non-parametric Mann-Whitney-Wilcoxon test was applied with Bonferroni correction. Statistical significance was accepted at $p < 0.05$.

1.3 Results

To investigate the extent to which PEF treatment alters photosynthetic apparatus function, *C. vulgaris* was treated with microsecond pulses (10 µs, 19 kV/cm) using either single pulse (8 J/mL) or 10 pulses (80 J/mL). These parameters were selected based on literature [21,54] and prior experience demonstrating effects on algae membrane permeability. Emission spectra showed pulse number-dependent changes, with 80 J/mL producing greater fluorescence reduction than 8 J/mL (data not shown). Based on this energy dependence, 80 J/mL treatment was selected for detailed temporal characterization.

1.3.1 Microsecond Pulse Effects on Emission Spectra

Excitation at 470 nm resulted in emission spectra where PEF treatment produced fluorescence reduction across the 600-800 nm range with maximum change at a peak of 685 nm (Fig. 2A). This reduction exhibited time-dependent progression: as time post-treatment increased, the extent of reduction increased, with the most pronounced effect observed at 24 h. Normalized spectra (Fig. 2B) showed peak position remained at 685 nm. Absorption spectra recorded before and after PEF treatment showed no detectable changes in peak positions or overall absorbance within experimental uncertainty (Fig. 3).

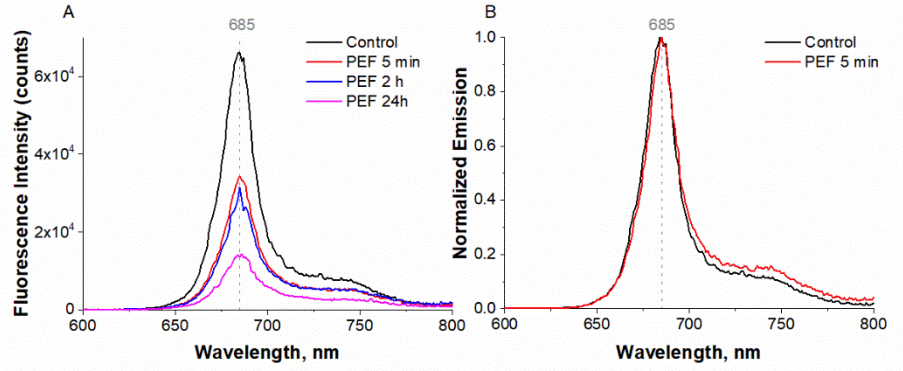

Figure 2 Fluorescence emission (470 nm excitation) spectra of *C. vulgaris* following PEF treatment (10 µs, 19 kV/cm, 80 J/mL). (A) Raw intensity at 5 min, 2 h, and 24 h post-treatment. (B) Emission spectra at 5 min normalized to the maximum intensity. Dashed line indicates peak at 685 nm.

Since 685 nm exhibited the maximum PEF-induced emission change, this wavelength was selected for time-resolved fluorescence lifetime measurements. Following PEF treatment, decay kinetics changed substantially: the PEF-treated sample exhibited both a shorter fluorescence lifetime and a steeper decay slope compared to control (Fig. 4A). Quantitative analysis showed effective fluorescence lifetime shortened from 1.71 ± 0.05 ns (control) to 0.83 ± 0.03 ns (5 min, 80 J/mL), demonstrating photosystem alterations.

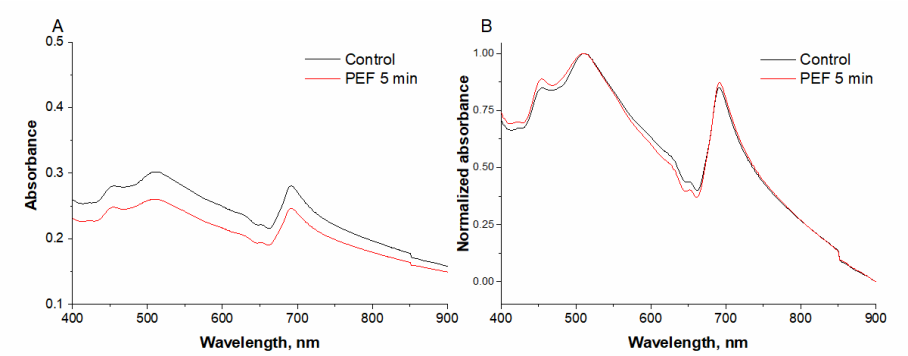

Figure 3 UV-Vis absorption spectra (400-900 nm) of *C. vulgaris* suspensions measured 5 min after PEF treatment (10 µs, 19 kV/cm, 80 J/mL; red) and untreated control (black). (A) Raw absorbance spectra. (B) Absorbance spectra normalized to the maximum intensity.

To determine whether observed photosystem effects resulted from direct intracellular targeting or secondary consequences of plasma membrane disruption, membrane permeabilization was assessed in parallel. SYTOX Green fluorescence in cells reached approximately 70% at 5 min and decreased to 55% by 24 h (Fig. 4B). Conversely, supernatant fluorescence increased dramatically from approximately 12% at 5 min to 83% at 24 h, while untreated samples remained at 3-5% throughout.

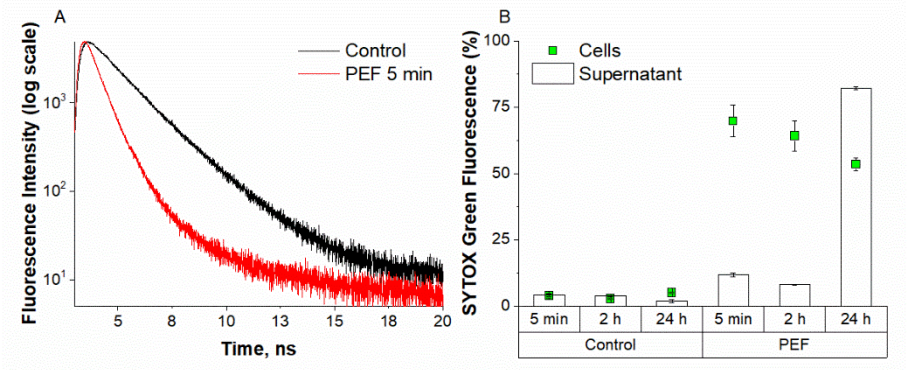

Figure 4 (A) Time-resolved fluorescence decay kinetics at 685 nm emission (470 nm excitation, log scale) 5 min after PEF. (B) SYTOX Green fluorescence measured in cells (green) and supernatant (white) at 5 min, 2 h, and 24 h post-treatment (10 µs, 19 kV/cm, 80 J/mL).

1.3.2 Nanosecond Pulse Effects at Fixed Field Strength

Following the observation of fluorescence kinetics changes under microsecond PEF treatment, these effects were explored using nanosecond pulses. Since nanosecond pulses are substantially shorter than microsecond pulses, achieving the same energy level (80 J/mL) requires either a higher

number of pulses or increased electric field strength. These parameter differences can result in distinct biological outcomes. Therefore, nanosecond treatments were performed under a fixed energy condition (80 J/mL) using pulse durations of 10 ns, 60 ns, and 90 ns.

To enable direct comparison with the microsecond regime, 90 ns pulses were first applied at 19 kV/cm, matching the field strength used for microsecond pulses, while the pulse number was adjusted to deliver the same total energy (80 J/mL). Subsequently, electric field strength was increased (26-86 kV/cm) to evaluate field-strength dependence under nanosecond conditions, while maintaining constant delivered energy (80 J/mL). For each nanosecond condition, fluorescence lifetime decay constants and plasma membrane permeabilization were measured 5 min after treatment. Fluorescence decay constants decreased with increasing field strength for 60 ns and 90 ns pulses (Fig. 5A). Significant differences from control appeared at field strengths above 38 kV/cm for 60 ns pulses and above 26 kV/cm for 90 ns pulses. In contrast, 10 ns pulses produced no significant changes across the entire field strength range tested.

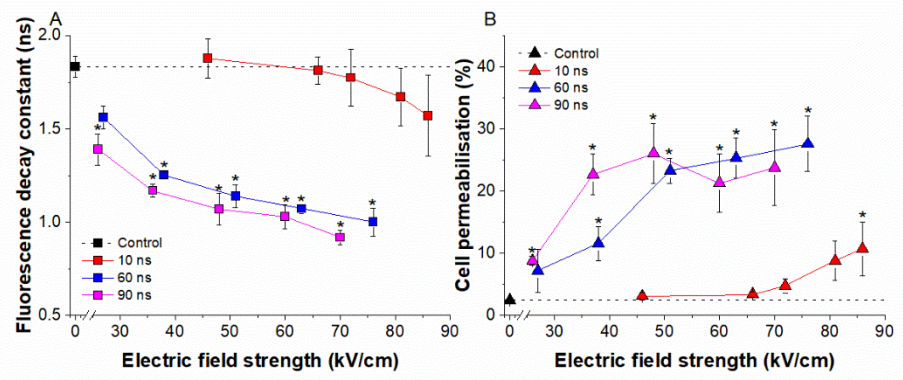

Figure 5 Nanosecond PEF field strength dependencies at 80 J/mL, measured 5 min post-treatment. (A) Fluorescence decay time constants. (B) Cell permeabilization. Asterisks indicate significant differences from control ($p < 0.05$).

Cell permeabilization showed similar field strength dependencies (Fig. 5B). For 60 ns pulses, permeabilization increased from approximately 8% at 26 kV/cm to 27% at 86 kV/cm. The 90 ns pulses exhibited comparable permeabilization levels, ranging from approximately 8% at 26 kV/cm to 24% at 86 kV/cm. No significant differences were observed between 60 ns and 90 ns treatments at equivalent field strengths. The 10 ns pulses showed minimal permeabilization (3-5%) across most field strengths, with a significant increase to approximately 11% only at the highest field strength tested (86 kV/cm).

1.3.3 Relationship Between Membrane Permeabilization and Photosystem Alterations

Microsecond pulses (10 μs, 19 kV/cm, 80 J/mL) produced ~70% permeabilization and a decay constant of 0.83 ± 0.03 ns. Under a matched field strength and total delivered energy condition (19 kV/cm, 80 J/mL; achieved by adjusting pulse number for the 90 ns regime), 90 ns pulses produced 10.5% ± 2.1% permeabilization and a decay constant of ~1.4 ns.

For 60 ns and 90 ns pulses at higher field strengths (≥26 kV/cm), both permeabilization and decay constant changes increased concurrently. No significant differences were observed between 60 ns and 90 ns treatments at equivalent field strengths. The 10 ns pulses demonstrated minimal effects on both parameters across all field strengths tested (26-86 kV/cm), with maximum permeabilization of 11% at 86 kV/cm and no significant decay constant changes.

1.4 Discussion

The present study showed that following PEF treatment, *C. vulgaris* fluorescence spectra decreased with the largest change at the 685 nm peak, which is the characteristic emission of chlorophyll *a* in photosystem II. This decrease resulted from substantially shortened chlorophyll fluorescence lifetime (from 1.71 ns in untreated cells to 0.83 ns at 5 min post-treatment). Absorption spectra and emission peak position remained unchanged throughout, indicating that the same chlorophyll population responds differently rather than being lost or degraded. These observations indicate that PEF-induced alterations in chlorophyll fluorescence result from enhanced non-radiative energy dissipation pathways [56], not from pigment loss or photodestruction. Furthermore, this provides mechanistic explanation for the photosystem II quantum yield (F_v/F_m) decrease documented by Straessner et al. [28], whose work demonstrated PEF effects on algal photosystem function but could not resolve the underlying mechanisms.

These fluorescence changes were not transient. Instead, fluorescence lifetime values failed to recover to control levels and continued to decline over the 24 h observation period. This deterioration was accompanied by progressive cell lysis, indicated by a substantial increase in DNA release into the supernatant (from 12% to 83%). This suggests irreversible damage and activation of secondary cellular processes. Krust et al. (2022) [21] demonstrated that PEF-treated *C. vulgaris* releases a cell death inducing factor

capable of triggering death in neighboring cells, which may contribute to the progressive deterioration observed in our measurements.

Comparing the two pulse regimes at equivalent field strength and energy reveals something beyond a simple difference in magnitude. Microsecond pulses produced approximately 70% permeabilization alongside 51% reduction in fluorescence lifetime. The larger permeabilization response suggests that membrane disruption was the dominant effect, with photosynthetic impairment potentially arising as a secondary consequence rather than from direct field interaction with the chloroplast. A plausible pathway involves pores created in the plasma membrane permitting ion redistribution, which alters the cytosolic chemical environment. These cytosolic changes could then propagate into the chloroplast stroma, collapsing the transthylakoid pH gradient that normally drives both ATP synthesis and photoprotective regulation [27]. Luminal acidification resulting from gradient collapse activates energy-dependent quenching, in which pH-sensitive conformational changes in light-harvesting complexes redirect absorbed excitation energy toward non-radiative thermal dissipation rather than photochemistry [27]. This would directly manifest as shortened fluorescence lifetime without loss of chlorophyll [57], consistent with our absorption data. Whether pH perturbation in *C. vulgaris* can produce the fluorescence changes we observe has been addressed experimentally: Chorvatova et al. (2020) [53] demonstrated in intact *Chlorella* sp. cells that externally induced acidification caused a gradual decrease in red fluorescence intensity at 680 nm accompanied by shortening of the fluorescence lifetime, lending indirect support to the final step of this proposed pathway. The qualitative match with our data is notable, though not complete. Under severe acidification, Chorvatova et al. additionally observed a shift of the red emission peak toward 690-700 nm and increased green fluorescence [53], neither of which appeared in our spectra, suggesting that the perturbation in our case was moderate rather than severe. Whether the cytosolic disturbance under our experimental conditions is sufficient to collapse the stromal gradient within the 5 min measurement window remains to be tested directly. The proposed sequence of events is summarized in Figure 6.

Nanosecond pulses tell a different story. At the same conditions, permeabilization fell to 10.5%, yet fluorescence lifetime shortened by approximately 18%. This is a proportionally larger photosynthetic response than the degree of membrane disruption alone would predict. The shift in ratio is difficult to explain purely through secondary ion flux effects. It may instead point toward some degree of direct field interaction with intracellular structures, since pulses shorter than the membrane charging time constant

theoretically allow partial field penetration into the cell interior [1,46]. However, membrane permeabilization did occur under nanosecond conditions, meaning the two potential mechanisms cannot be cleanly separated. Direct, primary damage to the photosynthetic apparatus independent of plasma membrane effects therefore remains a hypothesis rather than a confirmed conclusion from these data.

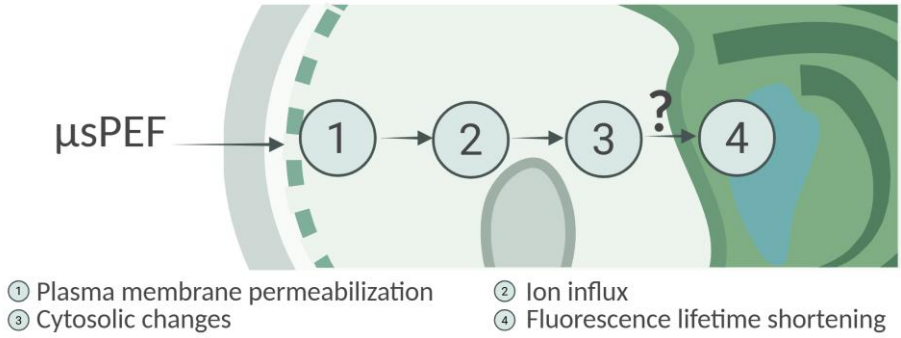

Figure 6 Proposed sequence of cellular events in *C. vulgaris* following microsecond PEF (µsPEF) treatment. Numbers indicate sequential steps: (1) plasma membrane permeabilization, (2) ion influx, (3) cytosolic changes, (4) fluorescence lifetime shortening. Dashed membrane boundary indicates permeabilization. Question mark between steps 3 and 4 reflects that the mechanistic link between cytosolic disruption and photosynthetic apparatus response remains inferred rather than directly demonstrated.

Thermal damage was also considered as a possible contributor to the observed changes. At equivalent total energy (~80 J/mL), theoretical calculations predict similar bulk temperature rise (~17°C) for all pulse conditions. Direct temperature measurement inside the treatment chambers was not feasible in the present configuration. Despite this thermal equivalence, biological effects differed sharply between pulse regimes. Microsecond pulses (10 µs, 19 kV/cm) caused substantial permeabilization (~70%) together with pronounced fluorescence lifetime shortening. In contrast, 10 ns pulses (86 kV/cm) produced minimal effects: ~11% permeabilization with no significant fluorescence changes, and this held despite the largest total pulse number being delivered at the highest repetition frequency tested (5 Hz), where any cumulative thermal or frequency-dependent contributions would be most expected to manifest. Taken together, these observations indicate that pulse duration-dependent electrical interactions, rather than bulk thermal input, govern treatment efficacy under the tested conditions.

Interpretation of observed results revealed limitations inherent to implemented experimental design for investigating direct versus indirect chloroplast targeting by PEF. Measurements at 5 min post-treatment are

already too distant and reflect equilibrated secondary effects rather than immediate PEF-induced changes. Transient effects occurring within seconds of pulse application escape detection, particularly relevant for ns pulses where rapid membrane resealing could mask short-lived perturbations. Direct measurements of chloroplast envelope integrity or stromal pH are needed to determine whether the photosystem alterations result from intracellular field penetration or from ion flux through plasma membrane pores. The energy level used (80 J/mL) may have been too high to observe subtle differences between pulse duration effects, potentially masking the distinct mechanisms of μsPEF and nsPEF.

A further methodological consideration concerns the attribution of 685 nm fluorescence changes to specific photosystem components. At room temperature, fluorescence at 685 nm originates predominantly from the inner antenna complexes of PSII (CP-43 and CP-47) and the associated peripheral LHCII, with PSI contributing primarily at longer wavelengths (720–735 nm) [57]. The tight energetic coupling between these antenna complexes and the PSII reaction centre means that the observed fluorescence changes at 685 nm may reflect disruption at the antenna level, altered energy transfer between antenna and reaction centre, or reaction centre damage, and the present data do not allow these contributions to be separated [57]. Low-temperature (77 K) fluorescence spectroscopy, which provides clear separation between PSII emission peaks (685 nm, 695 nm) and PSI emission (720-735 nm), would enable definitive attribution of PEF-induced changes to specific photosystem components [58]. The present findings are therefore interpreted as reflecting predominantly PSII-associated function, consistent with established wavelength assignments in the literature, while acknowledging that comprehensive photosystem-specific characterization would require additional spectroscopic approaches. Additionally, the single-exponential fitting used for decay analysis yields a single τ integrating contributions from multiple photosynthetic components. Resolving these contributions individually would require multiexponential analysis, which is planned for future work.

Future work will address these limitations through two approaches: development of a treatment-measurement chamber for real-time fluorescence acquisition, and in parallel, experiments combining SNARF-1 pH monitoring with optimized PEF parameters (reduced energy, higher field strengths, shorter pulses) to better resolve direct versus indirect chloroplast targeting mechanisms.

1.5 Key Findings

PEF treatment induced measurable alterations in the photosynthetic apparatus of microalgae *C. vulgaris*, detected as shortened chlorophyll fluorescence lifetime at 685 nm. Following microsecond pulse treatment (19 kV/cm, 10 μs, 80 J/mL), fluorescence lifetime decreased from 1.71 ns to 0.83 ns. Absorption spectra showed minor reduction that was not statistically significant, confirming that the chlorophyll population remained intact and the observed fluorescence changes arose from enhanced non-radiative energy dissipation rather than pigment loss. This finding provides a mechanistic basis for interpreting the PSII quantum yield (F_v/F_m) decreases in microalgae documented in earlier studies but not mechanistically resolved.

The relationship between photosynthetic alterations and membrane permeabilization in C. vulgaris depended on pulse duration. Microsecond pulses (19 kV/cm, 10 μs, 80 J/mL) produced approximately 70% permeabilization coinciding with 51% fluorescence lifetime reduction, a pattern consistent with plasma membrane disruption as the primary event triggering downstream photosynthetic changes through ion redistribution and subsequent collapse of the transthylakoid pH gradient. Nanosecond pulses at equivalent field strength and energy (19 kV/cm, 90 ns, 80 J/mL) produced considerably lower permeabilization (10.5%) alongside an 18% lifetime reduction. The relationship between the two parameters was inverted relative to the microsecond regime: the proportional fluorescence response exceeded the degree of membrane disruption, whereas microsecond pulses produced the opposite pattern. This asymmetry is difficult to explain through secondary ion flux effects alone and may point toward some contribution from direct field interaction with intracellular structures, though this could not be confirmed within the parameters tested.

Thermal damage was excluded as the dominant mechanism. Based on theoretical energy conversion calculations, all pulse conditions at equivalent total energy (~80 J/mL) are estimated to produce a similar bulk temperature rise (~17°C). Direct temperature measurement inside the treatment chambers was not feasible in the present configuration. Yet biological effects varied dramatically between regimes: microsecond pulses caused substantial permeabilization and fluorescence changes, while 10 ns pulses (86 kV/cm, 80 J/mL) produced minimal effects at the same energy input. This strongly suggests that pulse duration, not thermal input, governs treatment efficacy under the tested conditions.

CHAPTER 2. Response Context Modulation in Sequential Plasma-PEF Treatment

2.1 Introduction

PEF treatment in aqueous media is never purely electrical. Pulse delivery generates reactive oxygen and nitrogen species (RONS) as an intrinsic byproduct: electrode-adjacent electrochemical reactions and field-driven processes in the surrounding liquid phase produce hydroxyl radicals, superoxide, hydrogen peroxide, and reactive nitrogen species during and immediately after each pulse [31,59]. These species are not merely incidental contaminants of the treatment. They can promote lipid peroxidation, introducing chemical modifications that deform lipid tails and increase bilayer defect density, thereby augmenting membrane permeability independently of the transmembrane potential the pulse induces [35,60]. This means that what appears to be a purely electrical permeabilization event is, in practice, a combined electro-oxidative perturbation, and the relative contributions of voltage-driven pore formation and oxidation-driven membrane modification to the final biological outcome are difficult to separate under standard PEF conditions. Whether this oxidative component actively shapes downstream biological execution, or simply accompanies it, cannot be determined under standard PEF conditions, where electrical and oxidative inputs cannot be varied independently.

This matters because it limits mechanistic interpretation. Under identical pulse parameters, differences in ROS accumulation, whether due to electrode material, medium composition, treatment volume, or pulse number, can alter permeabilization extent, persistence, and downstream cell fate [31,35]. At the same time, cells differ in their capacity to buffer oxidative stress and repair membrane damage after pulsing. Together, the oxidative environment set by the treatment and the cellular redox state at the moment of exposure determine how an initial permeabilization event evolves. Here, response context refers to this combined setting that controls whether cells recover, leak progressively, or lose function. From this perspective, permeabilization is necessary to explain many PEF effects, yet it is not sufficient to predict fate [61–63].

Microalgae provide a particularly suitable system in which to examine whether oxidative context meaningfully alters the biological outcome of a fixed electrical input. A critical feature is the documented temporal dissociation between permeabilization and fate. In wall-bearing species such as *C. vulgaris*, macromolecular release and loss of viability unfold during

post-treatment incubation rather than during the pulse itself [20,21], establishing that post-pulse processes, rather than the electrical event alone, govern the final outcome. This dissociation is less accessible in more electrically sensitive cell systems, where the window between permeabilization and death is compressed to the point where the two become experimentally inseparable. *C. vulgaris* also requires substantially higher field strengths to achieve permeabilization [64,65] and tolerates various cultivation conditions [22], meaning the permeabilization event itself does not preclude subsequent biological observation. Together, these features create an experimentally accessible window between electrical initiation and biological outcome, a window in which oxidative context may operate and within which multiple independently trackable endpoints, permeabilization extent, macromolecular release, metabolic competence, and death pathway engagement, can be monitored across defined time points.

If oxidative context partially determines the biological outcome of PEF, then delivering a controlled and tunable oxidative perturbation prior to the pulse, independently of the electrical input, should produce measurably different responses to an otherwise identical treatment. Cold atmospheric plasma offers a means to do exactly this. Plasma, the fourth state of matter, can be generated at atmospheric pressure and near-ambient temperature through electrical discharge in gas. These non-equilibrium plasmas produce reactive oxygen and nitrogen species (RONS) spanning a wide range of lifetimes, from short-lived radicals such as OH and O_3 to longer-lived stable products such as H_2O_2 and reactive nitrogen species including NO and NO_2 [66,67]. Both can affect cells under direct exposure conditions. In indirect plasma-liquid systems, however, short-lived radicals decay before reaching the suspension. The biologically relevant dose is therefore carried by the longer-lived products, which accumulate in the treated medium and constitute an operationally measurable oxidative input delivered to the cells. This makes plasma a controlled ROS source: it allows oxidative context to be systematically varied while the electrical input remains fixed, directly testing whether the oxidative component of a PEF treatment is a meaningful determinant of biological outcome rather than a passive byproduct.

Plasma treatment does not, however, deliver reactive species in isolation. It simultaneously modifies bulk suspension properties, including temperature, pH, and conductivity [66,68]. Each of these shifts can independently influence electroporation efficiency and post-treatment recovery [69]. Attributing observed biological outcomes to oxidative context therefore requires explicit separation of direct plasma-cell effects from these medium-mediated changes.

Studies combining plasma and PEF in mammalian and microbial systems have reported not only enhanced permeabilization but also altered downstream responses, including shifts in cell death pathway engagement [35,36,70–72]. These observations suggest that plasma-induced cellular conditioning may redirect the biological pathway through which cells respond to subsequent electrical stress, rather than simply intensifying permeabilization. In microalgae, plasma applications have so far focused primarily on inactivation for harmful algal bloom control and on plasma-activated water effects on growth [73–75], with some evidence that sub-lethal exposures can stimulate growth in certain species [76]. Whether plasma pretreatment produces comparable state-dependent effects in photosynthetic microorganisms remains unclear.

Among plasma sources, gliding arc discharge (GAD) generates non-equilibrium plasma that glides along diverging electrodes, producing high concentrations of reactive nitrogen species alongside reactive oxygen species [77]. GAD operates at atmospheric pressure with scalable throughput, making it suited for treatment of liquid suspensions [78].

Accordingly, plasma exposure is applied here not merely to intensify PEF effects, but to alter the cellular response context in which an otherwise identical PEF treatment is delivered.

Aim of this chapter: To determine whether oxidative context established by gliding arc discharge plasma prior to pore formation shapes the biological execution of a fixed PEF input in *C. vulgaris*.

Objectives:

1. To characterize GAD plasma-induced modifications in treatment suspension (temperature, pH, conductivity, reactive species) across the voltage range 130-250 V.
2. To quantify how oxidative preconditioning by plasma alters the biological execution of a fixed PEF input (25 kV/cm, 7 μs), assessing permeabilization, macromolecular release, metabolic fate, morphology, and cell death pathway engagement across post-treatment time points.
3. To distinguish direct plasma-cell effects from secondary medium effects by comparing sequential plasma-PEF treatment with matched control protocols, including thermal pretreatment, plasma-activated supernatant, and conductivity-matched exchange.

2.2 Materials and Methods

Algae Cultivation

C. vulgaris UTEX 395 cells were inoculated into a glass bubble column photobioreactor (PBR) containing BG-11 medium at final optical density of 0.1 at 750 nm. The PBR was a 1,000 mL glass vessel (61 cm in length and 5 cm in diameter) with a downstream aeration tube. Cells were cultivated under standardized conditions: temperature maintained at 22°C ± 1°C, illumination provided by fluorescent lamps delivering photosynthetic photon flux density of 90 μmol/m²/s, and photoperiod set to 16:8 hours light:dark cycle with CO_2 and air-gas mixture supplementation. Cell cultures were grown until reaching stationary growth phase on day 7, at which point the algal biomass was harvested and concentrated to 5 g/L using centrifugation (3,000 × g, 15 min). Final biomass concentration was verified by optical density measurements (OD at 750 nm) using a pre-established dry biomass calibration curve (R^2 = 0.962).

Gliding Arc Discharge Plasma Processing

Sequential treatment methodology was employed with plasma processing preceding PEF application, based on literature demonstrating superior efficacy of this treatment order [70,79]. System configuration. The gliding arc discharge (GAD) plasma system comprised three main components: plasma reactor, power supply system, and gas supply system (Fig. 7). The plasma reactor utilized two knife-shaped electrodes (52 mm length, 25 mm width) with electrode gap maintained at 1 mm at the top. The system was powered by a G2000 high voltage/medium frequency generator (Redline Technologies Elektronik GmbH) with a high-voltage transformer turn ratio of 1:33. The generator output voltage was adjustable from 90 V to 250 V while maintaining frequency at 270 kHz and signal duty cycle of 0.35 during discharge operation. Compressed air served as the plasma-forming gas and was introduced through dual injection points: top injection at 13.39 L/min and tangential injection at 9.44 L/min, resulting in total air flow rate of 22.8 L/min. Discharge voltage was measured using Rigol DS4012 oscilloscope (Rigol Technologies) equipped with Tektronix P6015A high-voltage passive probe (Tektronix). Current monitoring was performed using Pintek PA-699 current probe (Pintek Electronics). Algal or algae cultivation medium samples (10 mL) were placed in petri dishes positioned 30 mm below the electrode assembly. Treatment duration was standardized at 300 seconds for all plasma exposures. The plasma discharge occurred in the air gap between the knife-shaped electrodes, not within the liquid sample. Reactive species generated in the gas phase were subsequently transported to the liquid surface by the airflow and absorbed into

the suspension. This configuration represents indirect plasma exposure, in which plasma-generated species reach the biological sample through gas-liquid mass transfer rather than direct plasma-liquid contact.

Throughout this chapter, voltage values (130-250 V) refer to the power supply output voltage (V_s), not the plasma discharge voltage. For convenience, plasma pretreatment at V_s = 130 V is referred to as 'low-voltage plasma' and at V_s = 250 V as 'high-voltage plasma'.

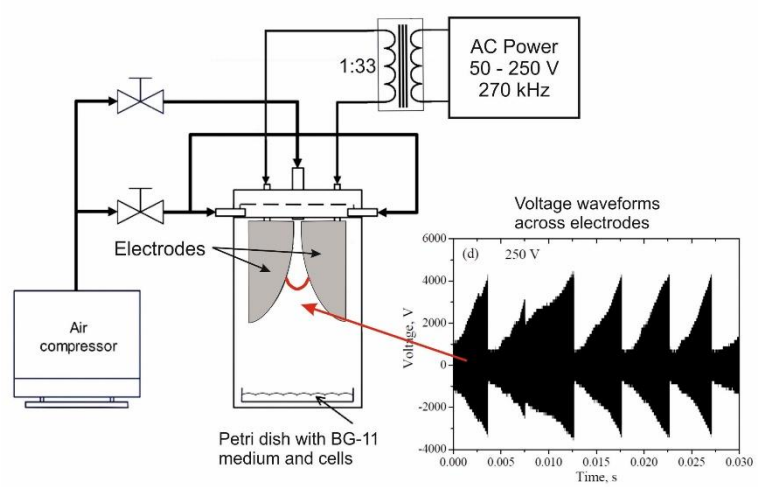

Figure 7 A schematic view of the gliding arc discharge plasma system.

Pulsed Electric Field Processing

Following plasma pretreatment, both plasma-exposed and control algal suspensions underwent pulsed electric field processing using a custom-designed Marx generator system. The generator featured a two-module configuration with 12-stage architecture, enabling generation of electrical pulses with variable durations. Module A2 was equipped with 0.25 μF capacitors while Module A3 contained 1 μF capacitors, both utilizing 5 kV polypropylene capacitors offering high repetition rates and 11 kV/μs rise time. The system was powered by a variable AC/DC high-voltage unit (model CCPF-500-4P) providing 220/4000 V output, with voltage control achieved through analog 0-10 V signals corresponding to 0-4 kV output range. Capacitor charging occurred in parallel via diodes, followed by series discharge through the load using thyristor switches (TA20401203SQ) with maximum operating specifications of 4000 V and 1200 A. Each thyristor was individually controlled through separate driver modules managed by the control unit via optical interface. System control was achieved using ARM STM32F072RBT6 microcontroller enabling control of charging voltage, capacitor module selection, pulse number determination, and repetition

timing. Protection against short circuits was provided through series-connected resistors and inductances that limited maximum current and regulated current rise rate. Exponential unipolar electrical pulses of 7 µs duration were generated using 2 mm electroporation cuvettes (VWR International, Taiwan). Electric field pulses were delivered at 25 kV/cm strength in two configurations: single pulse or ten-pulse sequences. The resulting energy densities were 2.78 J/mL for single pulse and 27.78 J/mL for ten-pulse treatment. These parameters were selected based on previous optimization studies to achieve irreversible cell membrane permeabilization (see Paper II of this thesis). Voltage measurements across the load were conducted using voltage dividers while current measurements utilized non-contact ammeters, with pulse visualization performed using external oscilloscope.

Control Treatments and Experimental Design

Positive Controls

Sonicated algal suspension served as positive control for complete cell disruption. Concentrated algae suspension (5 mL) was placed in 15 mL plastic centrifuge tubes and processed using a Vibra Cell ultrasonic device (Sonics & Materials Inc., USA) at 40% power amplitude, 20:30 s ON:OFF pulsation mode for 20 minutes total operating time. Samples were maintained in ice bath during sonication to prevent overheating. Heat-treated algae suspension was used as additional positive control for caspase 3-like activity evaluation, with cells incubated at 50°C for 2 hours and analyzed at 2 hours post-treatment.

Sequential Treatment Protocols

Multiple treatment protocols were designed to differentiate direct plasma effects from secondary phenomena:

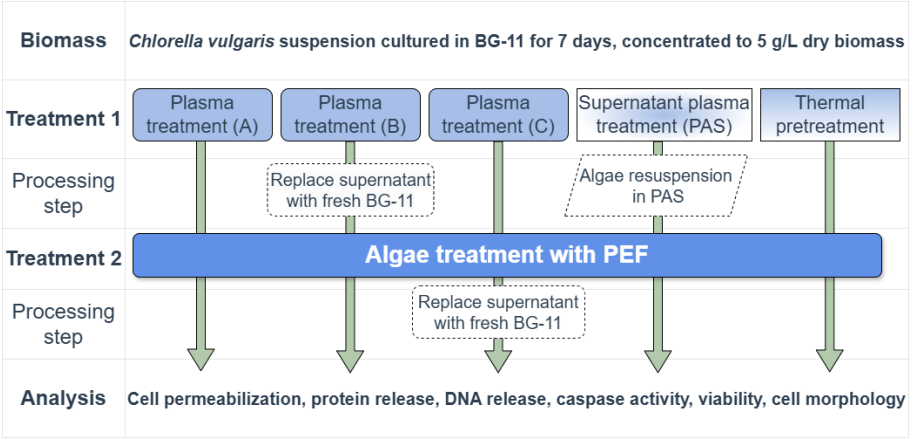

Figure 8 A schematic view of the experiments. Adapted from Paper V of this thesis.

Protocol A: Direct combined plasma and PEF treatment. Protocol B: Plasma treatment with immediate supernatant replacement using untreated BG-11 medium before PEF application (assessing conductivity effects). Protocol C: Plasma and PEF treatment followed by supernatant replacement with untreated BG-11 medium. Plasma-Activated Supernatant (PAS) Protocol: Plasma treatment of *C. vulgaris* supernatant only, followed by immediate algal resuspension and PEF exposure. Temperature control experiments utilized thermal pretreatment matching plasma-induced heating profiles. Treatment temperatures and durations were determined from suspension temperature measurements showing heating plateau achievement after ~150 seconds, with peak temperatures of 41, 46, 49, and 54°C corresponding to Vs values of 130, 170, 210, and 250 V, respectively.

Analytical Methods

Plasma Characterization and Medium Analysis

Air plasma emission spectra were analyzed to characterize plasma composition and properties. Primary spectral analysis was conducted using Flame UV-VIS flame-emission spectrometer (Ocean Insight, Orlando, FL, USA) operating in the 200-1000 nm wavelength range. Measurement parameters included integration time of 0.375 s, accumulation of 10 scans, with each plasma spectrum measured three times to calculate average values. Additional plasma composition analysis was performed using IFU AOS4 acousto-optic emission spectrometer (operating range 250-800 nm), which utilizes a tunable acoustic-optical filter (AOTF). This spectrometer featured a solid-state monochromator/grating with spectral resolution of 0.05 nm at 250 nm and 0.5 nm at 800 nm. Emission spectra measurements were conducted at the center between electrodes, 35 mm from the top, with accumulation of 3 scans performed for each measurement. BG-11 freshwater microalgae growth medium was utilized as test sample for plasma effect evaluation, collected after PAS protocol. Physical and chemical property changes were monitored before and after treatment. Temperature variations during plasma processing were measured using two chromel-alumel thermocouples immersed into the medium near the surface, with reported values representing the average of both measurements. Due to immediate temperature drop upon sample removal from treatment chamber, pH and electrical conductivity measurements were performed 5 minutes post-treatment without temperature compensation, using Orion 720Aplus meter (Thermo Scientific™, USA) and conductivity meter equipped with InLab 738-ISM probe (Mettler Toledo, USA). Nitrate and nitrite concentrations in suspension were determined before and after treatment using commercial test kits (Merck KGaA, Germany) following manufacturer's protocols. Hydrogen peroxide concentrations were determined

using iodometric assay. Iodine standards (0.2-1 mM in 1 M acetic acid:2.5 M KI:H_2O = 10:0.5:1) were used to construct calibration curves based on absorbance at 450 nm. Samples (1 mL) were mixed with 5 mL acetic acid and 0.5 mL KI, incubated in darkness for 5 minutes, and measured at 450 nm to calculate peroxide content from the calibration curve. These assays quantify stable, long-lived dissolution products that accumulate in the liquid phase following plasma treatment, as primary short-lived radicals decay within microseconds and cannot be directly measured in solution.

Membrane Permeabilization Analysis

Algal cell membrane permeability was assessed using SYTOX Green dye (Thermo Fisher Scientific, USA). SYTOX Green penetrates cells only when membranes lose integrity and emits fluorescence upon binding nucleic acids. Treated and control samples were diluted to OD=1 (750 nm wavelength) with sterile BG-11 medium after 2 and 24-hour incubation at room temperature. Each sample was mixed with fluorescent dye (2 μM final concentration) and incubated for 5 minutes in darkness. Fluorescence intensity was measured using LS-50B luminescence spectrometer (PerkinElmer Inc, UK) with excitation at 490 nm, emission at 500-550 nm, 5 nm slit width, 200 nm/min scan speed, and peak intensity measured at 525 nm.

DNA Release Assessment

Nucleic acid leakage into supernatant was quantified using dual methodologies. SYTOX Green fluorescence was measured in supernatant following the staining protocol described above, with additional centrifugation (10,000 × g, 1 minute) to eliminate cellular debris. Also, DNA concentration in supernatant was quantified using Qubit 4 Fluorometer with dsDNA HS Assay Kit (Thermo Fisher Scientific, USA) according to manufacturer's protocol.

Metabolic Activity Evaluation

Microalgal viability was determined using 2,3,5-triphenyltetrazolium chloride (TTC) reduction to red 1,3,5-triphenylformazan (TPF) by mitochondrial dehydrogenases in viable cells. The protocol was modified from Lin et al. (2001). Concentrated algal samples (5 g/L) were centrifuged (1800 × g, 10 min) and pellets resuspended in 1 mL TTC solution (0.5% TTC in 0.05 M Tris-HCl buffer, pH 7.5, sterilized using 0.22 μm filter). Mixtures were incubated for 24 hours at room temperature in darkness. TPF extraction involved heating at 70°C for 15 minutes, then mixing with n-hexane (1:2 ratio). After centrifugation, the hexane phase was analyzed spectrophotometrically at 492 nm.

$$\text{Cell metabolic activity (\%)} = \frac{\text{Treated sample Abs 492 nm}}{\text{Untreated sample Abs 492 nm}} \times 100$$

Protein Quantification and Analysis

Soluble protein concentration in sample supernatants was determined using ROTI Quant universal assay (Roth, Germany) following manufacturer's protocol. After 24-hour incubation, treated and control samples were centrifuged (4,000 × g, 5 min) and supernatants used for protein quantification. Results were compared against bovine serum albumin (BSA) standard curve (Thermo Fisher Scientific, USA) and expressed as protein mass percentage based on dry biomass (%DBM). Supernatants were analyzed by SDS-PAGE using TV200Y electrophoresis unit (Scie-Plas Ltd., UK) according to modified protocols described in literature.

Free Amino Acid Determination

Free amino acids were quantified using modified Ninhydrin method with SUNRISE Microplate Absorbance Reader at 570 nm. After 24-hour incubation, treated and control samples were centrifuged (4,000 × g, 5 min) and supernatants used for amino acid quantification. Results were compared against leucine solution standard curve (Carl Roth, Germany) and expressed as free amino acid mass percentage based on dry biomass.

Caspase Activity Assessment

Colorimetric caspase assay employed Ac-DEVDpNA substrate (Cayman Chemical Company, Michigan, USA). Assays were performed in reaction buffer (50 mM Tris-HCl pH 7.5, 0.3% Triton-100, 1.0 mM DTT) with 0.2 mM Ac-DEVDpNA. Reaction mixtures were incubated at 37°C for 2 hours. Caspase 3-like activity was determined by spectrophotometric quantification of free pNA ($\lambda = 405$ nm).

Microscopic Analysis

Morphological examination was conducted on samples treated with direct plasma and/or PEF at 24/72 hours post-treatment using bright-field microscopy. Analysis employed inverted microscope Nikon Eclipse Ti-E with Plan-flour ELWD 20x/0.45 objective (Nikon Instruments, Japan) equipped with NIS-Elements software (Nikon Instruments, Japan).

Statistical Analysis

The study presents n independent experiments (n = 3-6) with internal duplicates or triplicates depending on experimental design. Calculated averages and standard deviations are displayed in figures. Statistical significance was evaluated using one-way analysis of variance (ANOVA). Gel electrophoresis was performed at least three times with representative images selected for publication.

2.3 Results

2.3.1 Plasma Characterization and Medium Analysis

Plasma characterization.

GAD plasma exhibited voltage-dependent electrical behavior. Waveform analysis showed serrated voltage patterns with associated current variations characteristic of gliding arc operation. Discharge duration increased from 1.71 ± 0.29 ms at 50 V to 5.21 ± 0.61 ms at V_s = 250 V, indicating longer sustained discharge at higher supply voltage (for more details see Paper I of this thesis).

The emission spectra demonstrated that excited nitrogen species dominated the air plasma. Prominent N_2 emission peaks were observed at 316 nm, 337 nm, 353 nm, 358 nm, and 379 nm (Fig.9).

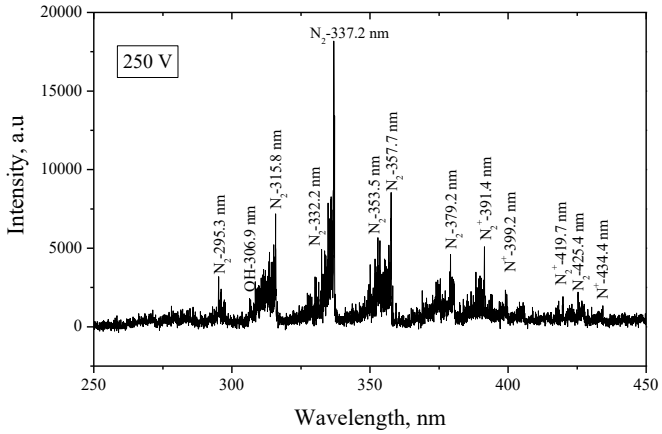

Figure 9 Optical emission spectrum of air plasma when input voltage was 250 V. Adapted from Paper I of this thesis.

Additional plasma composition analysis, using IFU AOS4 acousto-optic emission spectrometer, confirmed the presence of molecular nitrogen ions (N_2^+) with emission lines at 391 nm, 419 nm, and 470 nm (Fig. 10A). The intensity of N_2^+ emission lines increased with voltage.

Nitrogen oxide species (NO_γ) were detected at 236 nm, 246 nm, 258 nm, and 283 nm wavelengths, with intensity increasing from 1,300 to 18,900 counts across the voltage range (Fig. 10A). Atomic oxygen species were identified at 777.4 nm and 844.6 nm, though at significantly lower intensities than nitrogen species. Hydroxyl radicals (•OH) were detected at 306.9 nm, attributed to water vapor presence in ambient air.

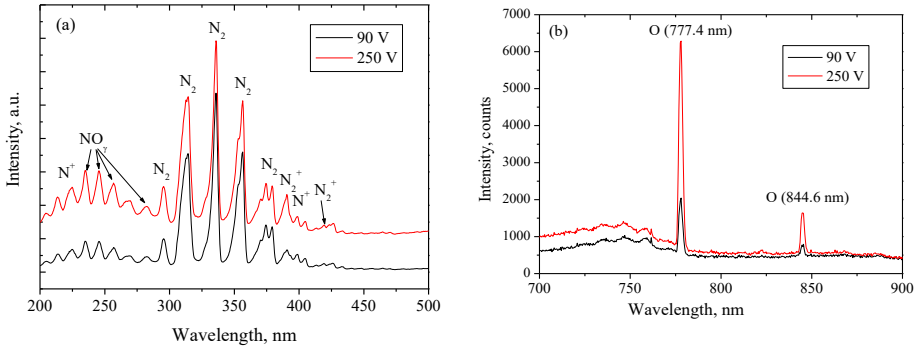

Figure 10 Emission spectra of the air plasma when the input voltage was 90 V and 250 V. Adapted from Paper I of this thesis.

Physical and chemical changes in BG-11 medium.

Plasma treatment induced systematic modifications to the BG-11 microalgae medium properties in a voltage-dependent manner. Medium temperature increased with voltage, reaching plateau values of 41, 46, 49, and 54 °C corresponding to V_s = 130, 170, 210, and 250 V, respectively (Fig. 11a). The pH decreased from approximately 7.5 to ~7.0 at the highest voltage (Fig. 11b). Conductivity increased from ~1.85 mS/cm (control) to 2.40 mS/cm at V_s = 90 V and 3.34 mS/cm at V_s = 250 V (Fig. 12a). This enhancement correlated with the formation of ionic species in the treated medium.

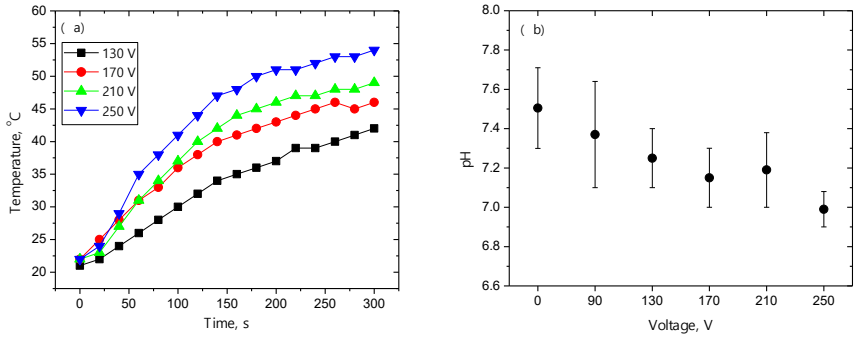

Figure 11 The dependence of the medium temperature on the used voltage (a) and variation of pH values (b). Adapted from Paper I of this thesis.

Chemical analysis of the treated medium quantified stable long-lived products of plasma-liquid interactions (Fig. 12b). Nitrite (NO_2^-) concentrations rose from 0.13 mM to 1.67 mM, while nitrate (NO_3^-) increased from 23.3 mM to 28.9 mM across the 90 V to 250 V voltage range. Hydrogen peroxide (H_2O_2) increased from 5.9 mM to 17.4 mM at maximum supply voltage.

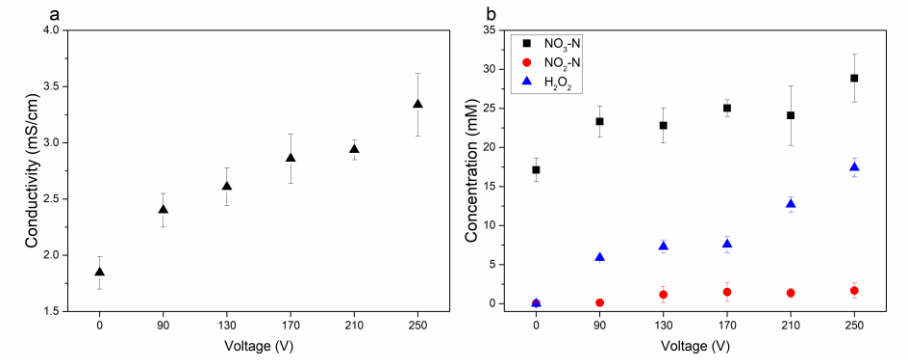

Figure 12 The variation of the conductivity (a) and concentration of nitrites, nitrates, and hydrogen peroxide (b) in liquid medium as a function of the output voltage. Adapted from Paper I of this thesis.

2.3.2 Single-Modality Baseline Responses

PEF treatment without prior plasma exposure produced increased permeabilization with increasing pulse number at 2 h that became less pronounced during incubation. Two hours after exposure, a single pulse (25 kV/cm, 7 µs) resulted in ~14% SYTOX-positive cells, whereas 10 pulses exceeded 60% (Fig. 13A). After 24 h, SYTOX uptake increased in both conditions and reached ~70%, reducing the difference between one and ten pulses (Fig. 13B). In parallel, DNA signal in the supernatant increased strongly after PEF. Quantitative assay confirmed DNA release exceeding 20 mg/L (Fig. 13C), accompanied by complete loss of metabolic activity under ten-pulse conditions (Fig. 13D).

Protein release into the supernatant reached approximately 23% of total dry biomass, with no increase in amino acid release compared to untreated samples (Fig. 14). Morphological examination of ten-pulse treated samples revealed cell aggregation at 24 hours (data not shown), progressing to decreased cell concentration and bacterial overpopulation by 72 hours (Fig. 16B).

Plasma exposure without subsequent PEF produced voltage-dependent effects relative to untreated controls. At V_s = 130 V, plasma treatment did not increase SYTOX uptake by cells, supernatant DNA signal, or protein release beyond control levels after 2 or 24 hours (Fig. 13, 14, 15). Metabolic activity and morphological features remained similar to untreated samples (Fig. 13D, 16C).

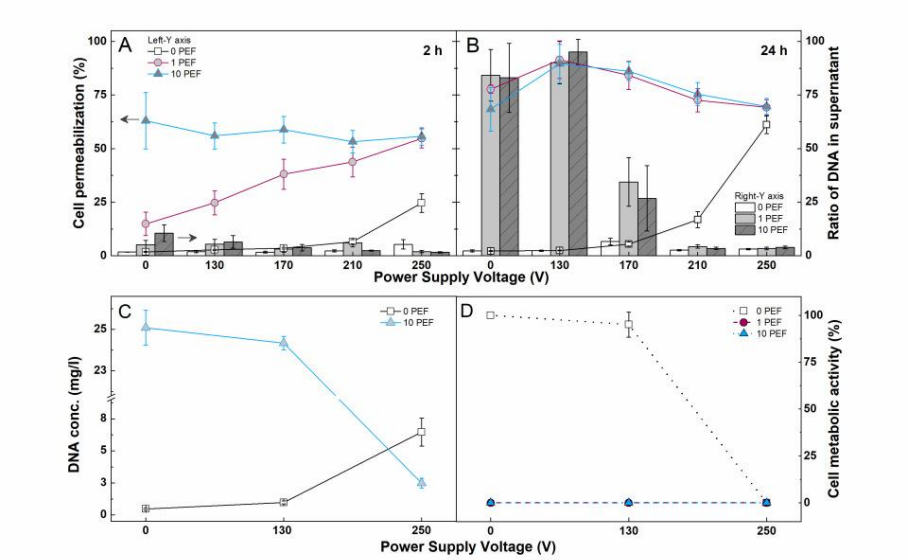

Figure 13 Plasma and PEF treatment induced changes in the cell permeability and DNA release into supernatant after 2 h (A) and 24 h (B). The line and symbol represent cell permeabilization data (left-Y axis) and the columns represent DNA release (right-Y axis). Plasma and PEF treatment induced changes in DNA release into the supernatant (C) and cellular metabolic activity after 24 h (D). The numbers (0; 1; 10) represent the number of applied PEF pulses. Adapted from Paper V of this thesis.

At higher voltages, plasma alone induced membrane permeabilization and loss of metabolic activity, though macromolecular release remained limited. At V_s = 250 V, the SYTOX-positive fraction reached ~25% after 2 hours and increased to ~60% after 24 hours (Figs. 13A, B). In contrast, the amount of extracellular DNA remained low. The amount of SYTOX in the supernatant accounted for ~4%, and the quantitative assay yielded ~6 mg/L of DNA at 24 hours (Figs. 13B, C). Protein release remained below 5% DBM, and SDS-PAGE did not show additional bands relative to untreated controls (Figs. 14, 15). Metabolic activity was completely lost at 24 hours (Fig. 13D). Microscopy revealed intact cell morphology without visible disintegration or aggregation at 72 hours (Fig. 16E).

2.3.3 Voltage-Dependent Response Patterns in Sequential Plasma-PEF Treatment

Sequential plasma pretreatment followed by PEF produced plasma voltage dependent differences in membrane permeabilization, macromolecular release, metabolic activity, and morphology (Figs. 13-16). The following

sections compare low-voltage (V_s = 130 V) and high-voltage (V_s = 250 V) plasma pretreatment, as defined in Methods.

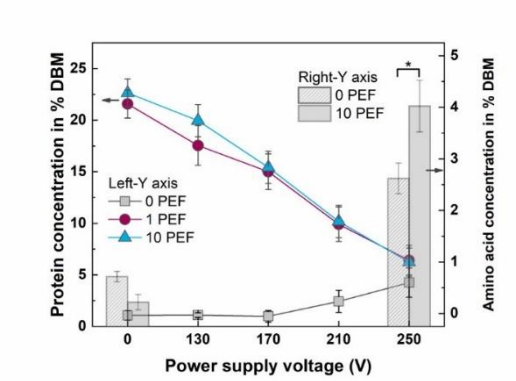

Figure 14 Plasma and PEF treatment induced changes in protein and amino acid release 24 hours after treatment. Lines and symbols represent protein concentration (left Y axis); columns represent amino acid concentration (right Y axis). Numbers (0; 1; 10) indicate the number of applied PEF pulses. Data represent means and standard deviations from at least six biological replicates. Statistical significance (*) is indicated only where differences are less visually apparent; obvious differences (e.g., protein decrease with increasing voltage) were not marked. Adapted from Paper V of this thesis.

At low plasma voltage (V_s = 130 V), sequential plasma-PEF treatment produced an outcome pattern comparable to the PEF-only baseline. At 2 h, cell permeability reached ~25% with a single pulse and ~55% with 10 pulses (Fig. 13A). By 24 h, permeabilization increased and stabilized near ~90% regardless of pulse number (Fig. 13B). In parallel, the supernatant DNA signal rose to ~90% of the fluorescence maximum (Fig. 13B), and quantitative assay confirmed DNA release >20 mg/L (Fig. 13C). Protein release remained in the same range as PEF-only treatment (~20% DBM) (Fig. 14), and SDS-PAGE profiles showed no qualitative shift in the dominant bands relative to PEF alone (Fig. 15). Metabolic activity was completely abolished at 24 h (Fig. 13D). Morphological changes matched the PEF-alone trajectory: aggregation at 24 h, progressing to reduced apparent cell concentration and bacterial overpopulation by 72 h (Fig. 16D).

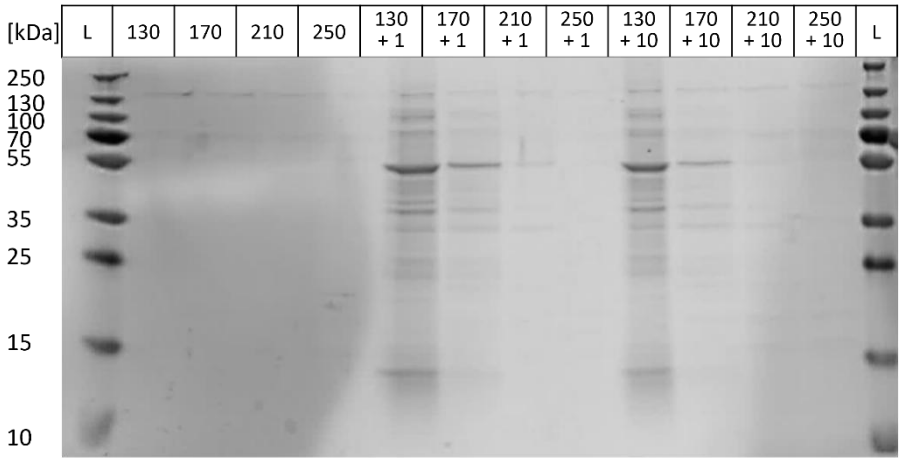

Figure 15 SDS-PAGE analysis of the soluble protein extracts obtained by plasma and PEF treatment. Numbers above the gel tracks indicate the applied voltage of plasma generator (V) and (+) the number of PEF pulses. Adapted from Paper V of this thesis.

Plasma pretreatment markedly altered how PEF was expressed: at 2 h, adding a single PEF pulse after high-voltage plasma (V_s = 250 V) increased permeabilization roughly four-fold compared with a single pulse without plasma (~55% vs ~15%) (Fig. 13A), reaching levels similar to a 10-pulse PEF treatment. However, macromolecular release was suppressed. At 24 h, combined treatment maintained high permeabilization (≥70%) and complete metabolic inactivation (Figs. 13B, D). However, DNA remained <5% of total fluorescence in the supernatant, with quantitative release ~2 mg/L even after 10 pulses (vs ~25 mg/L for PEF alone) (Figs. 13B, C). Protein release fell below ~6% of dry biomass and became undetectable by SDS-PAGE at the highest-voltage combinations (Figs. 14, 15). In parallel, free amino acid concentrations increased under high-voltage combined conditions (Fig. 14). Morphologically, cells remained similar to untreated controls even after prolonged incubation, lacking the aggregation/disintegration patterns typical of the PEF-only endpoint (Fig. 16F).

Across intermediate voltages, increasing plasma voltage was associated with high cell permeability but progressively lower DNA and protein release.

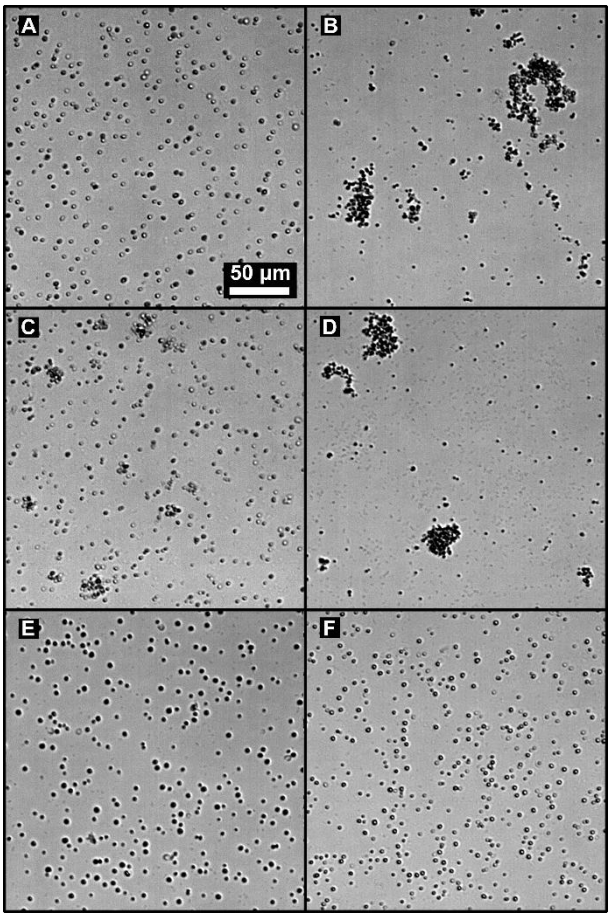

Figure 16 Bright field microscopy images taken 72 hours after treatment. Untreated samples(A); samples treated with PEF (10 pulses) only (B); samples treated with 130V plasma only (C); samples treated with both 130V plasma and PEF (D); samples treated with 250V plasma only (E); samples treated with both 250V plasma and PEF (F). Adapted from Paper V of this thesis.

2.3.4 Differentiation of Primary and Secondary Plasma-Induced Effects

To separate direct plasma-cell interaction from secondary changes in the medium (heating, conductivity shifts, and long-lived reactive species), sequential plasma-PEF outcomes were compared with control protocols that reproduced individual secondary factors while keeping the PEF exposure constant (Fig. 8).

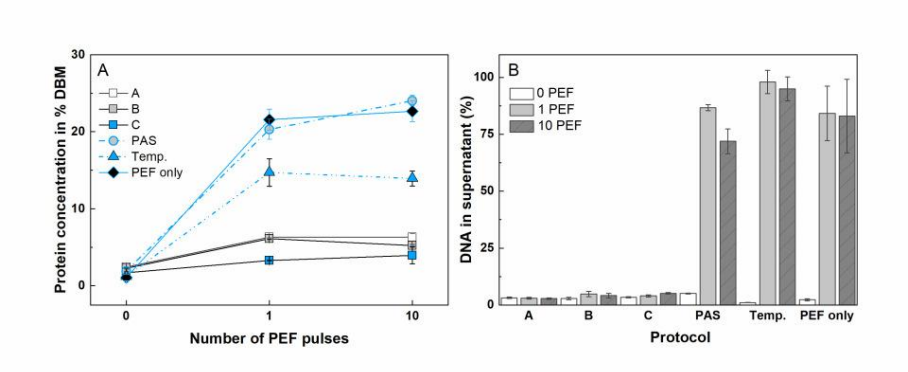

Figure 17 Effect of treatment protocols on protein (A) and DNA (B) release into the supernatant 24 hours post-treatment. Protocols A, B, and C represent direct plasma treatments, compared against secondary effect controls: Plasma Activated Solution (PAS), Temperature simulation (Temp.), and PEF alone. Protein concentration is expressed as a percentage of dry biomass (DBM). Error bars represent standard deviation (from at least 6 biological replicates). Detailed protocol configurations are illustrated in Figure 6. Adapted from Paper V of this thesis.

Protocols designed to eliminate plasma-induced conductivity changes by replacing the supernatant with untreated BG-11 either immediately before PEF exposure or after PEF exposure did not abolish the voltage-dependent outcome pattern. Reduced protein and DNA release at high plasma voltage persisted despite supernatant replacement (Fig. 17), indicating that bulk conductivity shifts or continued incubation in plasma-modified medium were not required for the effect.

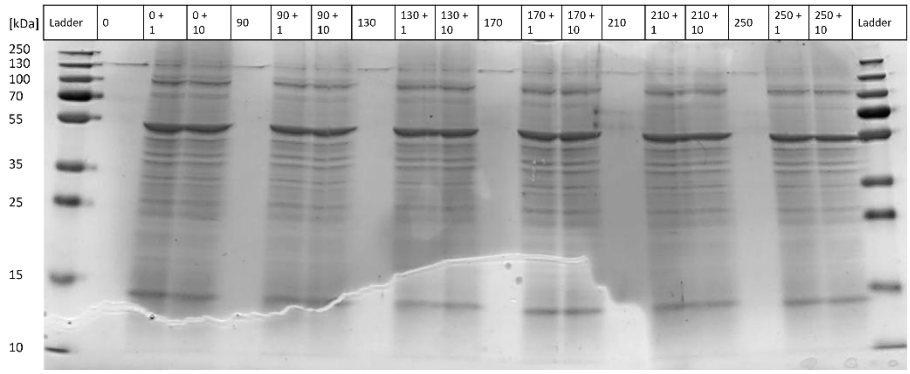

Figure 18 SDS-PAGE analysis of the protein extracts obtained by PEF only and PAS protocol. Numbers above the gel tracks indicate the applied plasma voltage (V) and (+) the number of PEF pulses. Adapted from Paper V of this thesis.

Similarly, exposure to PAS alone did not reproduce the high-voltage response pattern. When the medium was plasma-treated only and the cells were resuspended prior to PEF exposure, the release of proteins and DNA remained comparable to the PEF-only baseline across all voltage (Fig. 17). The SDS-PAGE profiles of these samples retained the characteristic band

pattern observed after PEF treatment rather than showing suppression, as seen after direct high-voltage plasma exposure (Fig. 18). Therefore, long-lived plasma products in the medium were insufficient to generate the reduced protein and DNA release observed after direct plasma pretreatment.

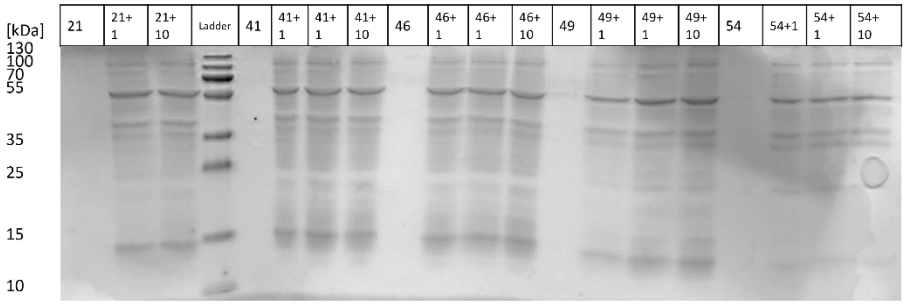

Figure 19 SDS-PAGE analysis of the protein extracts obtained by PEF only and temperature protocol. Numbers above the gel tracks indicate the applied treatment temperature (°C) and (+) the number of PEF pulses. Adapted from Paper V of this thesis.

Thermal pretreatment that replicated the temperature range associated with plasma (41-54 °C, or 130-250 V) followed by PEF treatment did not reproduce the reduced macromolecular release characteristic of high-voltage plasma pretreatment. At the highest simulated temperature (54 °C + PEF), protein release was substantially higher than in the direct high-voltage plasma-PEF condition (approximately 15% DBM versus less than 5% after 250 V plasma + PEF) (Fig. 17A). DNA release exhibited a similar trend (Fig. 17B).

Additionally, to evaluate the direct impact of plasma exposure on protein detectability, a BSA suspension was subjected to plasma treatment at 250 V for 5 minutes. SDS-PAGE analysis revealed no reduction in band intensity or the appearance of lower-molecular-weight bands, which would indicate fragmentation (Fig. 20A). Fluorescence spectra showed only a minor peak shift and a small increase in signal intensity (Fig. 20B).

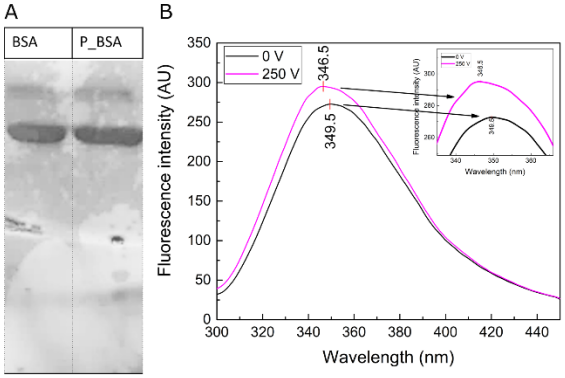

Figure 20 Effects of high-voltage plasma exposure on BSA. (A) SDS-PAGE profile and (B) fluorescence emission spectra measured before treatment and after 5 min exposure to GAD plasma at 250 V. Adapted from Paper V of this thesis.

Taken together, these comparisons show that the reduced macromolecular release observed after high-voltage plasma-PEF treatment could not be reproduced by isolated medium heating, PAS exposure, or conductivity-related supernatant replacement, and is unlikely to reflect plasma-driven loss of protein detectability under the analytical conditions used.

2.3.5 Modulation of Caspase 3-Like Activity by Plasma and PEF Exposure

Caspase 3-like activity was quantified 2 h after treatment to assess whether plasma exposure altered cell death signaling pathways activated by PEF. PEF treatment alone induced a pronounced increase in caspase 3-like activity, reaching approximately 250% relative to the untreated control and exceeding the activity observed in the heat-shock positive control (Fig. 21).

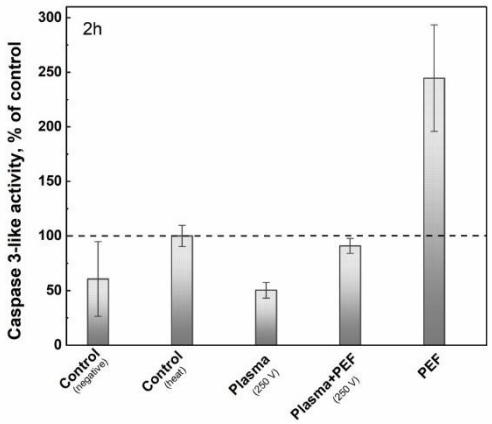

Figure 21 Modulation of Caspase 3-like activity in *C. vulgaris* 2 hours post-treatment. Cells were exposed to high-intensity plasma (250 V), PEF alone (10 pulses, 25 kV/cm), or the combined sequence (Plasma+PEF). Data represent the mean percentage relative to the heat shock positive control (indicated by the dashed line at 100%) ± standard deviation from at least three biological replicates. Adapted from Paper V of this thesis.

In contrast, plasma exposure produced an opposing effect. Cells exposed to GAD plasma exhibited strongly suppressed caspase 3-like activity, regardless of whether plasma treatment was applied alone or followed by PEF (Fig. 21). At the high voltage plasma (250 V), caspase activity remained below baseline control levels, despite complete loss of metabolic activity and high membrane permeabilization.

2.4 Discussion

The central finding of this study is that plasma pretreatment redirects how a fixed PEF exposure is biologically expressed in *C. vulgaris*. When identical PEF parameters were applied (25 kV/cm, 7 µs, 10 pulses), low-voltage plasma pretreatment (V_s = 130 V) produced the typical PEF phenotype: extensive DNA and protein release, elevated caspase 3-like activity, and progressive morphological disintegration during post-treatment incubation. In contrast, high-voltage plasma pretreatment (V_s = 250 V) yielded a qualitatively different outcome: complete metabolic inactivation with strong macromolecular retention, preserved cellular architecture for at least 72 h, and suppression of caspase activity below control levels. This voltage-dependent divergence in biological outcome under identical electrical input is summarized schematically in Figure 22.

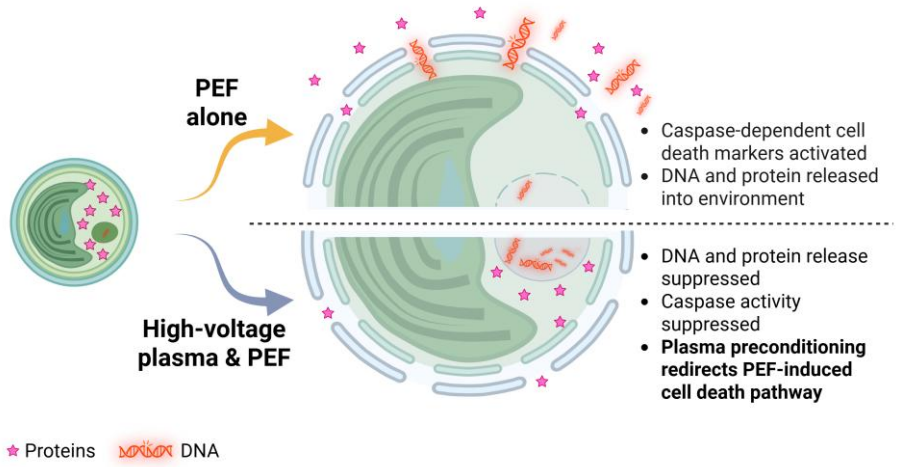

Figure 22 Schematic summary of voltage-dependent outcome bifurcation in sequential plasma-PEF treatment of *C. vulgaris* 24 h after treatment. The untreated cell (left) contains proteins (pink stars) and DNA (orange) within an intact membrane. Following PEF alone, or low-voltage plasma pretreatment combined with PEF (upper path), membrane permeabilization is accompanied by caspase-dependent programmed cell death markers and progressive release of proteins and DNA into the surrounding environment. Following high-voltage plasma pretreatment combined with PEF (lower path), membrane permeabilization occurs but macromolecular contents are retained intracellularly, caspase activity is suppressed.

This divergence was not explained by differences in gross membrane permeability. Both low- and high-voltage plasma-PEF sequences reached comparable SYTOX Green uptake at 24 h. However, their downstream pathways diverged sharply. Since the electrical input stayed the same, it appears that plasma pretreatment must have altered the cellular state in which

the permeabilization occurred. This led to a change in the downstream biological outcomes.

Control experiments constrain the origin of the high-voltage phenotype. Temperature-matched pretreatment, plasma-activated supernatant exposure, and conductivity-controlled supernatant replacement all failed to reproduce the reduced macromolecular release observed after direct high-voltage plasma pretreatment, and BSA controls excluded plasma-driven loss of protein detectability under the analytical conditions used. Together, these comparisons indicate that secondary medium effects are insufficient and that direct plasma-cell interaction is required, with discharge voltage providing a clear axis for mechanistic investigation even if the responsible plasma component is not yet isolated.

The high-voltage plasma-PEF phenotype does not correspond to either of the programmed cell death pathways associated with PEF treatment in *C. vulgaris*. Apoptosis would manifest as elevated caspase activity, membrane blebbing, and controlled cellular dismantling with macromolecular release [80,81]. Necrosis, although caspase-independent, proceeds through uncontrolled membrane rupture leading to bulk content release and structural disintegration [80]. Neither pattern was observed here. Instead, the data show a combination that is incompatible with both: membrane permeabilization without bulk macromolecular release, suppressed rather than elevated caspase activity, and preserved cellular architecture sustained over 72 h. This phenotype has not been previously reported in plasma-PEF studies and represents a qualitatively distinct biological response that falls outside established death classification frameworks.

The mechanism underlying this voltage-dependent divergence is not yet resolved. What the experimental design does establish is where the relevant modification must operate. Since identical PEF parameters produced opposite outcomes depending on prior plasma exposure, the change must occur before permeabilization rather than during it. The control experiments further localize this effect. The high-voltage phenotype requires something that direct plasma-cell contact provides and that neither heating, long-lived reactive species accumulation in the medium, nor conductivity changes can replicate.

Whether the disconnect between dye entry and macromolecular escape arises from plasma-induced modifications to the cell envelope, from disruption of intracellular execution pathways, or from some combination of these cannot be distinguished from the present data. What the results do establish is that cellular response context shapes how a fixed electrical input translates into phenotype. Conventional electroporation frameworks often treat permeabilization as the primary determinant of outcome. These findings

suggest that in *C. vulgaris*, permeabilization is necessary but not sufficient. The downstream consequences depend on processes that plasma pretreatment disrupts or redirects.

This interpretation aligns with evidence that PEF-induced macromolecular release in microalgae depends substantially on post-pulse processes. Scherer et al. (2019) demonstrated that extraction-relevant protein recovery from *C. vulgaris* is strongly driven by events occurring after loss of viability, likely involving enzymatic activity triggered by cell death rather than the electrical pulse itself [20]. Krust et al. (2022) demonstrated that *C. vulgaris* contains a cell death-inducing factor that is released upon disruption (whether by PEF or mechanical methods) and can trigger death in neighboring cells. This indicates that post-treatment outcomes in microalgal populations involve not only passive diffusion but also active biological signaling among cells [21]. Whether plasma pretreatment acts at the level of the cell envelope, intracellular signaling, or enzymatic execution remains unresolved, but the caspase data provides a more direct window into this question.

The shift in caspase 3-like activity further supports a change in PEF execution logic rather than increased damage. PEF treatment alone produced a pattern consistent with classical PEF-induced cell death in microalgae: elevated caspase 3-like activity reaching approximately 250% of control, substantial DNA and protein release, and progressive morphological deterioration culminating in aggregation and bacterial overgrowth. This trajectory aligns with evidence that extraction-relevant macromolecular release from *C. vulgaris* depends substantially on post-pulse enzymatic processes triggered by cell death rather than the electrical pulse itself [20], and that disrupted cells release a death-inducing factor capable of propagating lysis through neighboring populations [21]. High-voltage plasma pretreatment yielded an opposing trajectory. Despite comparable membrane permeabilization, caspase 3-like activity fell below baseline levels, macromolecular release was strongly suppressed, and cellular morphology remained intact at 72 hours. If high-voltage plasma disrupts the execution machinery required for autolytic processes, whether by modifying envelope structure, depleting required cofactors, or inactivating key enzymes, the result would be a permeabilized cell that is metabolically inactivated but cannot complete the downstream processes required for bulk release.

Caspase-independent death pathways are well established in mammalian systems and include routes such as paraptosis and autophagy-dependent cell death, alongside regulated necrosis programs that proceed without caspase activation [82]. These pathways differ in their terminal phenotype. Some, like necroptosis, culminate in membrane rupture and content release. Others, such

as oxeiptosis, proceed through ROS-sensing circuits without inflammatory signaling or extensive macromolecular leakage [83,84]. The high-voltage plasma-PEF phenotype in *C. vulgaris* shares some features with these contained death modes. However, direct alignment with any mammalian pathway would be premature. The phylogenetic distance between green microalgae and mammalian systems is substantial [81], the molecular machinery governing cell death execution in microalgae remains incompletely characterized, and the present data do not include pathway-specific markers beyond caspase 3-like activity [85]. What can be stated is that the phenotype is real, reproducible, and distinct. Its mechanistic basis warrants dedicated investigation.

The microbiological dynamics observed during post-treatment incubation provide independent, population-level support for the retention phenotype. That PEF-disrupted algal cells release bioavailable carbon and nitrogen capable of sustaining bacterial growth is not a self-evident assumption. Chapter 3 of this thesis establishes it directly: lysate-growth assays confirmed that Delftia sp. proliferates in PEF-treated algal extract at rates comparable to fresh growth medium, and antimicrobial screening showed no inhibitory activity in the released material. Given this, the conventional PEF-like trajectory, with its substantial macromolecular efflux, would be expected to create permissive conditions for opportunistic bacterial growth, and this is precisely what was observed: aggregation followed by bacterial overgrowth during post-treatment incubation. Under high-voltage plasma-PEF conditions, where macromolecular release was strongly suppressed, these downstream signatures were absent. The two outcomes are therefore not only biochemically distinct but ecologically distinguishable, and the convergence of molecular and population-level evidence on the same conclusion strengthens confidence in the retention phenotype even where its mechanistic basis remains unresolved.

Methodologically, a major strength of this work is the explicit separation of direct plasma-cell interaction from secondary medium effects. This is an essential distinction in plasma biology, where temperature shifts and long-lived reactive species can otherwise dominate interpretation [72]. The multi-timepoint window (2-72 h) also demonstrates that the high-voltage phenotype is sustained rather than a simple delay of conventional lysis. These findings have implications for both fundamental understanding and application. Mechanistically, they support the view that PEF outcome is shaped by cellular state, not permeabilization alone. Practically, the high-voltage phenotype, metabolic inactivation without bulk release, may prove useful for applications requiring inactivation without product leakage, though process optimization

would be required. The main limitations relevant for interpretation are that the responsible direct plasma component was not isolated; amino acids were quantified as leucine equivalents, limiting biochemical specificity; and caspase 3-like activity is an operational readout that cannot, by itself, identify the executing protease class or pathway in microalgae [85]. Finally, the study focuses on one wall-bearing green alga; generalization will require comparative testing across taxa and envelope architectures.

2.5 Key Findings

GAD plasma treatment induced systematic voltage-dependent modifications in BG-11 medium. At 250 V, temperature reached 54°C, pH decreased to 7, conductivity rose to 3.3 mS/cm, and reactive species accumulated (NO_2^- 1.67 mM, NO_3^- 28.9 mM, H_2O_2 17.4 mM). Direct biological effects of plasma on *C. vulgaris* were observed only at high voltage. 250 V plasma exposure alone caused ~25% membrane permeabilization and metabolic inactivation, while lower voltages produced no significant cellular effects.

Sequential plasma-PEF treatment produced voltage-dependent response patterns that could not be predicted from individual treatments. Low-voltage plasma pretreatment (130 V) followed by PEF (25 kV/cm, 7 μs, 10 pulses) yielded a conventional PEF-like phenotype: high membrane permeabilization, substantial DNA and protein release, metabolic inactivation, and progressive morphological deterioration. High-voltage plasma pretreatment (250 V) followed by identical PEF parameters produced a fundamentally different outcome: comparable membrane permeabilization but strongly suppressed macromolecule release, preserved morphology at 72 h, and metabolic inactivation without bulk lysis.

Control experiments established that this divergence required direct plasma-cell interaction. Thermal pretreatment matching plasma-induced temperatures (41-54°C), plasma-activated supernatant exposure, and conductivity-matched medium exchange all failed to reproduce the high-voltage phenotype. Secondary medium effects alone were insufficient.

Cell death pathway analysis revealed that plasma pretreatment altered death execution in *C. vulgaris*. PEF alone produced the classical PEF-induced pattern: elevated caspase 3-like activity (approximately 250% of control), substantial macromolecule release, and progressive morphological deterioration. High-voltage plasma pretreatment fundamentally altered this trajectory. Despite comparable membrane permeabilization, caspase 3-like activity was suppressed below control levels, macromolecule release was strongly reduced, and cellular morphology remained intact at 72 h. This pattern is distinct from classical PEF-induced cell death in microalgae and does not fit either caspase-mediated apoptotic pathways or necrotic lysis.

CHAPTER 3. PEF Effects on Microalgae-Bacteria Co-culture

3.1 Introduction

Industrial microalgae cultivation is rarely axenic. Bacteria persist in open ponds and many photobioreactor systems, where they can alter algal growth, reshape biomass composition, and complicate downstream processing [86]. PEF has been established as an effective method for extracting intracellular proteins from *C. vulgaris*, with reported yields of approximately 20-30% of cell dry weight at field strengths of 25-40 kV/cm under monoculture conditions [13,15,20]. Whether comparable extraction efficiency and purity can be achieved from non-axenic cultures, where bacterial proteins may co-extract alongside algal material, is therefore a practically relevant but largely unresolved question. For microalgal biorefineries, this matters: the question is not whether PEF disrupts algae under controlled conditions, but whether it can do so selectively enough in mixed populations to support clean product recovery without additional purification steps.

A first-order biophysical expectation suggests that selective responses should be achievable. According to the Schwan equation, the induced transmembrane voltage scales linearly with cell radius under a given external field [1,38]. This implies that larger eukaryotic microalgae reach the critical permeabilization threshold at lower field strengths than smaller bacteria. However, cell architecture is not the only determinant of PEF susceptibility. Growth phase has been identified as a significant modulator of bacterial electrical resistance in monoculture studies, though the direction of the effect is species-dependent: stationary-phase *Listeria* and *Salmonella* cells show increased resistance relative to exponential-phase counterparts [62,87,88], while exponential-phase *E. coli* strains tend to be more susceptible [61]. Whether comparable state-dependent variation occurs in bacteria co-existing with microalgae, and whether it can be exploited for selective treatment, has not been examined. Whether algal PEF susceptibility varies with growth phase has received limited attention in the literature. In practice, PEF-based extraction from microalgae is conventionally applied at the end of cultivation, when total biomass concentration reaches its maximum and harvest is economically justified [13,15,20,89]. As a consequence, there has been little practical motivation to treat cultures at earlier stages, and whether electrical susceptibility changes across growth phases remains an open question that this chapter addresses directly. Co-cultures introduce additional determinants of effective exposure and damage. Aggregation, cell-to-cell shielding,

extracellular polymers, and conductivity microgradients can distort local fields, while metabolic coupling and stress adaptation can shift membrane composition, repair capacity, and death pathways. In this context, treatment outcome may be governed as much by community organization and physiological state as by species identity. This possibility extends the response-context principle developed earlier in the dissertation to the community scale: if cellular state shapes individual PEF outcomes, then differential states across co-existing populations may determine community-level selectivity.

Evidence for differential electrical susceptibility in mixed populations exists, but it is not yet tailored to the algae-bacteria scenario that dominates microalgal biotechnology [90]. Simonis et al. reported selective inactivation in acid whey, achieving >3 $\log_{10}$ reduction of *Saccharomyces cerevisiae* (yeast) while reducing *Lactobacillus* (bacteria) populations by only 1-2 $\log_{10}$ under identical treatment conditions (25 kV/cm, 100 μs) [40]. Similarly, Rego et al. showed selective elimination of predatory microorganisms (rotifers and ciliated protozoans) in *C. vulgaris* cultures (900 V/cm, 50 Hz, 65 μs) while maintaining algal viability [39]. These examples support feasibility of selectivity in principle, yet direct tests of microalgae-bacteria selectivity remain uncommon, despite their frequent co-occurrence in industrial and natural aquatic systems.

Whether community context can override monoculture-based expectations is particularly plausible because interaction outcomes themselves can switch with environment. High-throughput analysis of *Chlamydomonas-Escherichia coli* communities across over 500 environmental conditions revealed that pH, nutrient availability, and carbon source identity function as master switches controlling interaction outcomes [91]. Because bacterial membrane composition, metabolic activity, and stress tolerance shift across growth phases, electrical susceptibility in co-cultures may vary with cultivation timing, not only with treatment parameters. If cultivation conditions act as master variables for interaction structure, then responses to electrical stress may likewise depend on the starting physiological state of each population rather than on cell architecture alone.

If cell size governs electrical susceptibility as electroporation theory predicts, algae should be consistently inactivated at field strengths that leave smaller bacteria largely unaffected. However, if physiological state modulates susceptibility, bacterial responses may vary with growth phase even under constant PEF parameters. This study tests both possibilities.

Selectivity in this context is defined operationally: algal protein recovery without proportional bacterial protein contamination in the extract. From this

perspective, selectivity is not a theoretical size effect but an emergent outcome of physiology, community context, and post-treatment dynamics. The bacterial isolate used here, *Delftia* sp., was previously isolated from *C. vulgaris* cultures [see Paper III of this thesis]. It is a gram-negative, rod-shaped bacterium belonging to the Betaproteobacteria, commonly encountered in microalgal cultivation systems and aquatic environments, making it an ecologically relevant rather than arbitrarily chosen model contaminant.

Aim of this chapter: To investigate how physiological state and community context affect PEF responses in algae-bateria co-cultures, and to evaluate whether differential susceptibility enables selective algal protein extraction.

Objectives:

1. To characterize medium-dependent community dynamics and identify conditions supporting substantial bacterial populations for PEF testing.
2. To quantify species-specific PEF susceptibility and its dependence on growth phase and treatment energy.
3. To evaluate whether differential susceptibility enables selective algal protein extraction from co-cultures.

3.2 Materials and Methods

Bacterial Strain

The bacterial isolate used in this study, identified as *Delftia* sp. (GenBank accession OP777498.1, 98% identity to *D. tsuruhatensis*), was previously isolated and characterized from *C. vulgaris* (UTEX 395) cultures at the Arizona Center for Algae Technology and Innovation (for more details see Paper III of this thesis). The strain was maintained on tryptic soy agar at 30°C and cultured aerobically in tryptic soy broth (TSB) with shaking at 30°C for 24 hours prior to co-culture inoculation.

Algae Cultivation

Microalgal Culture. *C. vulgaris* (SAG strain 211-12, University of Göttingen) axenic pre-cultures were maintained in TAP medium at 21 ± 1°C under 90 μmol m^{-2} s^{-1} photosynthetic photon flux density with 16:8 hour light:dark cycles and continuous shaking at 150 rpm. Cultures were harvested during stationary phase (7 days) for experimental use.

Co-culture Establishment and Monitoring

Medium Formulations. *C. vulgaris* grows primarily autotrophically, fixing CO_2 as its carbon source, while *Delftia* sp. is strictly heterotrophic. Organic carbon availability therefore directly determines bacterial physiological state

before PEF treatment. Three media were selected to vary this: TAP provides organic carbon (17.49 mM acetic acid) supporting both organism growth; BG-11 relies on CO_2 as the sole carbon source, limiting bacterial growth; BG+AA supplements BG-11 with 17.49 mM acetic acid, matching TAP carbon content. Complete medium compositions are provided in Table S1 at Paper III of this thesis.

Co-culture Protocols. Experiments were conducted in sterile 250 mL Erlenmeyer flasks under controlled conditions (see Microalgal Culture). Standardized inocula of OD_{750} = 0.1 for *C. vulgaris* and OD_{600} = 0.01 for *Delftia* sp. were used. Parallel monoculture controls were maintained under identical conditions. Cultivation extended to 7 days without external CO_2 supplementation, with daily sampling for population and chemical analysis.

Population Monitoring. Cell viability and mortality were assessed using flow cytometry (Attune™ Nxt) with differential fluorescent staining. SYTO® 9 (0.5 μM) provided total cell counts, YO-PRO-1® (0.5 μM) assessed membrane integrity (dead/damaged cells), and fluorescein diacetate (FDA, 0.5 μM) indicated algae metabolic activity. Chlorophyll-a autofluorescence distinguished algal from bacterial populations. Standard calculations determined viability and mortality percentages for each population.

Chemical Analysis. Daily centrifuged supernatants were analyzed for NH_4^+, NO_2^-, and NO_3^- using colorimetric test kits (Merck KGaA), and acetic acid via enzymatic assays (Megazyme). pH was measured using a calibrated electrode. For more details look into Paper III of this thesis.

Pulsed Electric Field Treatment

PEF System Configuration. Treatments employed a continuous-flow system with transmission-line pulse generator delivering rectangular pulses. The treatment chamber housed plane-parallel stainless-steel electrodes separated by 2 mm gap within a polycarbonate structure designed for sterile operation.

Treatment Protocols. Two energy levels were investigated. Low-energy treatment (PEF 1: 40 kV/cm, 1 μs, 0.2 Hz, 4 J/mL) was designed to achieve selective algal inactivation while leaving bacterial populations partially intact. High-energy treatment (PEF 2: 40 kV/cm, 1 μs, 5 Hz, 100 J/mL) was applied to assess whether conditions targeting both cell types simultaneously would preclude selective extraction. Treatments were applied at three time points during co-culture development. Day 1: Early exponential phase (active bacterial proliferation). Day 3: Late exponential/early stationary transition (bacterial starvation onset). Day 7: Stationary phase (established community structure).

Aseptic Processing. Cell suspensions (100 mL) in sterile sealed flasks were connected via sterile tubing to the PEF system. Peristaltic pumping at 0.05 mL/s ensured uniform treatment. Samples were collected at 0-, 2-, and 24-hours post-treatment to capture immediate and delayed effects.

Protein Extraction Studies. For extraction experiments, co-cultures were concentrated to 5 g/L dry weight through centrifugation (10,000 × g, 5 minutes) prior to treatment. High-pressure homogenization (HPH) served as mechanical disruption control (EmulsiFlex-C3, 2000 bar, 5 passes with ice cooling).

Protein Extraction and Quality Analysis

Extraction Protocols. Following PEF or HPH treatment, samples underwent aqueous extraction with gentle stirring. Supernatants were separated through centrifugation (15,000 × g, 15 minutes), filtered (0.45 μm), and concentrated using ultrafiltration (10 kDa MWCO). Protein concentration was determined using Bradford assay with bovine serum albumin as standard. Extraction yield was calculated as protein recovered per cell dry weight.

SDS-PAGE Analysis. Protein profiles were characterized through sodium dodecyl sulfate polyacrylamide gel electrophoresis optimized for 10-250 kDa separation. Samples were mixed with Laemmli buffer containing β-mercaptoethanol, heated at 95°C for 5 minutes, and electrophoresed at constant voltage. Protein visualization employed Coomassie brilliant blue staining. Molecular weight determination utilized standard protein markers with GelAnalyzer software for band intensity quantification ($R^2 > 0.99$).

Antimicrobial Activity Testing. Algal extracts were assessed for antimicrobial properties through agar diffusion assays against *Delftia* sp. and *Escherichia coli*. Additionally, bacterial growth curves in diluted algal extracts were monitored spectrophotometrically.

Statistical Analysis

All experiments were conducted with ≥3 biological replicates. Viability and related quantitative datasets were evaluated using one-way ANOVA under defined conditions of interest, followed by Tukey's HSD for post-hoc comparisons. Data are presented as means ± SD, with statistical significance set at $p < 0.05$.

3.3 Results

3.3.1 Medium-Dependent Community Dynamics

The cultivation of *C. vulgaris* and *Delftia* sp. in different growth media revealed distinct interaction patterns and biomass production levels.

In TAP medium, which contains abundant organic carbon (17.49 mM acetic acid), bacterial populations showed rapid proliferation which reached peak cell concentration (1.5-2×10^8 cells/mL) within the first 24 hours of cultivation. During this period acetic acid was completely depleted from the medium. This swift resource consumption established nutrient-limiting conditions early in the cultivation period. Following nutrient depletion, bacterial proliferation ceased and prolonged starvation initiated gradual bacterial death, with mortality increasing from day 3 onwards. Under these nutrient-limiting conditions, algal populations exhibited notably slower growth compared to monoculture controls. By day 7, co-cultured algae achieved only ~ 4×10^7 cells/mL, while monocultures reached 7×10^7 cells/mL, representing a 40% reduction compared to monoculture concentrations (see Figs. 4A and B, at Paper III of this thesis).

Under BG-11 conditions (0.02 mM citrate), bacterial growth was minimal (<1 × 10^7 cells/mL) which followed fast decline in viability from day 3 (see Figs. 4C and D, at Paper III of this thesis). Algal cell concentrations in co-culture exceeded monoculture concentrations, with enhanced cell densities apparent from day 2 onward. BG-11 monocultures reached 4-6×10^7 cells/mL by day 7, while co-cultures achieved approximately 6×10^7 cells/mL.

Supplementing BG-11 medium with acetic acid (BG+AA) supported bacterial growth up to ~ 3-6 ×10^7 cells (see Figs. 4E and F, at Paper III of this thesis). After reaching this peak, the population gradually declined, consistent with patterns observed in TAP co-cultures. Co-cultured *C. vulgaris* achieved approximately 8×10^7 cells/mL by day 7, almost two-fold higher than BG+AA monocultures. In contrast, algal monocultures in BG+AA remained at concentrations similar to BG-11 monocultures (~4×10^7 cells/mL). Chemical analysis detected rapid acetic acid consumption in co-cultures (similar to TAP medium), while monocultures showed no detectable reduction over the cultivation period. Ammonium concentrations were higher in bacteria-containing samples compared to algal monocultures.

Based on these cultivation patterns, TAP medium was selected for subsequent PEF treatment experiments due to substantial bacterial populations enabling co-culture analysis under treatment conditions.

For more details regarding this subject see Paper III of this thesis.

3.3.2 Differential PEF Susceptibility Between Species

PEF treatments were applied at three time points (days 1, 3, and 7) using two energy protocols: low-energy treatment (4 J/mL, designated PEF 1) and high-energy treatment (100 J/mL, designated PEF 2). Flow cytometry with differential staining enabled simultaneous tracking of algal and bacterial populations within co-cultures.

C. vulgaris demonstrated remarkably consistent susceptibility to electrical treatment regardless of growth phase, medium composition, or bacterial presence (Fig. 23A, B, C). Low-energy treatment (PEF 1) achieved greater than 95% algal inactivation across all experimental conditions tested. High-energy treatment (PEF 2) produced complete algal inactivation in nearly all cases, with cell death (mortality) approaching 100% within hours of treatment.

Bacterial populations exhibited substantially more complex response patterns that varied with both growth phase and culture conditions (monoculture vs. co-culture).

In bacterial monocultures, day 1 treatments produced minimal inactivation (Fig. 23D). Low-energy treatment (PEF 1) achieved less than 20% mortality within 2 hours, while high-energy treatment (PEF 2) produced approximately 40-50% inactivation, with maximal effects observed only after 24-hour incubation.

Day 3 monoculture treatments revealed peak bacterial susceptibility (Fig. 23E). Both PEF 1 and PEF 2 achieved 70-80% bacterial inactivation within 2 hours, representing a 10-fold increase in susceptibility compared to day 1.

By day 7, bacterial monocultures showed high baseline mortality (>50%) even without PEF treatment due to prolonged nutrient depletion (Fig. 23F). PEF treatment at this time point produced minimal additional inactivation, as most bacteria were already dead before electrical treatment.

In co-cultures with algae, bacterial responses to PEF at days 1 and 3 followed similar patterns to monocultures, with day 3 showing maximum susceptibility (70-85% inactivation) (Figs. 23G, H). However, day 7 co-cultured bacteria displayed a distinct response in which early (2 h) PEF-induced inactivation was followed by full recovery and enhanced viability by 24 h compared to untreated controls (Fig. 23I).

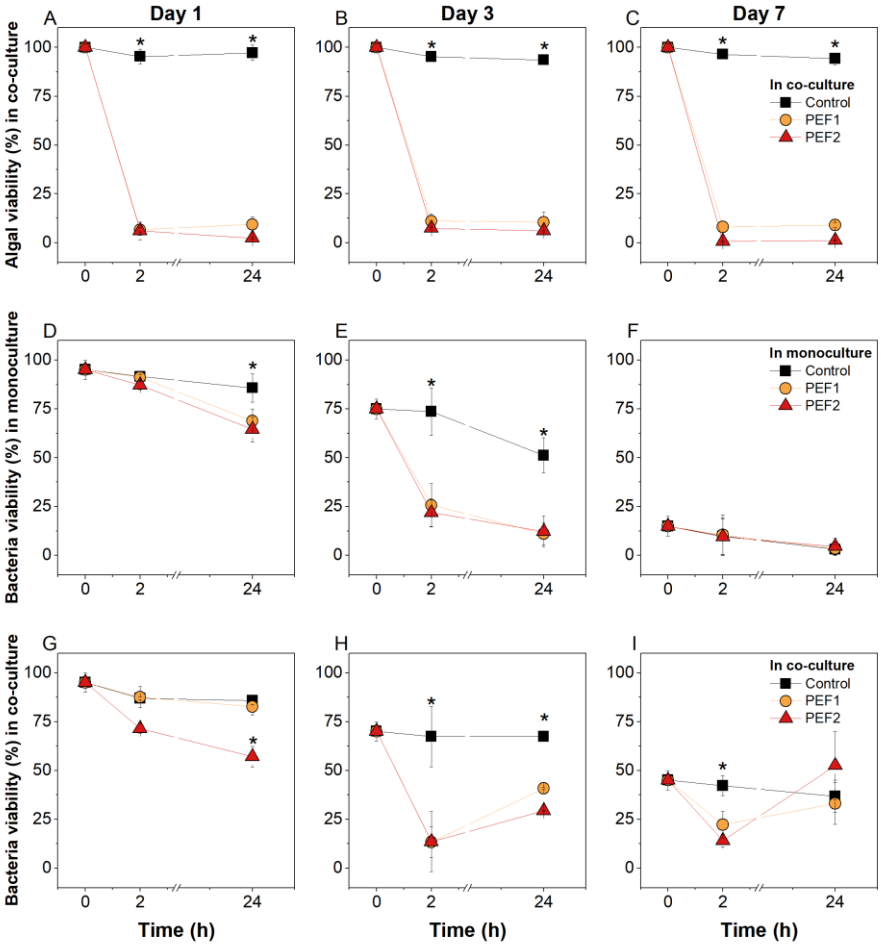

Figure 23 PEF induced changes in *C. vulgaris* algae (A, B, C) and *Delftia* sp. bacteria viability when the bacteria were cultivated alone (D, E, F) or in co-culture with algae (G, H, I). PEF treatments were performed on days 1 (A, D, G), 3 (B, E, H) and 7 (C, F, I) of cultivation, and viability changes were determined 2 h and 24 h PEF post-treatment. Untreated samples were used as a control. Adapted from Paper IV of this thesis.

3.3.3 Post-Treatment Community Dynamics

Extended monitoring revealed temporal changes in bacterial populations following PEF treatment of day 7 co-cultures. Beginning approximately 2 hours post-treatment, bacterial populations initiated rapid proliferation that continued for at least 24 hours (Fig. 24). By 24 hours post-treatment, PEF 2 samples contained up to 4-fold higher bacterial concentrations compared to untreated control cultures.

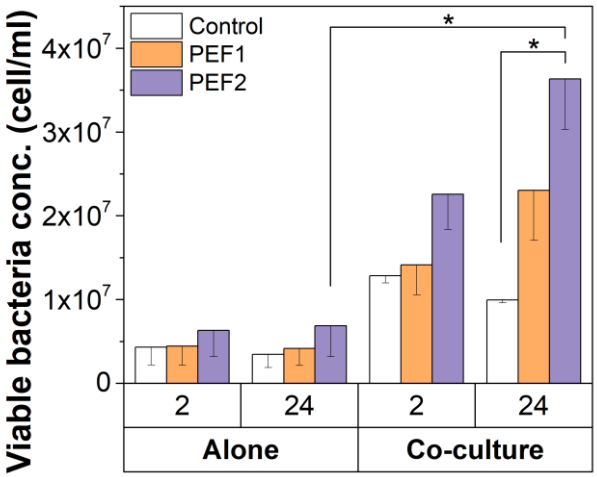

Figure 24 Viable *Delftia* sp. bacteria count 2 h and 24 h post PEF treatment on day 7. Bacteria were cultured alone or in co-culture with *C. vulgaris*. Adapted from Paper IV of this thesis.

This response was observed exclusively in co-culture samples, never appearing in bacterial monocultures treated under identical conditions. The magnitude of bacterial proliferation showed direct correlation with applied electrical energy, with PEF 2 treatments consistently producing greater proliferation than PEF 1.

3.3.4 Nutrient Release from Disrupted Algal Cells

Agar diffusion assays using PEF-treated algal monoculture lysates showed no inhibition zones against *Delftia* sp. (Fig. 25) or control *E. coli* strains (see Supp. Fig. 2, at Paper IV of this thesis), indicating absence of antimicrobial compounds.

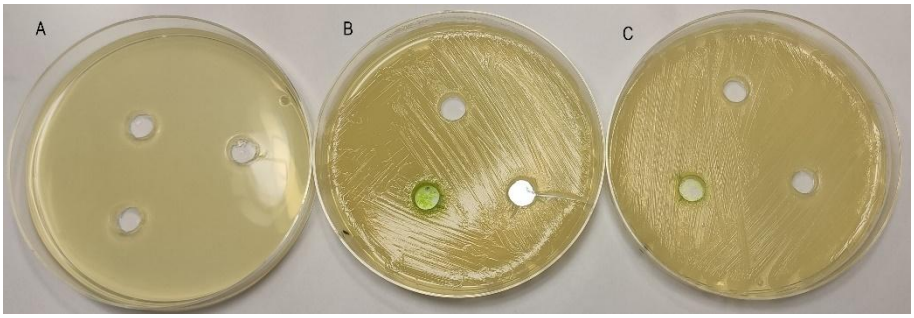

Figure 25 Antibacterial effect of *C. vulgaris* PEF1, PEF2 and HPH extract on *Delftia* sp. First Petri dish without bacteria and algal extract (A). Other plates with bacteria and wells with extracts from cultured algae alone (B) or in combination with bacteria (C). Adapted from Paper IV of this thesis.

Spectrophotometric monitoring of *Delftia* sp. freshly inoculated into PEF-treated algal monoculture lysates showed growth kinetics comparable to those in fresh TAP (Fig. 26).

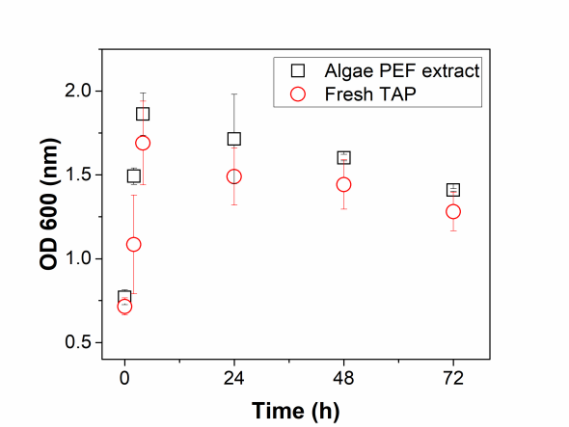

Figure 26 *Delftia* sp. optical density changes during cultivation in *C. vulgaris* PEF treated extract and fresh TAP medium. Adapted from Paper IV of this thesis.

3.3.5 Selective Algal Protein Extraction

Given the demonstrated bacterial proliferation following PEF treatment of co-cultures, the potential for bacterial protein contamination in algal extracts required systematic investigation.

PEF treatment achieved protein extraction yields approximately 25% of algal dry weight (Fig. 27). Yields showed non-significant variations across different conditions: algal monocultures versus co-cultures, and PEF 1 versus PEF 2 energy levels. HPH extraction exceeded 50% of algal dry weight, marginally higher than PEF treatment.

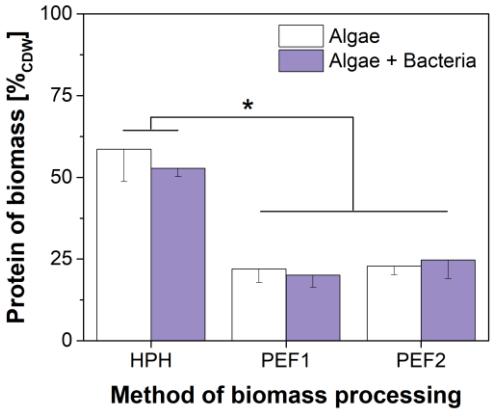

Figure 27 HPH and PEF facilitated protein extraction from *C. vulgaris* biomass cultivated alone or in co-culture with *Delftia* sp. bacteria. Adapted from Paper IV of this thesis.

SDS-PAGE analysis revealed differences in protein composition between treatment methods and culture conditions (Fig. 28). PEF-treated algal monocultures established the characteristic algal protein pattern, with major bands distributed across the 10-250 kDa range. PEF-treated co-culture samples displayed protein patterns similar to monoculture samples across all energy levels tested.

In contrast, HPH-treated co-culture samples revealed a novel protein band at approximately 27 kDa (molecular weight determination $R^2 = 0.992$) that was absent from all other sample types. This band appeared consistently across multiple experimental replicates of HPH-treated co-cultures but never appeared in HPH-treated monocultures or any PEF-treated samples.

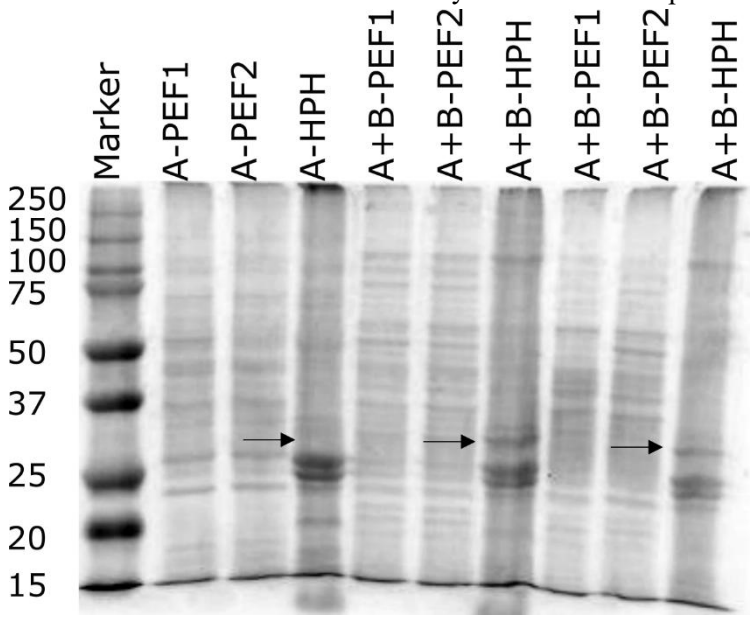

Figure 28 Visualization of protein extracts obtained by HPH and PEF treatment by SDS-PAGE. Samples obtained from concentrated *C. vulgaris* biomass (5 g/l) cultivated alone (A) or co-cultivated with bacteria (A+B). Adapted from Paper IV of this thesis.

3.4 Discussion

The application of PEF to microalgae-bacteria co-cultures revealed effects that extend beyond anticipated outcomes for single-population treatments. Algal responses were robust and reproducible, whereas bacterial fate depended strongly on cultivation stage and, critically, on whether algal biomass was present. This positions PEF as more than a disruption technique: in mixed systems it can act as a trigger that shifts community trajectories (extraction vs. bioconversion), depending on timing and post-treatment handling.

PEF treatment achieved algal inactivation exceeding 95% across all tested conditions, even at relatively low specific energy input (4 J/mL). This high inactivation persisted at 24 h, indicating that outcomes are shaped not only by immediate membrane permeabilization but also by delayed post-treatment processes during incubation. This effectiveness remained consistent regardless of bacterial presence, with protein release patterns stabilizing at approximately 25% of cell dry weight. These values are comparable to those reported in prior monoculture studies [16,21,92]. The sustained inactivation observed 24 h may be consistent with release of cell death inducing factors (CDIF) by PEF-treated algae, as demonstrated by Krust et al. (2022) [21]. However, this should be treated as a candidate mechanism rather than a settled explanation in the present system. This framing aligns with the assumption that selectivity in co-culture is governed not only by field parameters but by state-dependent dynamics after the pulse.

Bacterial susceptibility to PEF, in contrast, proved strongly growth-phase dependent. Maximum inactivation (70-80%) assessed by flow cytometry occurred on day 3 of cultivation, coinciding with starvation/long-term stationary conditions in *Delftia* sp. following exhaustion of available organic carbon (see Paper III of this thesis). During active growth on day 1, bacterial inactivation remained below 20% at the lower energy setting and increased only partially at higher energy input. This growth-phase dependence supports the hypothesis posed in the introduction: physiological state, not cell architecture alone, governs bacterial susceptibility to PEF in co-cultures. The pattern contradicts commonly reported trends for model bacteria (e.g., exponential-phase *E. coli* often showing higher vulnerability than stationary-phase cells under comparable fields), implying a species-by-medium-by-state interaction rather than a universal rule. In TAP-grown *Delftia*, starvation-associated remodeling could plausibly reduce repair capacity, alter envelope structure, and shift energy metabolism in ways that amplify electrical injury; alternatively, cell-envelope architecture specific to this isolate may dominate. Resolving these alternatives requires targeted characterization (membrane composition, stress-response proteins, and metabolic status across phases), because the observation is central to the chapter's "state vs. size" argument.

The most significant co-culture-specific outcome was the unexpected bacterial rebound observed at late cultivation, where viable *Delftia* sp. populations increased approximately four-fold within 24 h following PEF treatment (day 7 condition). Importantly, this rebound occurred in co-cultures but not in bacterial monocultures, arguing against a direct "stimulation" effect of PEF on bacteria and instead pointing to a resource-context explanation created by algal injury. The temporal coupling between algal disruption and

bacterial growth strongly suggests that damaged algal biomass becomes a substrate pool. In other words, PEF can convert part of the algal population into bioavailable carbon and nitrogen for the bacterial population, without external substrate addition. This interpretation is supported by the lysate-growth assays (bacterial growth in algal lysate) and the absence of inhibition in antimicrobial screening, which together indicate that the post-PEF extracellular environment is permissive for bacterial regrowth rather than suppressive.

Delftia sp. regrowth mechanism also clarifies why "selective treatment" should be defined carefully. The results support selective disruption/extraction rather than selective sterilization. This differential response between algae and bacteria has precedent in mixed-population studies. Simonis et al. (2019) achieved greater than 3 $\log_{10}$ reduction of *Saccharomyces cerevisiae* while reducing *Lactobacillus* populations by only 1-2 $\log_{10}$ in acid whey [40], and Aronsson et al. (2001) demonstrated higher yeast sensitivity compared to bacterial species in food matrices [93]. Such selectivity typically reflects fundamental biological differences in cell wall structure, membrane composition, and cellular organization between prokaryotic and eukaryotic cells. In the present system, algal cells underwent permeabilization sufficient to release intracellular proteins into the surrounding medium. Whereas bacterial cells subjected to identical fields largely retained envelope integrity, preventing substantial protein leakage even when a fraction of cells lost viability. This distinction is reflected in protein analysis. SDS-PAGE profiles from PEF-treated co-cultures matched algae-only extracts across the dominant molecular-weight range, and no additional bacterial-associated bands were detected under these conditions. By contrast, HPH treatment of the same co-culture produced a distinct band at ~27 kDa that was absent from algae-only HPH extracts and absent from PEF extracts. While this band is consistent with bacterial protein release during non-selective mechanical disruption, biochemical identification (e.g., LC-MS/MS) is required before assigning origin. By the operational definition established in the introduction, algal protein recovery without bacterial protein contamination, PEF achieved selectivity under the tested conditions, whereas HPH did not.

The selective disruption demonstrated here enables two fundamentally different processing strategies. First, in cascade bioprocessing applications, bacterial proliferation is not a contamination problem but rather the intended outcome. PEF-lysed algal material provides growth substrate for bacterial production of secondary metabolites such as biopolymers, pigments, and specialty chemicals without requiring external carbon or nitrogen supplementation. This approach could integrate algal cultivation for CO_2

capture with subsequent bacterial production stages, where PEF-treated algal lysate serves as growth medium for value-added compound synthesis. The strategy circumvents the substantial costs associated with maintaining axenic algal cultures, which industry reports estimate can account for significant fractions of production expenses [37]. Similar substrate utilization patterns have been demonstrated: Ricós-Muñoz et al. (2023) observed enhanced *Lactobacillus rhamnosus* growth in media supplemented with PEF-treated *Chlorella* and *Spirulina* extracts [94]. While established wastewater treatment systems operate on this sequential principle, where algae capture CO_2 and nutrients before bacteria process the algal biomass for products [95,96]. These observations collectively reposition PEF from a straightforward extraction technology into a tool for deliberate restructuring of microbial community dynamics, where selective population disruption creates conditions favoring targeted organisms. Here, extended contact between bacteria and lysed algae is desirable, and axenic cultivation becomes unnecessary.

The second approach emphasizes PEF as a viable method for treating co-cultured algae, which are cheaper and easier to maintain than axenic monocultures, while achieving extract purity equivalent to monoculture standards. SDS-PAGE analysis confirmed that protein profiles from PEF-treated co-cultures were identical to those from algae-only cultures, showing no bacterial protein contamination despite viable *Delftia* sp. presence throughout treatment. This capability addresses a major industrial constraint: axenic cultivation systems require substantial capital investment and operational costs [37], yet PEF treatment of non-axenic cultures produces extracts meeting the same quality standards. HPH treatment cannot ensure this equivalence. Mechanical disruption releases bacterial proteins during processing itself, producing the 27 kDa contamination band observed in co-cultured samples. However, maintaining extract purity with PEF requires one critical step: rapid bacterial elimination or alternative methods that prevent bacterial regrowth and secondary metabolite production. The bacterial proliferation observed on day 7 demonstrates that delayed separation allows bacteria to metabolize released algal components, leading to protein degradation, metabolite accumulation, and compromised product quality. These outcomes are particularly problematic for food and pharmaceutical applications where purity and safety standards are strict [97,98]. Industrial implementation therefore demands immediate biomass separation (within hours), temperature control during processing, or antimicrobial preservation methods that maintain extract integrity without introducing chemical contaminants.

Several limitations constrain interpretation. The mechanistic basis of *Delftia* susceptibility during starvation remains unresolved and should be tested by envelope and stress-physiology profiling across growth phases. The post-PEF metabolite environment driving bacterial regrowth was inferred functionally but not chemically mapped; quantifying dissolved organic carbon and key metabolite classes would convert the rebound interpretation from plausible to causal. The ~27 kDa band observed after HPH, though consistent with bacterial origin, requires biochemical confirmation. Finally, only one algal strain and one bacterial isolate were tested; broader validation across bacteria commonly present in non-axenic algal cultures is required to generalize extraction-selectivity claims.

3.5 Key Findings

Medium composition determined community dynamics between *C. vulgaris* and *Delftia* sp. TAP medium, containing abundant organic carbon (17.49 mM acetic acid), supported rapid bacterial proliferation reaching 1.5-2×10^8 cells/mL within the first days. BG-11 and BG+AA remained algae-dominant with minimal bacterial growth (<1×10^7 cells/mL). TAP was therefore selected for PEF selectivity testing.

PEF treatment revealed distinct susceptibility patterns between species. *C. vulgaris* demonstrated consistent susceptibility regardless of growth phase, medium composition, or bacterial presence: low-energy treatment (40 kV/cm, 1 μs, 4 J/mL) achieved >95% inactivation, high-energy treatment (40 kV/cm, 1 μs, 100 J/mL) exceeded 99% inactivation across all conditions. Bacterial responses differed fundamentally. *Delftia* sp. susceptibility depended strongly on growth phase: day 1 (exponential growth) showed minimal inactivation, day 3 (starvation) reached maximum susceptibility (70-80% inactivation), and day 7 showed high baseline mortality masking treatment effects.

Post-treatment bacterial dynamics revealed a co-culture-specific outcome. At day 7, surviving bacteria rebounded approximately four-fold within 24 h, but only in co-cultures. This regrowth never occurred in bacterial monocultures under identical treatment. Antibacterial assays showed no inhibition zones against *Delftia* sp. or *E. coli* from PEF-treated algal lysates, and bacterial growth kinetics in algal lysates matched fresh TAP medium. These results confirm that PEF-released algal substrates support bacterial proliferation rather than inhibit it.

Protein extraction analysis supported selective recovery from co-cultures. PEF achieved protein yields of approximately 25% of algal dry weight, comparable to monoculture reports. SDS-PAGE profiles from PEF-treated co-cultures were indistinguishable from algal monocultures. In contrast, HPH-treated co-cultures revealed an additional ~27 kDa band absent from all other samples. This band is consistent with bacterial protein contamination, though biochemical confirmation is required.

CONCLUSIONS

1. PEF treatment (19 kV/cm, 10 μs, 80 J/mL) shortened chlorophyll fluorescence lifetime at 685 nm in *C. vulgaris* from 1.71 ns to 0.83 ns without statistically significant absorption changes, indicating enhanced non-radiative energy dissipation rather than pigment degradation.
2. Photosynthetic responses depended on pulse duration: microsecond pulses reduced fluorescence lifetime by 51%, nanosecond pulses (90 and 60 ns) at equivalent energy by 18%, and 10 ns pulses at higher field strength (86 kV/cm) produced minimal effects despite equivalent estimated thermal input (~17°C).
3. Photosynthetic alterations and membrane permeabilization showed tight coupling under microsecond conditions: 51% fluorescence lifetime reduction coincided with ~70% permeabilization. Nanosecond pulses produced weaker but differently distributed effects (18% lifetime reduction, 10.5% permeabilization), with fluorescence changes exceeding permeabilization. Direct intracellular targeting independent of plasma membrane permeabilization could not be confirmed within the parameters tested.
4. GAD plasma induced voltage-dependent medium modifications in BG-11: at 250 V, temperature reached 54°C, pH decreased from ~7.5 to ~7.0, conductivity rose from ~1.85 mS/cm to 3.34 mS/cm, and reactive species accumulated (NO_2^- 1.67 mM, NO_3^- 28.9 mM, H_2O_2 17.4 mM). Direct biological effects on *C. vulgaris* were observed only at high voltage (250 V): ~25% permeabilization and metabolic inactivation.
5. Plasma pretreatment reshaped biological responses to fixed PEF parameters (25 kV/cm, 7 μs, 10 pulses) in a voltage-dependent manner. Low-voltage pretreatment (130 V) yielded a conventional PEF phenotype with high macromolecule release. High-voltage pretreatment (250 V) shifted cells to a permeable-but-retentive phenotype, suppressing release despite comparable permeabilization. PEF alone increased caspase 3-like activity (~250% of control), but high-voltage plasma reduced it below control, consistent with a non-classical, caspase-independent cell-death pathway.
6. Control protocols (thermal pretreatment, plasma-activated supernatant, conductivity-matched exchange) failed to reproduce the high-voltage phenotype, establishing that direct plasma-cell interaction is required for the voltage-dependent response divergence.

7. Medium composition determined community structure: TAP supported substantial bacterial populations (1.5-2×10^8 cells/mL), while BG-11 and BG+AA remained algae-dominant. TAP provided conditions for evaluating PEF selectivity in mixed cultures.
8. Species-specific PEF susceptibility differed fundamentally. *C. vulgaris* inactivation exceeded 95% at low energy (40 kV/cm, 1 μs, 4 J/mL) and 99% at high energy (40 kV/cm, 1 μs, 100 J/mL), regardless of growth phase or culture conditions. *Delftia* sp. susceptibility was growth phase-dependent: minimal at day 1, maximal at day 3 (70-80%), with post-treatment regrowth at day 7 in co-cultures only.
9. PEF treatment enabled selective algal protein extraction from co-cultures. Protein yields reached ~25% of dry weight with SDS-PAGE profiles indistinguishable from monocultures. HPH-treated co-cultures showed an additional ~27 kDa band, possibly indicating bacterial protein contamination, though this requires biochemical confirmation.

Statements for defense

1. PEF shortens chlorophyll fluorescence lifetime at 685 nm in *C. vulgaris* in a pulse duration-dependent manner without altering absorption spectra, indicating that photosynthetic apparatus impairment arises from enhanced non-radiative energy dissipation rather than pigment degradation.
2. Sequential plasma pretreatment (250 V power supply) followed by PEF decouples membrane permeabilization from macromolecule release, suppresses caspase-like activity, and induces a non-apoptotic, non-necrotic cell-death phenotype that differs from classical PEF-induced programmed cell death and requires direct plasma exposure.
3. PEF treatment (40 kV/cm, 1 μs, 4-100 J/mL) produces consistent algal inactivation (>95%) in *C. vulgaris* while *Delftia* sp. susceptibility is growth phase-dependent, enabling selective extraction of algal proteins from co-cultures without additional protein bands observed with mechanical disruption.

REFERENCES

[1] T. Kotnik, L. Rems, M. Tarek, D. Miklavčič, Membrane Electroporation and Electropermeabilization: Mechanisms and Models, Annual Review of Biophysics 48 (2019) 63–91. https://doi.org/10.1146/annurev-biophys-052118-115451.

[2] J. Teissié, M.P. Rols, An experimental evaluation of the critical potential difference inducing cell membrane electropermeabilization, Biophysical Journal 65 (1993) 409–413. https://doi.org/10.1016/S0006-3495(93)81052-X.

[3] L. Rems, X. Tang, F. Zhao, S. Pérez-Conesa, I. Testa, L. Delemotte, Identification of electroporation sites in the complex lipid organization of the plasma membrane, eLife 11 (2022) e74773. https://doi.org/10.7554/eLife.74773.

[4] M. Kandušer, D. Miklavčič, Electroporation in Biological Cell and Tissue: An Overview, in: Electrotechnologies for Extraction from Food Plants and Biomaterials, Springer, New York, NY, 2008: pp. 1–37. https://doi.org/10.1007/978-0-387-79374-0_1.

[5] J. Raso, W. Frey, G. Ferrari, G. Pataro, D. Knorr, J. Teissie, D. Miklavčič, Recommendations guidelines on the key information to be reported in studies of application of PEF technology in food and biotechnological processes, Innovative Food Science & Emerging Technologies 37 (2016) 312–321. https://doi.org/10.1016/j.ifset.2016.08.003.

[6] U. Probst, I. Fuhrmann, L. Beyer, P. Wiggermann, Electrochemotherapy as a New Modality in Interventional Oncology: A Review, Technol Cancer Res Treat 17 (2018) 1533033818785329. https://doi.org/10.1177/1533033818785329.

[7] V.Y. Reddy, E.P. Gerstenfeld, A. Natale, W. Whang, F.A. Cuoco, C. Patel, S.E. Mountantonakis, D.N. Gibson, J.D. Harding, C.R. Ellis, K.A. Ellenbogen, D.B. DeLurgio, J. Osorio, A.B. Achyutha, C.W. Schneider, A.S. Mugglin, E.M. Albrecht, K.M. Stein, J.W. Lehmann, M. Mansour, Pulsed Field or Conventional Thermal Ablation for Paroxysmal Atrial Fibrillation, New England Journal of Medicine 389 (2023) 1660–1671. https://doi.org/10.1056/NEJMoa2307291.

[8] T. Kotnik, W. Frey, M. Sack, S. Haberl Meglič, M. Peterka, D. Miklavčič, Electroporation-based applications in biotechnology, Trends in Biotechnology 33 (2015) 480–488. https://doi.org/10.1016/j.tibtech.2015.06.002.

[9] C. Delso, J.M. Martínez, G. Cebrián, S. Condón, J. Raso, I. Álvarez, Microbial Inactivation by Pulsed Electric Fields, in: J. Raso, V. Heinz, I. Alvarez, S. Toepfl (Eds.), Pulsed Electric Fields Technology for the Food Industry: Fundamentals and Applications, Springer International Publishing, Cham, 2022: pp. 169–207. https://doi.org/10.1007/978-3-030-70586-2_5.

[10] G. Ghoshal, Comprehensive review on pulsed electric field in food preservation: gaps in current studies for potential future research, Heliyon 9 (2023) e17532. https://doi.org/10.1016/j.heliyon.2023.e17532.
[11] J.M. Martínez, C. Delso, I. Álvarez, J. Raso, Pulsed electric field-assisted extraction of valuable compounds from microorganisms, Compr Rev Food Sci Food Saf 19 (2020) 530–552. https://doi.org/10.1111/1541-4337.12512.
[12] M.A. Alam, J.L. Xu, Z. Wang, Microalgae biotechnology for food, health and high value products, 2020. https://doi.org/10.1007/978-981-15-0169-2.
[13] L. Buchmann, I. Brändle, I. Haberkorn, M. Hiestand, A. Mathys, Pulsed electric field based cyclic protein extraction of microalgae towards closed-loop biorefinery concepts, Bioresource Technology 291 (2019) 121870. https://doi.org/10.1016/j.biortech.2019.121870.
[14] P.R. Postma, G. Pataro, M. Capitoli, M.J. Barbosa, R.H. Wijffels, M.H.M. Eppink, G. Olivieri, G. Ferrari, Selective extraction of intracellular components from the microalga Chlorella vulgaris by combined pulsed electric field–temperature treatment, Bioresource Technology 203 (2016) 80–88. https://doi.org/10.1016/j.biortech.2015.12.012.
[15] M. Coustets, V. Joubert-Durigneux, J. Hérault, B. Schoefs, V. Blanckaert, J.-P. Garnier, J. Teissié, Optimization of protein electroextraction from microalgae by a flow process, Bioelectrochemistry 103 (2015) 74–81. https://doi.org/10.1016/j.bioelechem.2014.08.022.
[16] L. Buchmann, L. Böcker, W. Frey, I. Haberkorn, M. Nyffeler, A. Mathys, Energy input assessment for nanosecond pulsed electric field processing and its application in a case study with *Chlorella vulgaris*, Innovative Food Science & Emerging Technologies 47 (2018) 445–453. https://doi.org/10.1016/j.ifset.2018.04.013.
[17] I. Papachristou, N. Nazarova, R. Wüstner, R. Lina, W. Frey, A. Silve, Biphasic lipid extraction from microalgae after PEF-treatment reduces the energy demand of the downstream process, Biotechnology for Biofuels and Bioproducts 18 (2025) 12. https://doi.org/10.1186/s13068-025-02608-7.
[18] R. Straessner, M. Nikolausz, A. Silve, N. Nazarova, R. Wuestner, I. Papachristou, S. Akaberi, K. Leber, G. Mueller, W. Frey, Holistic exploitation of pulsed electric field (PEF)-treated and lipid extracted microalgae Auxenochlorella protothecoides, utilizing anaerobic digestion (AD), Algal Research (2022) 102950. https://doi.org/10.1016/j.algal.2022.102950.
[19] S. Akaberi, D. Krust, G. Müller, W. Frey, C. Gusbeth, Impact of incubation conditions on protein and C-Phycocyanin recovery from Arthrospira platensis post- pulsed electric field treatment, Bioresource

Technology 306 (2020) 123099. https://doi.org/10.1016/J.BIORTECH.2020.123099.
[20] D. Scherer, D. Krust, W. Frey, G. Mueller, P. Nick, C. Gusbeth, Pulsed electric field (PEF)-assisted protein recovery from Chlorella vulgaris is mediated by an enzymatic process after cell death, Algal Research 41 (2019) 101536. https://doi.org/10.1016/J.ALGAL.2019.101536.
[21] D. Krust, C. Gusbeth, A.S.K. Müller, D. Scherer, G. Müller, W. Frey, P. Nick, Biological signalling supports biotechnology – Pulsed electric fields extract a cell-death inducing factor from Chlorella vulgaris, Bioelectrochemistry 143 (2022) 107991. https://doi.org/10.1016/J.BIOELECHEM.2021.107991.
[22] C. Safi, B. Zebib, O. Merah, P.Y. Pontalier, C. Vaca-Garcia, Morphology, composition, production, processing and applications of Chlorella vulgaris: A review, Renewable and Sustainable Energy Reviews 35 (2014) 265–278. https://doi.org/10.1016/j.rser.2014.04.007.
[23] S. Bensalem, D. Pareau, B. Cinquin, O. Français, B. Le Pioufle, F. Lopes, Impact of pulsed electric fields and mechanical compressions on the permeability and structure of Chlamydomonas reinhardtii cells, Sci Rep 10 (2020) 2668. https://doi.org/10.1038/s41598-020-59404-6.
[24] H. Kirchhoff, Chloroplast ultrastructure in plants, New Phytologist 223 (2019) 565–574. https://doi.org/10.1111/nph.15730.
[25] J. Widzgowski, A. Vogel, L. Altrogge, J. Pfaff, H. Schoof, B. Usadel, L. Nedbal, U. Schurr, C. Pfaff, High light induces species specific changes in the membrane lipid composition of Chlorella, Biochemical Journal 477 (2020) 2543–2559. https://doi.org/10.1042/BCJ20200160.
[26] J. Hryc, R. Szczelina, M. Markiewicz, M. Pasenkiewicz-Gierula, Lipid/water interface of galactolipid bilayers in different lyotropic liquid-crystalline phases, Front. Mol. Biosci. 9 (2022). https://doi.org/10.3389/fmolb.2022.958537.
[27] M.D.L. Trinh, S. Masuda, Chloroplast pH Homeostasis for the Regulation of Photosynthesis, Frontiers in Plant Science 13 (2022). https://www.frontiersin.org/articles/10.3389/fpls.2022.919896 (accessed March 31, 2023).
[28] R. Straessner, C. Eing, M. Goettel, C. Gusbeth, W. Frey, Monitoring of Pulsed Electric Field-Induced Abiotic Stress on Microalgae by Chlorophyll Fluorescence Diagnostic, IEEE Trans. Plasma Sci. 41 (2013) 2951–2958. https://doi.org/10.1109/TPS.2013.2281082.
[29] J. Sheng, R. Vannela, B.E. Rittmann, Evaluation of Cell-Disruption Effects of Pulsed-Electric-Field Treatment of Synechocystis PCC 6803, Environ. Sci. Technol. 45 (2011) 3795–3802. https://doi.org/10.1021/es103339x.
[30] F. Bai, C. Gusbeth, W. Frey, P. Nick, Nanosecond pulsed electric fields modulate the expression of the astaxanthin biosynthesis genes psy, crtR-b and bkt 1 in Haematococcus pluvialis, Sci Rep 10 (2020) 15508. https://doi.org/10.1038/s41598-020-72479-5.

[31] K. Červinková, P. Vahalová, M. Poplová, T. Zakar, D. Havelka, M. Paidar, V. Kolivoška, M. Cifra, Modulation of pulsed electric field induced oxidative processes in protein solutions by pro- and antioxidants sensed by biochemiluminescence, Sci Rep 14 (2024) 22649. https://doi.org/10.1038/s41598-024-71626-6.
[32] L. Rems, M. Viano, M.A. Kasimova, D. Miklavčič, M. Tarek, The contribution of lipid peroxidation to membrane permeability in electropermeabilization: A molecular dynamics study, Bioelectrochemistry 125 (2019) 46–57. https://doi.org/10.1016/j.bioelechem.2018.07.018.
[33] D. Wiczew, N. Szulc, M. Tarek, Molecular dynamics simulations of the effects of lipid oxidation on the permeability of cell membranes, Bioelectrochemistry 141 (2021) 107869. https://doi.org/10.1016/j.bioelechem.2021.107869.
[34] K. Balantič, V.U. Weiss, E. Pittenauer, D. Miklavčič, P. Kramar, The role of lipid oxidation on electrical properties of planar lipid bilayers and its importance for understanding electroporation, Bioelectrochemistry 153 (2023) 108498. https://doi.org/10.1016/j.bioelechem.2023.108498.
[35] C.M. Wolff, J.F. Kolb, K.-D. Weltmann, T. von Woedtke, S. Bekeschus, Combination Treatment with Cold Physical Plasma and Pulsed Electric Fields Augments ROS Production and Cytotoxicity in Lymphoma, Cancers (Basel) 12 (2020) 845. https://doi.org/10.3390/cancers12040845.
[36] A. Steuer, C.M. Wolff, T. Von Woedtke, K.-D. Weltmann, J.F. Kolb, Cell stimulation versus cell death induced by sequential treatments with pulsed electric fields and cold atmospheric pressure plasma, PLoS ONE 13 (2018) e0204916. https://doi.org/10.1371/journal.pone.0204916.
[37] T.P. Lam, T.-M. Lee, C.-Y. Chen, J.-S. Chang, Strategies to control biological contaminants during microalgal cultivation in open ponds, Bioresource Technology 252 (2018) 180–187. https://doi.org/10.1016/j.biortech.2017.12.088.
[38] H.P. Schwan, Electrical Properties of Tissue and Cell Suspensions, in: Advances in Biological and Medical Physics, Elsevier, 1957: pp. 147–209. https://doi.org/10.1016/B978-1-4832-3111-2.50008-0.
[39] D. Rego, L.M. Redondo, V. Geraldes, L. Costa, J. Navalho, M.T. Pereira, Control of predators in industrial scale microalgae cultures with Pulsed Electric Fields, Bioelectrochemistry 103 (2015) 60–64. https://doi.org/10.1016/j.bioelechem.2014.08.004.
[40] P. Simonis, S. Kersulis, V. Stankevich, K. Sinkevic, K. Striguniene, G. Ragoza, A. Stirke, Pulsed electric field effects on inactivation of microorganisms in acid whey, International Journal of Food Microbiology 291 (2019) 128–134. https://doi.org/10.1016/j.ijfoodmicro.2018.11.024.
[41] T. Kotnik, D. Miklavčič, T. Slivnik, Time course of transmembrane voltage induced by time-varying electric fields—a method for

theoretical analysis and its application, Bioelectrochemistry and Bioenergetics 45 (1998) 3–16. https://doi.org/10.1016/S0302-4598(97)00093-7.
[42] J. Teissie, Electropermeabilization of the Cell Membrane, in: S. Li, J. Cutrera, R. Heller, J. Teissie (Eds.), Electroporation Protocols, Springer New York, New York, NY, 2014: pp. 25–46. https://doi.org/10.1007/978-1-4614-9632-8_2.
[43] P.T. Vernier, Z.A. Levine, Y.-H. Wu, V. Joubert, M.J. Ziegler, L.M. Mir, D.P. Tieleman, Electroporating Fields Target Oxidatively Damaged Areas in the Cell Membrane, PLOS ONE 4 (2009) e7966. https://doi.org/10.1371/journal.pone.0007966.
[44] S.J. Beebe, K.H. Schoenbach, Nanosecond Pulsed Electric Fields: A New Stimulus to Activate Intracellular Signaling, J Biomed Biotechnol 2005 (2005) 297–300. https://doi.org/10.1155/JBB.2005.297.
[45] I. Haberkorn, L. Siegenthaler, L. Buchmann, L. Neutsch, A. Mathys, Enhancing single-cell bioconversion efficiency by harnessing nanosecond pulsed electric field processing, Biotechnology Advances 53 (2021) 107780. https://doi.org/10.1016/j.biotechadv.2021.107780.
[46] K. Asadipour, M.B. Hani, L. Potter, B.L. Ruedlinger, N. Lai, S.J. Beebe, Nanosecond Pulsed Electric Fields (nsPEFs) Modulate Electron Transport in the Plasma Membrane and the Mitochondria, Bioelectrochemistry 155 (2024) 108568. https://doi.org/10.1016/j.bioelechem.2023.108568.
[47] P. Simonis, S. Kersulis, V. Stankevich, V. Kaseta, E. Lastauskiene, A. Stirke, Caspase dependent apoptosis induced in yeast cells by nanosecond pulsed electric fields, Bioelectrochemistry 115 (2017) 19–25. https://doi.org/10.1016/j.bioelechem.2017.01.005.
[48] B. Fuks, F. Homblé, Permeability and electrical properties of planar lipid membranes from thylakoid lipids., Biophys J 66 (1994) 1404–1414. https://doi.org/10.1016/S0006-3495(94)80931-2.
[49] T. Maurício, D. Couto, D. Lopes, T. Conde, R. Pais, J. Batista, T. Melo, M. Pinho, A.S.P. Moreira, M. Trovão, A. Barros, H. Cardoso, J. Silva, P. Domingues, M.R. Domingues, Differences and Similarities in Lipid Composition, Nutritional Value, and Bioactive Potential of Four Edible Chlorella vulgaris Strains, Foods 12 (2023) 1625. https://doi.org/10.3390/foods12081625.
[50] T. Takeshita, S. Ota, T. Yamazaki, A. Hirata, V. Zachleder, S. Kawano, Starch and lipid accumulation in eight strains of six *Chlorella* species under comparatively high light intensity and aeration culture conditions, Bioresource Technology 158 (2014) 127–134. https://doi.org/10.1016/j.biortech.2014.01.135.
[51] J.F. Allen, J. Forsberg, Molecular recognition in thylakoid structure and function, Trends Plant Sci 6 (2001) 317–326. https://doi.org/10.1016/s1360-1385(01)02010-6.

[52] G.H. Krause, E. Weis, Chlorophyll Fluorescence and Photosynthesis: The Basics, Annual Review of Plant Biology 42 (1991) 313–349. https://doi.org/10.1146/annurev.pp.42.060191.001525.
[53] A.M. Chorvatova, M. Uherek, A. Mateasik, D. Chorvat, Time-resolved endogenous chlorophyll fluorescence sensitivity to pH: study on Chlorella sp. algae, Methods Appl. Fluoresc. 8 (2020) 024007. https://doi.org/10.1088/2050-6120/ab77f4.
[54] V. Stankevic, P. Simonis, N. Zurauskiene, A. Stirke, A. Dervinis, V. Bleizgys, S. Kersulis, S. Balevicius, Compact Square-Wave Pulse Electroporator with Controlled Electroporation Efficiency and Cell Viability, Symmetry 12 (2020) 412. https://doi.org/10.3390/sym12030412.
[55] J.R. Lakowicz, B.R. Masters, Principles of Fluorescence Spectroscopy, Third Edition, J. Biomed. Opt. 13 (2008) 029901. https://doi.org/10.1117/1.2904580.
[56] T. Mirkovic, E.E. Ostroumov, J.M. Anna, R. van Grondelle, Govindjee, G.D. Scholes, Light Absorption and Energy Transfer in the Antenna Complexes of Photosynthetic Organisms, Chem. Rev. 117 (2017) 249–293. https://doi.org/10.1021/acs.chemrev.6b00002.
[57] G.C. Papageorgiou, Govindjee, eds., Chlorophyll a Fluorescence: A Signature of Photosynthesis, Springer Netherlands, Dordrecht, 2004. https://doi.org/10.1007/978-1-4020-3218-9.
[58] J.J. Lamb, G. Røkke, M.F. Hohmann-Marriott, Chlorophyll fluorescence emission spectroscopy of oxygenic organisms at 77 K, Photosynt. 56 (2018) 105–124. https://doi.org/10.1007/s11099-018-0791-y.
[59] O.N. Pakhomova, B.W. Gregory, I. Semenov, A.G. Pakhomov, Two Modes of Cell Death Caused by Exposure to Nanosecond Pulsed Electric Field, PLOS ONE 8 (2013) e70278. https://doi.org/10.1371/journal.pone.0070278.
[60] N. Kitajima, K. Makihara, H. Kurita, On the Synergistic Effects of Cold Atmospheric Pressure Plasma Irradiation and Electroporation on Cytotoxicity of HeLa Cells, International Journal of Molecular Sciences 26 (2025) 1093. https://doi.org/10.3390/ijms26031093.
[61] M. Somolinos, D. García, P. Mañas, S. Condón, R. Pagán, Effect of environmental factors and cell physiological state on Pulsed Electric Fields resistance and repair capacity of various strains of Escherichia coli, International Journal of Food Microbiology 124 (2008) 260–267. https://doi.org/10.1016/j.ijfoodmicro.2008.03.021.
[62] I. Álvarez, R. Pagán, J. Raso, S. Condón, Environmental factors influencing the inactivation of Listeria monocytogenes by pulsed electric fields, Letters in Applied Microbiology 35 (2002) 489–493. https://doi.org/10.1046/j.1472-765X.2002.01221.x.
[63] U.R. Pothakamury, H. Vega, Q. Zhang, G.V. Barbosa-Canovas, B.G. Swanson, Effect of Growth Stage and Processing Temperature on the

Inactivation of *E. coli* by Pulsed Electric Fields, Journal of Food Protection 59 (1996) 1167–1171. https://doi.org/10.4315/0362-028X-59.11.1167.

[64] J. Knappert, C. McHardy, C. Rauh, Kinetic Modeling and Numerical Simulation as Tools to Scale Microalgae Cell Membrane Permeabilization by Means of Pulsed Electric Fields (PEF) From Lab to Pilot Plants, Front. Bioeng. Biotechnol. 8 (2020). https://doi.org/10.3389/fbioe.2020.00209.

[65] Y. Zhang, Z. Luo, F. Guo, Simulation of electroporation threshold based on the evolution of transmembrane potential and pore density, PeerJ 13 (2025) e19356. https://doi.org/10.7717/peerj.19356.

[66] R. Zhou, R. Zhou, P. Wang, Y. Xian, A. Mai-Prochnow, X. Lu, P.J. Cullen, K. (Ken) Ostrikov, K. Bazaka, Plasma-activated water: generation, origin of reactive species and biological applications, J. Phys. D: Appl. Phys. 53 (2020) 303001. https://doi.org/10.1088/1361-6463/ab81cf.

[67] A. Privat-Maldonado, A. Schmidt, A. Lin, K.-D. Weltmann, K. Wende, A. Bogaerts, S. Bekeschus, ROS from Physical Plasmas: Redox Chemistry for Biomedical Therapy, Oxid Med Cell Longev 2019 (2019) 9062098. https://doi.org/10.1155/2019/9062098.

[68] S. Sukhani, N. Punith, A. Ekatpure, G. Salunke, M. Manjari, R. Harsha, H.N. Chanakya, R. Lakshminarayana, Plasma-Activated Water as Nitrogen Source for Algal Growth: A Microcosm Study, IEEE Transactions on Plasma Science 49 (2021) 551–556. https://doi.org/10.1109/TPS.2021.3051728.

[69] G. Pucihar, T. Kotnik, M. Kandušer, D. Miklavčič, The influence of medium conductivity on electropermeabilization and survival of cells in vitro, Bioelectrochemistry 54 (2001) 107–115. https://doi.org/10.1016/S1567-5394(01)00117-7.

[70] E. Griseti, J. Kolosnjaj-Tabi, L. Gibot, I. Fourquaux, M.-P. Rols, M. Yousfi, N. Merbahi, M. Golzio, Pulsed Electric Field Treatment Enhances the Cytotoxicity of Plasma-Activated Liquids in a Three-Dimensional Human Colorectal Cancer Cell Model, Sci Rep 9 (2019) 7583. https://doi.org/10.1038/s41598-019-44087-5.

[71] T.-H. Chung, A. Stancampiano, K. Sklias, K. Gazeli, F.M. André, S. Dozias, C. Douat, J.-M. Pouvesle, J. Santos Sousa, É. Robert, L.M. Mir, Cell Electropermeabilisation Enhancement by Non-Thermal-Plasma-Treated PBS, Cancers 12 (2020) 219. https://doi.org/10.3390/cancers12010219.

[72] R. Mentheour, Z. Machala, Coupled Antibacterial Effects of Plasma-Activated Water and Pulsed Electric Field, Frontiers in Physics 10 (2022). https://www.frontiersin.org/articles/10.3389/fphy.2022.895813 (accessed October 27, 2022).

[73] R. Park, J.-G. Kim, H.-W. Kim, Prediction of varying microcystins during non-thermal plasma oxidation of harvested microalgal biomass,

Journal of Hazardous Materials 403 (2021) 123596. https://doi.org/10.1016/j.jhazmat.2020.123596.
[74] M. Bai, Z. Zhang, X. Xue, X. Yang, L. Hua, D. Fan, Killing Effects of Hydroxyl Radical on Algae and Bacteria in Ship's Ballast Water and on Their Cell Morphology, Plasma Chem Plasma Process 30 (2010) 831–840. https://doi.org/10.1007/s11090-010-9252-5.
[75] M. Beyrer, M.C. Pina-Perez, D. Martinet, W. Andlauer, Cold plasma processing of powdered Spirulina algae for spore inactivation and preservation of bioactive compounds, Food Control 118 (2020) 107378. https://doi.org/10.1016/j.foodcont.2020.107378.
[76] N.R.H. Rao, X. Chu, K. Hadinoto, Angelina, R. Zhou, T. Zhang, B. Soltani, C.G. Bailey, F.J. Trujillo, G.L. Leslie, S.W. Prescott, P.J. Cullen, R.K. Henderson, Algal cell inactivation and damage via cold plasma-activated bubbles: Mechanistic insights and process benefits, Chemical Engineering Journal 454 (2023) 140304. https://doi.org/10.1016/j.cej.2022.140304.
[77] J. Pawłat, P. Terebun, M. Kwiatkowski, B. Tarabová, Z. Kovaľová, K. Kučerová, Z. Machala, M. Janda, K. Hensel, Evaluation of Oxidative Species in Gaseous and Liquid Phase Generated by Mini-Gliding Arc Discharge, Plasma Chem Plasma Process 39 (2019) 627–642. https://doi.org/10.1007/s11090-019-09974-9.
[78] M. Zhu, Z. Wang, J. Chen, L. Liu, W. Xi, F. Zhang, L. Guo, D. Liu, M. Rong, Gliding arc discharge used for water activation: the production mechanism of aqueous NO and its role in sterilization, J. Phys. D: Appl. Phys. 56 (2022) 035202. https://doi.org/10.1088/1361-6463/aca340.
[79] C.M. Wolff, J.F. Kolb, S. Bekeschus, Combined In Vitro Toxicity and Immunogenicity of Cold Plasma and Pulsed Electric Fields, Biomedicines 10 (2022) 3084. https://doi.org/10.3390/biomedicines10123084.
[80] D. Tang, R. Kang, T.V. Berghe, P. Vandenabeele, G. Kroemer, The molecular machinery of regulated cell death, Cell Res 29 (2019) 347–364. https://doi.org/10.1038/s41422-019-0164-5.
[81] K.C. Kasuba, S.L. Vavilala, J.S. D'Souza, Apoptosis-like cell death in unicellular photosynthetic organisms — A review, Algal Research 12 (2015) 126–133. https://doi.org/10.1016/j.algal.2015.07.016.
[82] S. Hanson, A. Dharan, J. P. V., S. Pal, B.G. Nair, R. Kar, N. Mishra, Paraptosis: a unique cell death mode for targeting cancer, Front. Pharmacol. 14 (2023). https://doi.org/10.3389/fphar.2023.1159409.
[83] P. Scaturro, A. Pichlmair, Oxeiptosis—a cell death pathway to mitigate damage caused by radicals, Cell Death & Differentiation 25 (2018) 1191–1193. https://doi.org/10.1038/s41418-018-0134-3.
[84] P. Scaturro, A. Pichlmair, Oxeiptosis: a discreet way to respond to radicals, Current Opinion in Immunology 56 (2019) 37–43. https://doi.org/10.1016/j.coi.2018.10.006.

[85] M.M. Barreto Filho, P.M. Durand, N.E. Andolfato, A. Jordaan, H. Sarmento, I.L. Bagatini, Programmed cell death in the coccoid green microalga Ankistrodesmus densus Korshikov (Sphaeropleales, Selenastraceae), European Journal of Phycology 57 (2022) 193–206. https://doi.org/10.1080/09670262.2021.1938240.
[86] H. Wang, W. Zhang, L. Chen, J. Wang, T. Liu, The contamination and control of biological pollutants in mass cultivation of microalgae, Bioresource Technology 128 (2013) 745–750. https://doi.org/10.1016/j.biortech.2012.10.158.
[87] P.C. Wouters, N. Dutreux, J.P.P.M. Smelt, H.L.M. Lelieveld, Effects of Pulsed Electric Fields on Inactivation Kinetics of Listeria innocua, Applied and Environmental Microbiology 65 (1999) 5364–5371. https://doi.org/10.1128/AEM.65.12.5364-5371.1999.
[88] I. Álvarez, J. Raso, A. Palop, F.J. Sala, Influence of different factors on the inactivation of Salmonella senftenberg by pulsed electric fields, International Journal of Food Microbiology 55 (2000) 143–146. https://doi.org/10.1016/S0168-1605(00)00173-2.
[89] G.P. 't Lam, P.R. Postma, D.A. Fernandes, R.A.H. Timmermans, M.H. Vermuë, M.J. Barbosa, M.H.M. Eppink, R.H. Wijffels, G. Olivieri, Pulsed Electric Field for protein release of the microalgae Chlorella vulgaris and Neochloris oleoabundans, Algal Research 24 (2017) 181–187. https://doi.org/10.1016/j.algal.2017.03.024.
[90] R. Ramanan, B.H. Kim, D.H. Cho, H.M. Oh, H.S. Kim, Algae-bacteria interactions: Evolution, ecology and emerging applications, Biotechnology Advances 34 (2016) 14–29. https://doi.org/10.1016/j.biotechadv.2015.12.003.
[91] C. Gopalakrishnappa, Z. Li, S. Kuehn, Environmental modulators of algae-bacteria interactions at scale, Cels 15 (2024) 838-853.e13. https://doi.org/10.1016/j.cels.2024.08.002.
[92] V. Stankevič, K. Jonynaitė, A. Taha, S. Keršulis, A. Dervinis, S. Kurčevskis, S. Tolvaišienė, A. Stirkė, N. Žurauskienė, The Advancement and Utilization of Marx Electric Field Generator for Protein Extraction and Inducing Structural Alterations, Applied Sciences 14 (2024) 3886. https://doi.org/10.3390/app14093886.
[93] K. Aronsson, M. Lindgren, B.R. Johansson, U. Ronner, Inactivation of microorganisms using pulsed electric fields: the influence of process parameters on Escherichia coli, Listeria innocua, Leuconostoc mesenteroides and Saccharomyces cere¨isiae, Emerging Technologies (2001).
[94] N. Ricós-Muñoz, A. Rivas Soler, J.M. Castagnini, R. Moral, F.J. Barba, M.C. Pina-Pérez, Improvement of the probiotic growth-stimulating capacity of microalgae extracts by pulsed electric fields treatment, Innovative Food Science & Emerging Technologies 83 (2023) 103256. https://doi.org/10.1016/j.ifset.2022.103256.

[95] X. Chen, Z. Hu, Y. Qi, C. Song, G. Chen, The interactions of algae-activated sludge symbiotic system and its effects on wastewater treatment and lipid accumulation, Bioresource Technology 292 (2019) 122017. https://doi.org/10.1016/j.biortech.2019.122017.
[96] J. Wang, X. Wang, Z. Yu, S. Huang, D. Yao, J. Xiao, W. Chen, Z. Wang, F. Zan, Using algae bacteria consortia to effectively treat coking wastewater: Performance, microbial community, and mechanism, Journal of Cleaner Production 334 (2022) 130269. https://doi.org/10.1016/j.jclepro.2021.130269.
[97] O.N. Barberi, C.J. Byron, K.M. Burkholder, A.T. St. Gelais, A.K. Williams, Assessment of bacterial pathogens on edible macroalgae in coastal waters, J Appl Phycol 32 (2020) 683–696. https://doi.org/10.1007/s10811-019-01993-5.
[98] G. Wu, D. Zhuang, K.W. Chew, T.C. Ling, K.S. Khoo, D. Van Quyen, S. Feng, P.L. Show, Current Status and Future Trends in Removal, Control, and Mitigation of Algae Food Safety Risks for Human Consumption, Molecules 27 (2022) 6633. https://doi.org/10.3390/molecules27196633.

APPENDIX

List of Scientific Conferences

The results obtained during the doctoral studies were presented at 16 scientific conferences, of which 10 were international:

International conferences:

1. 19th international conference on plasma physics and applications (CPPA 2021), August 31 – September 3, 2021, Bucharest, Romania. “Treatment of Chlorella vulgaris by gliding arc discharge plasma”. Poster presentation.
2. Electroporation-based technologies and treatments: international scientific workshop and postgraduate course, November 14–20, 2021, Ljubljana, Slovenia. “Pulsed electric field and plasma assisted treatment of microalgae Chlorella vulgaris”. Poster presentation.
3. 3rd Baltic biophysics conference, October 6–7, 2022, Vilnius, Lithuania. “Pulsed electric field (PEF) treatment of marine microalgae”. Poster presentation.
4. 4th World congress on electroporation and pulsed electric fields in biology, medicine, and food & environmental technologies, October 9–13, 2022, Copenhagen, Denmark. “Combination of cold plasma and pulsed electric field for microalgae treatment”. Poster presentation.
5. SICT 2023 / Plasma Tech 2023 / Tribology 2023 joint conferences, April 26–28, 2023, Lisbon, Portugal. “Treatment of microalgae by gliding arc plasma and pulsed electric field”. Oral presentation.
6. 8th international conference on advanced plasma technologies, May 14–18, 2023, Gozd Martuljek, Slovenia. “Extraction of valuable compounds from microalgae using plasma and pulsed electric field treatment”. Poster presentation.
7. International bioelectrics symposium 2023, September 10–13, 2023, Lisbon, Portugal. “Investigation of the combined effect of plasma and pulsed electric field treatment on Chlorella vulgaris microalgae”. Oral presentation.
8. 4th workshop on plasma applications for smart and sustainable agriculture, 2024, Belgrade, Serbia. “Treatment of marine and fresh water microalgae by gliding arc discharge plasma”. Poster presentation.
9. International Conference on Plasma Medicine and 9th International Workshop on Plasma for Cancer Treatment, September 8–13, 2024, Portorož, Slovenia. “Treatment of fresh and marine water microalgae by

combined gliding arc discharge plasma and pulsed electric field". Oral presentation.

10. 5th World congress on electroporation and pulsed electric fields in biology, medicine, and food & environmental technologies, September 15–19, 2024, Rome, Italy. "Unveiling the interplay between gliding arc discharge (GAD) plasma pretreatment and pulsed electric field (PEF) on Chlorella vulgaris microalgae". Poster presentation.

National conferences:

11. FizTeCh 2020, 2020, Vilnius. "Interaction between Chlorella vulgaris microalgae and dominant bacteria of their microbiome during autotrophic cultivation". Oral presentation.
12. 44th Lithuanian National Physics Conference, October 6–8, 2021, Vilnius. "Treatment of Chlorella vulgaris by plasma". Poster presentation.
13. FizTeCh 2021, October 20–21, 2021, Vilnius. "Application of plasma treatment for the extraction of valuable compounds from microalgae used in wastewater bioremediation". Oral presentation.
14. FizTeCh 2022, October 19–20, 2022, Vilnius. "Treatment of microalgae using cold plasma and pulsed electric field". Oral presentation.
15. FizTeCh 2023, October 18–19, 2023, Vilnius. "Uncovering novel effects of combined plasma and pulsed electric field (PEF) treatments on algae cells: Insights into cell death mechanisms". Oral presentation.
16. 17th National Conference on Marine Sciences and Technologies, May 14–16, 2025, Juodkrantė. "Investigation of the effect of gliding arc discharge plasma and pulsed electric field on C. vulgaris microalgal cells". Poster presentation.

SANTRAUKA

Įvadas

Impulsinio elektrinio lauko (IEL) technologija grindžiama trumpų (ns-ms) stiprių (V/cm-kV/cm) impulsų taikymu biologinėms sistemoms. Poveikio metu keičiasi ląstelės transmembraninis potencialas, todėl membranoje gali formuotis poros ir padidėti jos pralaidumas (permeabilizacija), dažnai vadinamas elektroporacija. Šis veikimo principas lemia platų technologijos pritaikomumą: molekulių įnešimą į ląstelę, viduląstelinių junginių išskyrimą, ląstelinių funkcijų moduliavimą ir selektyvią ląstelių inaktyvaciją.

IEL tyrimų raida skirtingose biologinėse sistemose yra netolygi. Veikimo mechanizmai išsamiausiai išaiškinti žinduolių ir bakterijų ląstelėse, kur pavyko modeliuoti membranos porų dinamiką, nustatyti dozės-atsako ryšius, prognozuoti viduląstelinių struktūrų (mitochondrijų, branduolio) reakcijas ir šias žinias taikyti terapiniuose bei pramoniniuose kontekstuose. Mikrodumbliai, nepaisant daugiau nei du dešimtmečius besitęsiančių tyrimų, IEL poveikio atžvilgiu išlieka kur kas mažiau charakterizuoti. Literatūroje daugiausia dėmesio skiriama viduląstelinių junginių ekstrakcijai, o dažniausiai nagrinėjamos temos apima IEL impulsų parametrų ir taikymo režimų derinimą, siekiant maksimaliai padidinti lipidų, baltymų ar pigmentų išeigą ir pagerinti tolesnį apdorojimą. Tuo tarpu fundamentali samprata išlieka ribota: nepakankamai identifikuotos pagrindinės IEL veikiamos ląstelinės struktūros, menkai aprašyti biofiziniai keliai, neaiškūs fotosintetinio aparato atsako mechanizmai.

Šis disbalansas kelia ir intelektinių, ir praktinių iššūkių, nes riboja ne tik IEL poveikio prognozavimą bei racionalų parametrų parinkimą, bet ir patikimą technologijos perkėlimą į taikomuosius sprendimus bei pramoninį mastelį. Tai ypač aktualu mikrodumblių sektoriui, kuris laikomas perspektyvia žaliosios ekonomikos plėtros kryptimi. Vis dėlto tiesiogiai perkelti žinduolių ir bakterijų sistemose sukauptas žinias mikrodumbliams yra problemiškas. Šie organizmai pasižymi struktūrinėmis ir biocheminėmis savybėmis, reikšmingai besiskiriančiomis nuo sistemų, kuriose IEL mechanizmai jau nustatyti. Chloroplastuose yra sudėtingos, išplėtotos tilakoidų membranų sistemos, struktūriškai besiskiriančios nuo mitochondrijų kristų. Jose veikia šviesos valdomos elektronų pernašos grandinės ir deguonies išsiskyrimo aparatas, kurio redokso chemija iš esmės skiriasi nuo respiracinio metabolizmo. *C. vulgaris* standi, daugiasluoksnė ląstelės sienelė sudaro papildomą dielektrinį barjerą, kurio žinduolių sistemose nėra. Membranų sudėtis taip pat reikšmingai skiriasi: mikrodumblių chloroplastų ir tilakoidų membranose dominuoja galaktolipidai, o ląstelėje yra išplėtota su

fotosinteze susijusi vidinių membranų sistema. Klausimas, ar žinduolių ir bakterijų sistemoms nustatyti elektroporacijos principai galioja mikrodumbliams, turintiems tokią apvalkalo architektūrą ir chloroplastu dominuojantį vidų, reikalauja empirinio tyrimo, o ne prielaidų.

Šioje disertacijoje mechanistinių žinių spragą siekiama spręsti sistemingai charakterizuojant IEL poveikį fotosintetinėms sistemoms trijuose organizacijos masteliuose: organeliniame, ląsteliniame ir bendrijos. Visame darbe pagrindinis modelinis organizmas yra *C. vulgaris*, vienaląstis žaliasis dumblis, kurio sferinė geometrija (skersmuo 3-8 μm) leidžia tiesiogiai taikyti nusistovėjusius elektroporacijos modelius. Jis turi vieną taurės formos chloroplastą, užimantį apie 40-60 % ląstelės tūrio, ir greitai auga apibrėžtomis sąlygomis. Plati ankstesnė šios rūšies charakterizacija suteikia esminį lyginamąjį kontekstą.

Kiekviename iš trijų organizacijos mastelių egzistuoja specifiniai žinių trūkumai, kuriuos ši disertacija siekia spręsti.

Organelių mastas: impulso trukmė atlieka esminį vaidmenį nustatant IEL poveikį biologiniam objektui. Veikiant išoriniu elektriniu lauku, transmembraninė įtampa vystosi per būdingą įkrovos laiko konstantą ($\tau = R \times C$), ląstelės membranos atžvilgiu paprastai esančią submikrosekundžių-mikrosekundžių diapazone. Impulsai, gerokai ilgesni už šį laiką, leidžia beveik visiškai poliarizuoti plazminę membraną ir skatina įprastą porų formavimąsi. Tačiau kai impulso trukmė artėja prie τ arba yra trumpesnė už jį, plazminė membrana nespėja visiškai poliarizuotis, ir ląstelės viduje gali susidaryti trumpalaikiai elektriniai laukai. Žinduolių ląstelėse parodyta, kad nanosekundinių impulsų poveikis gali sukelti mitochondrijų depoliarizaciją, kalcio išsiskyrimą iš viduląstelinių saugyklų ir aktyvuoti nuo kaspazių priklausomą apoptozę. Mielėse analogiškas apdorojimas aktyvina metakaspazes ir sužadina programuotos žūties kelius. Šie stebėjimai įtvirtino principą, kad pakankamai trumpi impulsai gali veikti viduląstelines organeles. Vis dėlto nefotosintetinėms organelėms, tokioms kaip mitochondrijos ar endoplazminis tinklas, nustatyti rezultatai negali būti tiesiogiai pritaikomi visoms viduląstelinėms struktūroms. Fotosintetinės organelės reikšmingai skiriasi struktūra ir funkcija, o ar nanosekundiniai impulsai analogiškai veikia chloroplastus, nėra visapusiškai ištirta. Ankstesni mikrodumblių tyrimai užfiksavo fotosintetinio efektyvumo sumažėjimą (F_v/F_m kritimą) ir su chloroplastais susijusių genų raiškos pokyčius po IEL apdorojimo, tačiau iki šiol neišspręsta, ar šie efektai kyla dėl tiesioginės elektrinės sąveikos su chloroplastų membranomis, ar netiesiogiai, dėl plazminės membranos permeabilizacijos ir vėlesnio citosolio homeostazės sutrikimo.

Ląstelinis mastas: IEL poveikis vandeninėje terpėje niekada nėra vien elektrinis. IEL impulsų metu elektrodų paviršiuje vykstančios elektrocheminės reakcijos neišvengiamai generuoja reaktyviąsias deguonies ir azoto formas (RDAF), kurios gali oksiduoti membranos lipidus ir padidinti jos pralaidumą nepriklausomai nuo transmembraninio potencialo. Tai reiškia, kad tai, kas atrodo kaip grynai elektrinis permeabilizacijos įvykis, iš tikrųjų yra kombinuotas elektro-oksidacinis poveikis, kurio atskiros dedamosios standartinėmis IEL sąlygomis negali būti keičiamos nepriklausomai viena nuo kitos. Ar oksidacinė dedamoji aktyviai formuoja tolesnę biologinę reakciją, ar tik ją lydi, lieka neaišku. Šio apribojimo įveikimui šaltoji atmosferos plazma suteikia unikalią galimybę: kaip kontroliuojamas išorinis RDAF šaltinis, ji leidžia sistemingai keisti oksidacinį kontekstą išlaikant fiksuotus IEL parametrus. Tyrimai žinduolių ir mikrobinėse sistemose rodo, kad kombinuotas plazmos ir IEL poveikis ne tik sustiprina permeabilizaciją, bet ir gali keisti ląstelių mirties kelius. Ar plazmos apdorojimas prieš IEL sukelia panašius atsako konteksto pokyčius mikrodumbliuose, lieka neaišku.

Bendrijos mastas: mikrodumbliai tiek natūralioje aplinkoje, tiek pramoninio masto kultivavimo sistemose egzistuoja mikrobinėse bendrijose, kur bakterijų buvimas yra neišvengiamas. Dumbliai ir bakterijos ne tik koegzistuoja, bet ir sąveikauja, o sąveikos pobūdis kinta priklausomai nuo kultivavimo sąlygų: tokie veiksniai kaip pH, maistinių medžiagų prieinamumas ir anglies šaltinis gali tą pačią sąveikos porą paversti iš mutualistinės į konkurencinę. Šie pokyčiai keičia kiekvienos populiacijos fiziologinę būklę, o mitybinis statusas ir metabolinis aktyvumas veikia membranų savybes, streso toleranciją ir atsistatymo efektyvumą, todėl gali turėti įtakos IEL atsakui. Ląstelės dydis yra kitas svarbus aspektas: remiantis elektroporacijos teorija, mažesnėms ląstelėms, tokioms kaip bakterijos, membranos permeabilizacijai inicijuoti reikia stipresnio elektrinio lauko nei didesnėms eukariotinėms ląstelėms. Tačiau ši teorija paprastai taikoma monokultūroms, kur fiziologinė būsena yra apibrėžta. Kokultūrose sąveikų istorija formuoja kiekvienos populiacijos būklę dar prieš taikant IEL, todėl jautrumas poveikiui gali priklausyti nuo kultivavimo konteksto. Ar augimo fazė ir bendrijos dinamika keičia IEL poveikio mastą taip, kaip monokultūrų tyrimai negali numatyti, tiesiogiai nėra tirta.

Tyrimo tikslas ir uždaviniai

Ištirti IEL poveikį mikrodumblių sistemoms organelių, ląsteliniame ir bendrijos masteliuose, išplečiant nusistovėjusias elektrofiziologines paradigmas fotosintetiniams organizmams ir mišrioms mikroorganizmų populiacijoms.

Uždaviniai:

Organelių mastas: charakterizuoti IEL sukeltus chloroplasto funkcijos pokyčius *C. vulgaris* taikant fluorescencija grindžiamus tyrimus ir įvertinti jų ryšį su plazminės membranos permeabilizacija.

Ląstelinis mastas: nustatyti, ar išankstinis ląstelių apdorojimas slenkančio lankinio išlydžio plazma keičia fiksuotų IEL parametrų biologinę išraišką *C. vulgaris*, tiriant permeabilizaciją, makromolekulių išsiskyrimą ir ląstelių mirties kelius.

Bendrijos mastas: ištirti, kaip fiziologinė būklė ir bendrijos kontekstas veikia IEL atsaką mikrodumblių ir bakterijų kokultūrose, ir įvertinti, ar skirtingas ląstelinis jautrumas IEL įgalina selektyvią baltymų ekstrakciją.

Teiginiai gynimui

1. IEL sutrumpina chlorofilo fluorescencijos gyvavimo trukmę ties 685 nm *C. vulgaris*, priklausomai nuo impulso trukmės, nekeisdamas absorbcijos spektro, indikuodamas, kad fotosintetinio aparato sutrikimas kyla dėl padidėjusio nespinduliuojančio energijos išsklaidymo, o ne dėl pigmentų degradacijos.

2. Plazmos apdorojimas (250 V maitinimo šaltinis), po kurio taikomas IEL, atskiria membranos permeabilizaciją nuo makromolekulių išsiskyrimo, slopina kaspazės tipo aktyvumą ir sukelia neapoptotinį, ne nekrotinį ląstelių mirties fenotipą, kuris skiriasi nuo klasikinės IEL sukeltos programuotos ląstelių mirties ir reikalauja tiesioginio plazmos poveikio.

3. IEL apdorojimas (40 kV/cm, 1 μs, 4-100 J/mL) sukelia stabilią *C. vulgaris* inaktyvaciją (>95 %), o *Delftia* sp. jautrumas priklauso nuo augimo fazės, kas leidžia selektyviai išskirti dumblių baltymus iš ko-kultūrų be papildomų baltymų juostų, stebimų mechaninio suardymo atveju.

Medžiagos ir metodai

Pirmas skyrius: *C. vulgaris* buvo auginama burbulinių kolonų fotobioreaktoriuose BG-11 terpėje ir koncentruojama iki 5 g/L sausosios masės IEL eksperimentams. IEL apdorojimui naudoti du impulsų generatoriai: tranzistorinis elektroporatorius, generavęs mikrosekundinius impulsus (10 μs), ir koaksialinės perdavimo linijos generatorius, generavęs nanosekundinius impulsus (10, 60 ir 90 ns). Nanosekundiniame režime IEL impulsų energija buvo visais atvejais išlaikoma ta pati (80 J/mL), tik gaunama derinant skirtingo elektrinio lauko stiprį (19-86 kV/cm) ir impulsų skaičių. Tai leido tiesiogiai lyginti skirtingų impulsų trukmių poveikį. Pigmentų integralumas vertintas registruojant sugerties spektrus. Fluorescencijos matavimams naudotas Edinburgh F920 spektrofluorometras, žadinant 470 nm bangos ilgiu, emisijos spektrai registruoti 600-800 nm intervale. Fluorescencijos gyvavimo trukmės analizė atlikta laiko koreliuojamo

vienfotonio skaičiavimo (TCSPC) metodu, siekiant charakterizuoti gesimo kinetiką. Membranos permeabilizacija vertinta naudojant SYTOX Green nukleorūgščių dažą, fluorescenciją matuojant tiek ląstelių nuosėdose, tiek supernatantuose praėjus 5 min, 2 val. ir 24 val. po apdorojimo. Toks eksperimentinis dizainas leido gretinti optinius fotosistemos funkcijos matavimus su membranos pralaidumo būkle.

Antras skyrius: Nuosekliam plazmos-IEL apdorojimui naudota slenkančio lankinio išlydžio plazma, kurios maitinimo šaltinio įtampa buvo 90–250 V diapazone. Plazmos charakterizacija apėmė optinę emisijos spektroskopiją, naudojant Flame UV-VIS (200–1000 nm) ir IFU AOS4 akusto-optinius spektrometrus reaktyviosioms rūšims identifikuoti. Terpės modifikacijos kiekybiškai įvertintos visame įtampos diapazone: nustatyti temperatūros profiliai, pH pokyčiai, laidumo poslinkiai ir ilgai išliekančių reaktyviųjų rūšių koncentracijos. Sistemingi kontroliniai bandymai atskyrė tiesioginius plazmos ir ląstelių sąveikos efektus nuo antrinių terpės modifikacijų. Kontroliniai variantai apėmė tiesioginę plazmos ekspoziciją, plazma aktyvuotą terpę, temperatūriškai suderintą išankstinį apdorojimą ir laidumu suderintus supernatanto pakeitimo protokolus. Fiksuotas IEL protokolas buvo 25 kV/cm, 7 μs, su 1 arba 10 impulsų. Ląsteliniai atsakai vertinti keliais analitiniais lygmenimis: membranos permeabilizacija, baltymų išsiskyrimas (kiekybiškai Bradfordo metodu, kokybiškai natrio dodecilsulfato poliakrilamido gelio elektroforeze (angl. SDS-PAGE)), DNR išsiskyrimas, laisvosios aminorūgštys, metabolinis aktyvumas, morfologinis vertinimas ir kaspazės-3 tipo aktyvumas.

Trečias skyrius: Bakterijos buvo aptiktos ir išgrynintos iš C. vulgaris suspensijos, o jų tapatybė nustatyta morfologiniais, biocheminiais ir molekuliniais metodais, įskaitant 16S rRNR geno sekvenavimą. Kokultūros buvo sudarytos trijose terpėse (TAP, BG-11, BG-11 su acto rūgštimi (BG+AA)), siekiant charakterizuoti nuo mitybos priklausomą sąveikų dinamiką. Populiacijos analizuotos tėkmės citometrija (Attune NxT), taikant diferencinį dažymą (SYTO 9, YO-PRO-1, FDA). Cheminė analizė apėmė maistinių medžiagų suvartojimo stebėseną (NH_4^+, NO_2^-, NO_3^-, acto rūgštis). IEL apdorojimui naudota nuolatinio srauto sistema, taikant du energijos režimus: mažos energijos (4 J/mL; 1 μs, 40 kV/cm) ir didelės energijos (100 J/mL; 1 μs, 40 kV/cm). Apdorojimas taikytas 1, 3 ir 7 kokultūros kultivavimo dienomis. Mechaninio ardymo kontrolei naudota aukšto slėgio homogenizacija (HPH; 2000 bar, 5 ciklai). Baltymų koncentracija nustatyta Bradfordo metodu, o SDS-PAGE analizė naudota baltymų profiliams palyginti tarp apdorojimo metodų ir kultivavimo sąlygų. Dumblių lizatų

antimikrobinis aktyvumas tirtas agarinės difuzijos ir bakterijų augimo kreivių metodais.

Rezultatai ir jų aptarimas

Pirmas skyrius: IEL sukelti fotosintetinės sistemos funkcijos pokyčiai.

Po mikrosekundinių impulsų apdorojimo (10 μs, 19 kV/cm, 80 J/mL) sugerties spektrai nepakito: nebuvo stebėta nei piko poslinkio, nei reikšmingo intensyvumo sumažėjimo. Tai indikuoja, kad chlorofilo populiacija nebuvo prarasta ar degraduota po IEL apdorojimo. Tuo tarpu, emisijos spektrai rodė progresuojantį intensyvumo mažėjimą, piko padėčiai išliekant ties 685 nm. Laiko skiriamoji fluorescencijos gyvavimo trukmės analizė ties 685 nm parodė, kad intensyvumo sumažėjimas atitiko trumpėjančią gesimo kinetiką: gyvavimo trukmė sumažėjo nuo 1,71 ± 0,05 ns neapdorotose ląstelėse iki 0,83 ± 0,03 ns praėjus 5 minutėms po apdorojimo (sumažėjimas viršijo 50 %). Membranos permeabilizacija pasiekė apie 70 %.

Tolesnėje analizėje palyginti nanosekundiniai ir mikrosekundiniai impulsai esant ekvivalentiškam IEL lauko stipriui (19 kV/cm) ir energijai (80 J/mL). Esant šioms sąlygoms, 90 ns impulsai sukėlė 10,5 % ± 2,1 % permeabilizaciją, o fluorescencijos gyvavimo trukmė sumažėjo iki maždaug 1,4 ns. Abu efektai buvo gerokai silpnesni nei taikant mikrosekundinius impulsus, nepaisant identiškos IEL impulsų energijos.

Toliau nanosekundiniame režime įvertinta impulso trukmės (10, 60, 90 ns) ir lauko stiprio (26-86 kV/cm) įtaka atskleidė skirtingas priklausomybes. Esant 90 ns ir 60 ns impulsams, didėjantis lauko stipris sustiprino tiek fluorescencijos gyvavimo trukmės mažėjimą, tiek membranos permeabilizaciją. Esant 86 kV/cm, gyvavimo trukmė sumažėjo iki maždaug 0,9 ns, o permeabilizacija pasiekė 24-27 %. Reikšmingų skirtumų tarp 60 ns ir 90 ns apdorojimo esant tiems patiems lauko stipriams nebuvo. Priešingai, 10 ns impulsai visame tirtame lauko stiprių diapazone sukėlė tik minimalų poveikį: didžiausia permeabilizacija siekė tik 11 % esant 86 kV/cm, o reikšmingų fluorescencijos gyvavimo trukmės pokyčių nebuvo stebėta.

Nustatyti optiniai pokyčiai, nepakitusi sugertis kartu su sumažėjusiu emisijos intensyvumu ir sutrumpėjusia fluorescencijos gyvavimo trukme, indikuoja, jog IEL poveikis lemia sustiprėjusią nespinduliuojančią energijos disipaciją, o ne pigmentų praradimą. Fluorescencijos pokyčius daugeliu apdorojimo režimų lydėjo membranos permeabilizacija. Tačiau pokyčių mastas tarp permeabilizacijos ir fluorescencijos kinetikų nebuvo tolygus. Mikrosekundinių impulsų atveju (19 kV/cm, 80 J/mL) permeabilizacija (70 %) viršijo fluorescencijos gyvavimo trukmės pokytį (51 %, lyginant su kontrole). Nanosekundinių impulsų atveju (90 ns, 19 kV/cm, 80 J/mL) santykis buvo priešingas (10,5 % ir 18 % atitinkamai), kas gali rodyti

skirtingus IEL poveikio mechanizmus. Mikrosekundinių impulsų atveju, kai permeabilizacija buvo ryški, galimas mechanizmas gali būti siejamas su plazminės membranos porų palengvintu jonų persiskirstymu pagal elektrocheminius gradientus, keičiančiu citosolio homeostazę ir galimai veikiančiu chloroplasto funkciją per stromos aplinkos pokyčius. Šią interpretaciją netiesiogiai palaiko Chorvatova et al. (2020), parodę, kad išorinė terpės acidifikacija *Chlorella* sp. lemia analogišką fluorescencijos intensyvumo mažėjimą ir gyvavimo trukmės trumpėjimą. Nanosekundinių impulsų atveju fluorescencijos rezultatų pokytis, lyginant su kontrole, buvo didesnis nei permeabilizacijos, kas gali būti siejamas su nsIEL tiesiogiu poveikiu viduląstelinėms struktūroms. Tačiau ši hipotezė išlieka nepatvirtinta.

Būtina pažymėti, jog rezultatų interpretacijas riboja kelios aplinkybės. Matavimai praėjus 5 minutėms po apdorojimo gali atspindėti antrinius procesus, o ne momentinius IEL sukeltus pokyčius. Trumpalaikiai efektai, pasireiškiantys per kelias sekundes po impulso, liko neužfiksuoti. Tai ypač aktualu nanosekundiniams impulsams, kai greitas porų užsidarymas gali užmaskuoti trumpai trunkančius sutrikimus. Šiems klausimams spręsti planuojami tolimesni tyrimai, apimantys tiesioginius chloroplasto apvalkalo integralumo matavimus, stromos pH stebėseną ir žemos temperatūros (70 K) fluorescencijos analizę.

Antras skyrius: dumblių atsako į IEL moduliavimas nuosekliame plazmos-IEL poveikio tyrime.

Plazmos charakterizacija parodė, kad slenkančio lankinio išlydžio plazma generavo azotu dominuojančius emisijos spektrus su ryškiais N_2 pikais ir nuo įtampos priklausomais N_2^+, NO_γ bei atominių deguonies rūšių intensyvumo didėjimais. Terpės modifikacijos didėjo didėjant išlydžio įtampai: temperatūra pasiekė 54 °C esant 250 V maitinimo šaltiniui, pH sumažėjo nuo maždaug 7,5 iki 7,0, laidumas padidėjo nuo 1,85 iki 3,34 mS/cm. Reaktyviųjų rūšių koncentracijos ženkliai išaugo: H_2O_2 nuo 5,9 iki 17,4 mM ir NO_2^- nuo 0,13 iki 1,67 mM.

Plazmos poveikis (be IEL) sukėlė nuo įtampos priklausomus biologinius efektus. Esant 130 V, plazmos apdorojimas nepadidino permeabilizacijos, DNR signalo ar baltymų išsiskyrimo virš kontrolės lygio. Metabolinis aktyvumas ir morfologija nepakito. Esant 250 V, permeabilizacija siekė apie 25 % po 2 valandų ir padidėjo iki 60 % po 24 valandų. DNR išsiskyrimas išliko mažas (apie 6 mg/L), o baltymų išsiskyrimas nesiekė 5 % sausos biomasės. Nepaisant visiško metabolinio aktyvumo praradimo, po 72 valandų ląstelės išlaikė natyvią morfologiją be matomų irimo požymių.

IEL apdorojimas (be plazmos) sukėlė nuo impulsų skaičiaus priklausomus efektus. Praėjus 2 valandoms po apdorojimo, vienas impulsas (25 kV/cm, 7

μs) lėmė apie 14 % membranos permeabilizaciją, dešimt impulsų viršijo 60 %. Po 24 valandų permeabilizacija padidėjo iki maždaug 70 % nepriklausomai nuo impulsų skaičiaus. DNR išsiskyrimas viršijo 20 mg/L, baltymų išsiskyrimas siekė apie 23 % sausos biomasės, o metabolinis aktyvumas buvo visiškai panaikintas taikant 10 impulsų.

Nuoseklus plazmos-IEL apdorojimas atskleidė nuo įtampos priklausomus atsakus, kurių nebuvo galima numatyti iš atskirų apdorojimų rezultatų. Kai identiški IEL parametrai (25 kV/cm, 7 μs, 10 impulsų) buvo taikomi po išankstinio plazminio apdorojimo, baigtys ryškiai išsiskyrė priklausomai nuo plazmos intensyvumo.

Žemos įtampos plazmos išankstinis apdorojimas (130 V) ir vėlesnis IEL sukėlė atsaką, panašų į vien IEL: didelę membranos permeabilizaciją, reikšmingą DNR išsiskyrimą į supernatantą (>20 mg/L) ir baltymų išsiskyrimą apie 20 % sausos biomasės. Po 2 valandų ląstelių pralaidumas siekė apie 25 % taikant vieną impulsą ir apie 55 % taikant 10 impulsų. Po 24 valandų permeabilizacija didėjo ir stabilizavosi ties maždaug 90 % nepriklausomai nuo impulsų skaičiaus. Morfologinis suirimas progresavo inkubacijos metu, atitinkant įprastą elektroporacijos ir ekstrakcijos modelį.

Aukštos įtampos plazmos išankstinis apdorojimas (250 V) ir vėlesnis tas pats IEL protokolas sukėlė kokybiškai kitokį atsaką. Po 2 valandų vieno impulso pridėjimas po 250 V plazmos padidino permeabilizaciją maždaug keturis kartus, palyginti su vienu impulsu be plazmos (maždaug 55 % palyginti su maždaug 15 %). Taikant 10 impulsų protokolą, membranos permeabilizacija išliko didelė (ne mažiau 70 % SYTOX teigiamų ląstelių po 24 valandų), o metabolinis aktyvumas buvo visiškai eliminuotas. Tačiau DNR išsiskyrimas išliko minimalus, iki maždaug 2 mg/L net po 10 impulsų, tai yra maždaug dešimtadalis lygio, stebėto taikant vien IEL ar žemos įtampos plazmos-IEL. Baltymų išsiskyrimas taip pat sumažėjo žemiau 5 % sausos biomasės. SDS-PAGE profiliai rodė ryškų juostų intensyvumo sumažėjimą, palyginti su kitomis apdorojimo sąlygomis. Po 72 valandų morfologinės savybės išliko santykinai išsaugotos, dumblių ląstelių suirimas nebuvo stebimas.

Kaspazės-3 tipo aktyvumas buvo kiekybiškai įvertintas praėjus 2 valandoms po apdorojimo. Vien IEL sukėlė ryškų padidėjimą, pasiekusį 250 % lyginant su neapdorota kontrole ir viršijusį šiluminio šoko teigiamą kontrolę. Priešingai, didelio intensyvumo plazmos ekspozicija stipriai slopino kaspazės-3 tipo aktyvumą, ir šis slopinimas išliko derinant didelės įtampos plazmos apdorojimą su vėlesniu IEL. Esant 250 V, kaspazės aktyvumas liko žemiau bazinės kontrolės lygių, nepaisant metabolinės inaktyvacijos ir didelės membranos permeabilizacijos.

Sistemingi kontroliniai bandymai leido atmesti keletą galimų šio nuo įtampos priklausomo atsako mechanistinių priežasčių. Plazma aktyvuota terpė (PAT) išsiskyrimo neatkartojo: kai plazma buvo taikoma tik terpei, o ląstelės prieš IEL ekspoziciją buvo resuspenduotos, baltymų ir DNR išsiskyrimas visuose plazmos įtampos lygiuose išliko panašus į vien IEL atsaką. Temperatūriškai suderintas išankstinis apdorojimas (41-54 °C), po kurio taikytas IEL, nesukėlė sumažėjusio makromolekulių išsiskyrimo. Laidumui kontroliuoti supernatanto pakeitimo protokolai taip pat nepašalino nuo įtampos priklausomo fenotipo. BSA kontrolės paneigė plazmos sukelto baltymų aptinkamumo praradimo hipotezę taikytomis analitinėmis sąlygomis.

Šie palyginimai rodo, kad antriniai plazmos sukeliami efektai terpėje, įskaitant temperatūros, laidumo pokyčius ir ilgai išliekančias reaktyviąsias rūšis, yra nepakankami paaiškinti aukštos plazmos įtampos fenotipą. Reikalinga tiesioginė plazmos ir ląstelių sąveika, o išlydžio įtampa veikia kaip pagrindinis veiksnys.

Šie rezultatai kontrastuoja su plazmos-IEL tyrimais žinduolių ir bakterijų sistemose, kur plazmos išankstinis apdorojimas paprastai sustiprina IEL sukeltą permeabilizaciją ir citotoksinį poveikį. Chung et al. (2020) parodė, kad plazma apdorotas PBS padidino elektropermeabilizacijos efektyvumą vėžio ląstelėse. Panašūs sinerginiai efektai aprašyti ir bakterijų inaktyvacijai. Tuo tarpu šiame darbe užfiksuotas aukštos įtampos fenotipas kokybiškai skiriasi nuo sustiprinto atsako paradigmos, nes apjungia didelę permeabilizaciją su užslopintu makromolekulių išsiskyrimu. Šį atsaką papildomai išskiria kaspazės-3 tipo aktyvumo slopinimas, rodantis, kad buvo aktyvuotas ne klasikinis IEL sukeltas ląstelių mirties kelias. Toks fenotipas anksčiau nebuvo užfiksuotas kombinuoto plazmos-IEL poveikio tyrimuose. Tai galimai siejama su oksidacinio streso sąlygota ląstelių mirtimi, tačiau tam patvirtinti reikalingi papildomi tyrimai.

Apibendrinant, gauti rezultatai rodo, kad membranos permeabilizacija nėra pakankamas rodiklis IEL biologinei baigčiai prognozuoti, kai ląstelės prieš tai yra veikiamos plazma. Ar šis IEL sukelto atsako pokytis kyla iš plazmos sukeltų ląstelės apvalkalo modifikacijų, ar iš viduląstelinių molekulinių kelių pokyčių, lieka neišspręsta. Aišku, kad stebėtam fenotipui nepakanka antrinių plazmos sukeliamų efektų terpėje, o būtina tiesioginio plazmos išlydžio ekspozicija. Tai patvirtina, kad ląstelės būklė IEL poveikio metu formuoja vėlesnį atsaką. Skirtingas *C. vulgaris* atsakas į kombinuotą plazmos-IEL apdorojimą tikėtinai atspindi struktūrines ir biochemines ypatybes, kurių nėra žinduolių sistemose: standžią ląstelės sienelę, chloroplastą, užimantį didelę dalį ląstelės tūrio, ir aktyvų fotosintetinį metabolizmą, pasižymintį

intensyviomis redokso reakcijomis. Tai patvirtina, kad žinduolių ląstelėms nustatyti principai tiesiogiai neperkeliami fotosintetiniams organizmams.

Trečias skyrius: skirtingas mikroorganizmų jautrumas IEL poveikiui ir jo priklausomybė nuo fiziologinės būklės.

Iš *C. vulgaris* kultūros išskirtas bakterijų izoliatas identifikuotas kaip *Delftia* sp. (GenBank identifikacinis kodas OP777498.1, 98 % panašumas į *D. tsuruhatensis*). Siekiant nustatyti, kaip kultivavimo sąlygos formuoja dumblių ir bakterijų sąveiką, kokultūros buvo sudarytos trijose, skirtingos sudėties, mitybinėse terpėse. TAP terpėje, kurioje dominuoja organinis anglies šaltinis (acto rūgštis), *C. vulgaris* ir *Delftia* sp. sąveika buvo konkurencinė. Bakterijų populiacija greitai, per 24 valandas, suvartojo visą prieinamą acto rūgštį, ir pasiekė 1,5-2×10^8 ląstelių/mL piką. Nuo trečios kultivavimo dienos bakterijų populiacija pradėjo mažėti dėl nepakankamo maistinių medžiagų kiekio. Tuo tarpu dumblių augimas šiomis sąlygomis buvo slopinamas: kokultūroje dumblių koncentracija 7 dieną pasiekė tik apie 60 % monokultūros lygio. BG-11 terpėje, kurioje organinės anglies kiekis minimalus, o azotas tiekiamas neorganine forma ($NaNO_3$), bakterijų augimas išliko minimalus (<1×10^7 ląstelių/mL). Dumblių populiacijos kokultūroje viršijo monokultūrų lygius apie 50 %, rodydamos mutualistinį sąveikos pobūdį. BG+AA terpėje, apjungiančioje BG-11 neorganinį azotą su papildomu organinės anglies šaltiniu (acto rūgštimi), buvo palaikomas tarpinis bakterijų kiekis, o dumblių augimas kokultūroje padidėjo apie 160 %, palyginti su monokultūra. Vis dėlto absoliuti dumblių ir bakterijų biomasė TAP terpėje buvo didžiausia, kas suteikė optimalias sąlygos tolimesniems tyrimams analizuoti IEL poveikį kokultūrų atžvilgiu.

Kokultūrų apdorojimo rezultatai atskleidė skirtingą dumblių ir bakterijų jautrumą IEL poveikiui. *C. vulgaris* demonstravo nuoseklų jautrumą elektriniam apdorojimui, nepriklausomai nuo augimo fazės ir bakterijų buvimo. Mažos energijos apdorojimas (4 J/mL) pasiekė >95 % dumblių inaktyvaciją visomis tirtomis eksperimentinėmis sąlygomis, o didelės energijos apdorojimas (100 J/mL) beveik visais atvejais sukėlė visišką dumblių inaktyvaciją.

Bakterijų atsakas esant identiškiems IEL parametrams stipriai priklausė nuo augimo fazės. 1 dieną, atitinkančią eksponentinį augimą, mažos energijos apdorojimas vertinant rezultatus po 2 valandų sukėlė <20 % mirtingumą, o didelės energijos apdorojimas lėmė apie 40-50 % inaktyvaciją. 3 dieną, sutampančią su perėjimu į badavimą po prieinamos organinės anglies išsekimo, jautrumas smarkiai padidėjo. Abu IEL energijos lygiai sukėlė 70-80 % bakterijų inaktyvaciją praėjus 2 val po apdorojimo. 7 dieną, atspindinčią ilgalaikę maistinių medžiagų stoką, bakterijų monokultūros rodė didelį bazinį

mirtingumą (>50 %) net be IEL. O IEL apdorojimas sukėlė tik minimalią papildomą inaktyvaciją. Tačiau vertinant pastaruosius rezultatus praėjus 24 val po IEL apdorojimo užfiksuotas netikėtas *Delftia* sp. populiacijos padidėjimas maždaug keturis kartus. Toks bakterijų populiacijos prieaugis nebuvo užfiksuotas bakterijų monokultūrose, apdorotose identiškomis sąlygomis. Šis 24 val laiko tarpas indikuoja jog bakterijų augimas galimai yra sąlygotas iš inaktyvuotų dumblių išsiskyrusių viduląstelinių junginių, kurie tampa substratu bakterijų proliferacijai. Gautos augimo kreivės patvirtino, kad į IEL apdorotų dumblių lizatas yra tinkamos sąlygos *Delftia* sp. augimui, ir prilygo bakterijų dauginimuisi šviežioje TAP terpėje. Taip pat atlikti antimikrobinio aktyvumo tyrimai neparodė jokio dumblių lizatų aktyvumo prieš tirtas bakterijas.

SDS-PAGE analizė atskleidė baltymų ekstrakcijai reikšmingą selektyvumą. Baltymų profiliai iš IEL apdorotų kokultūrų pagal metodo skiriamąją gebą nesiskyrė nuo dumblių monokultūrų profilių. Baltymų ekstrakcijos išeiga siekė apie 25 % sausos masės abiem IEL energijos lygiais. Priešingai, HPH apdorotuose kokultūrų mėginiuose atsirado nauja baltymų juosta ties maždaug 27 kDa, kurios nebuvo kitų tipų mėginiuose. Šios papildomos juostos kilmė nebuvo galutinai nustatyta, tačiau jos pasireiškimas specifiškai po HPH atitinka platesnį, mažiau selektyvų suardymą, būdingą aukšto slėgio homogenizacijai, kuri gali pažeisti tiek dumblių, tiek bakterijų ląsteles. Tai leidžia manyti, kad papildoma juosta galėjo kilti iš bakterinių baltymų, išsiskyrusių po HPH. Galutiniam patvirtinimui reikia papildomų tyrimų.

Apibendrinant, gauti rezultatai atskleidžia, kad IEL poveikis bendrijos mastelyje nėra tolygus. Nors dydžiu paremta elektroporacijos teorija prognozuoja didesnį bakterijų atsparumą, kokultūrų rezultatai rodo, kad bakterijų jautrumas priklauso nuo fiziologinės būklės, kurią formuoja kultivavimo sąlygų dinamika. Tai koreliuoja su antrame skyriuje nustatyta tendencija, kad ląstelinė būklė poveikio metu formuoja biologinę baigtį. Praktinė šio diferencinio jautrumo pasekmė yra tai, kad IEL apdorojimas įgalina selektyvią dumblių baltymų ekstrakciją iš kokultūrų be bakterinės kontaminacijos, kurios neišvengia mechaninio suardymo metodai. Vis dėlto selektyvumo išlikimas priklauso ne vien nuo diferencinio ląstelių suardymo apdorojimo metu, bet ir nuo po apdorojimo ekologinių baigčių, tokių kaip bakterijų proliferacija, sąlygota iš suardytų dumblių išsiskyrusių viduląstelinių junginių. Tai rodo, kad IEL poveikio vertinimas kokultūrose reikalauja ilgalaikės stebėsenos, apimančios ne tik momentinį ląstelinį atsaką, bet ir bendrijos dinamikos pokyčius.

Mokslinis naujumas ir praktinė reikšmė

Disertacija prisideda prie mechanistinio IEL poveikio mikrodumblių sistemoms supratimo trimis pagrindinėmis kryptimis.

Darbas pateikia pirmą sistemingą IEL sukeltų fotosintetinio aparato funkcijos pokyčių mikrodumbliuose charakterizaciją. Chlorofilo fluorescencijos gyvavimo trukmės matavimai parodė, kad IEL sutrumpina fluorescencijos gyvavimo trukmę nekeisdamas sugerties spektrų. Tai rodo pakitusius energijos disipacijos kelius, o ne pigmentų degradaciją. Šiuos efektus palyginus tarp skirtingų impulsų trukmių ir susiejus su plazminės membranos permeabilizacija, nustatyta, kad fotosintetinio aparato pažeidimo mastas tiesiogiai nekoreliuoja su membranos permeabilizacija. Tai reiškia, kad membranos pažeidimas ir fotosintetinės funkcijos sutrikimas yra susiję, tačiau neekvivalentūs IEL poveikio padariniai. Taip IEL poveikio supratimas viduląstelinių organelių lygmenyje išplečiamas nuo žinduolių mitochondrijų į fotosintetines sistemas. Praktine prasme, fluorescencijos gyvavimo trukmės matavimai leidžia neinvaziškai stebėti organelių funkciją IEL apdorojimo metu ir gali sudaryti pagrindą realaus laiko stebėsenai bei grįžtamojo ryšio valdymui, priešingai nei ilgai trunkantys pralaidumo ir gyvybingumo tyrimai.

Disertacijoje pirmą kartą charakterizuojami nuoseklaus plazmos-IEL apdorojimo efektai mikrodumbliuose. Identifikuojami nuo įtampos priklausomi atsako režimai, kuriems būtina tiesioginė plazmos ekspozicija, ir atskleidžiami nuo kaspazių nepriklausomi, neklasikiniai dumblių ląstelių žūties modeliai esant dideliam plazmos apdorojimo intensyvumui. Šie rezultatai parodo, kad kombinuotas plazmos-IEL apdorojimas mikrodumbliuose sukelia ląstelinius atsakus, kurie kokybiškai skiriasi nuo aprašytų žinduolių ląstelėse ir negali būti paaiškinti vien plazminės membranos permeabilizacija. Tai rodo, kad biologinė baigtis priklauso ne vien nuo IEL parametrų, bet ir nuo ląstelės būklės, suformuotos ankstesnio plazmos apdorojimo. Todėl kombinuoto plazmos-IEL apdorojimo optimizavimas reikalauja empirinio konkrečių apdorojimo sekų ir ląstelinės būklės sąlygų testavimo, kadangi atskirų apdorojimų sukeliami efektai negali būti naudojami prognozuojant kombinuoto poveikio baigčių.

Disertacija išplečia IEL analizę iš monokultūrų į mikrodumblių ir bakterijų kokultūras ir parodo, kad elektrinis jautrumas bendrijos lygiu priklauso nuo kultivavimo aplinkos. Nors *C. vulgaris* buvo tolygiai inaktyvuojama IEL poveikiu visomis tirtomis sąlygomis, *Delftia* sp. jautrumas stipriai kito priklausomai nuo augimo fazės (1, 3 ir 7 diena). Šis skirtingas jautrumas atveria praktinių taikymų galimybes. IEL apdorotų kokultūrų baltymų SDS-PAGE profiliai nesiskyrė nuo dumblių monokultūrų, o HPH apdorotose kokultūrose atsirado papildoma ~27 kDa juosta, galimai indikuojanti

bakterinių baltymų priemaišą. Tai rodo, kad IEL, skirtingai nei mechaninis suardymas, įgalina selektyvią dumblių baltymų ekstrakciją. Tačiau vėlyvose kokultūrose po IEL apdorojimo stebėtas bakterijų populiacijos prieaugis rodo, kad ši selektyvumas nėra automatiškas. Siekiant išvengti antrinės bakterinės kontaminacijos, būtina laiku atskirti dumblių biomasę nuo bakterijų, nes inkubacijos periodas, skirtas baltymų išsiskyrimui, kartu sudaro sąlygas bakterijų proliferacijai.

Apibendrinant, šie indėliai parodo, kad jautrumas elektriniam laukui fotosintetinėse sistemose nėra nulemtas vien plazminės membranos permeabilizacijos, o priklauso nuo fiziologinės sistemos būklės, įskaitant fotosintetinę funkciją ir augimo fazę. Tai nustato mechanistinį pagrindą tolesniam IEL poveikio tyrimui sudėtingose fotosintetinėse ir mišriose mikrobinėse sistemose.

1. IEL apdorojimas (19 kV/cm, 10 μs, 80 J/mL) sutrumpino chlorofilo fluorescencijos gyvavimo trukmę ties 685 nm *C. vulgaris* nuo 1,71 ns iki 0,83 ns be statistiškai reikšmingų absorbcijos pokyčių, kas rodo sustiprėjusią nespinduliuojančią energijos disipaciją, o ne pigmentų degradaciją.
2. Fotosintetiniai atsakai priklausė nuo impulso trukmės: mikrosekundiniai impulsai sumažino fluorescencijos gyvavimo trukmę 51 %, nanosekundiniai impulsai (90 ir 60 ns) esant ekvivalentiškai energijai 18 %, o 10 ns impulsai esant didesniam lauko stipriui (86 kV/cm) sukėlė minimalius efektus, nepaisant apskaičiuoto ekvivalentiško šiluminio poveikio (~17 °C).
3. Fotosintetiniai pokyčiai ir membranos permeabilizacija buvo glaudžiai susiję mikrosekundinių impulsų sąlygomis: 51 % fluorescencijos gyvavimo trukmės sumažėjimas lydėjo ~70 % permeabilizacija. Nanosekundiniai impulsai sukėlė silpnesnius, tačiau neproporcingus efektus (18 % gyvavimo trukmės sumažėjimas, 10,5 % permeabilizacija), kur fluorescencijos pokytis viršijo permeabilizacijos mastą. Tiesioginio viduląstelinio taikymo, nepriklausomo nuo plazminės membranos permeabilizacijos, tirtais parametrais patvirtinti nepavyko.
4. Slenkančio lankinio išlydžio plazma sukėlė nuo šaltinio maitinimo įtampos priklausomas BG-11 terpės modifikacijas: esant 250 V, temperatūra pasiekė 54 °C, pH sumažėjo nuo ~7,5 iki ~7,0, o laidumas padidėjo nuo ~1,85 mS/cm iki 3,34 mS/cm, susikaupė reaktyviosios rūšys (NO_2^- 1,67 mM, NO_3^- 28,9 mM, H_2O_2 17,4 mM). Tiesioginiai biologiniai efektai *C. vulgaris* stebėti tik esant aukštai įtampai (250 V): ~25 % permeabilizacija ir metabolinė inaktyvacija.
5. Išankstinis plazmos apdorojimas pakeitė biologinius atsakus į fiksuotus IEL parametrus (25 kV/cm, 7 μs, 10 impulsų) ir priklausė nuo įtampos. Žemos įtampos išankstinis apdorojimas (130 V) lėmė įprastą IEL fenotipą su dideliu makromolekulių išsiskyrimu. Aukštos įtampos išankstinis apdorojimas (250 V) perkėlė ląsteles į pralaidų, bet sulaikantį fenotipą, slopindamas išsiskyrimą, nepaisant panašios permeabilizacijos. Vien IEL padidino kaspazės-3 tipo aktyvumą (~250 % kontrolės), tačiau aukštos įtampos plazma jį sumažino žemiau kontrolės, kas indikuoja neklasikinį, nuo kaspazių nepriklausomą ląstelių mirties kelią.
6. Kontroliniai protokolai (šiluminis išankstinis apdorojimas, plazma aktyvuota terpė, laidumu suderinti pakeitimo protokolai) neatkartojo aukštos įtampos fenotipo, patvirtindami, kad nuo įtampos priklausomam atsako išsiskyrimui būtina tiesioginė plazmos ir ląstelių sąveika.

7. Terpės sudėtis lėmė bendrijos struktūrą: TAP palaikė reikšmingas bakterijų populiacijas (1,5-2×10^8 ląstelių/mL), o BG-11 ir BG+AA išliko dumblių dominuojamos. TAP suteikė sąlygas IEL selektyvumui mišriose kultūrose vertinti.
8. Rūšinis IEL jautrumas iš esmės skyrėsi. *C. vulgaris* inaktyvacija viršijo 95 % esant mažai energijai (40 kV/cm, 1 μs, 4 J/mL) ir 99 % esant didelei energijai (40 kV/cm, 1 μs, 100 J/mL), nepriklausomai nuo augimo fazės ar kultivavimo sąlygų. *Delftia* sp. jautrumas priklausė nuo augimo fazės: minimalus 1 dieną, didžiausias 3 dieną (70-80 %), su po apdorojimo stebėtu populiacijos ataugimu 7 dieną tik kokultūrose.
9. IEL apdorojimas įgalino selektyvią dumblių baltymų ekstrakciją iš kokultūrų. Baltymų išeiga siekė ~25 % sausos masės, o SDS-PAGE profiliai nesiskyrė nuo monokultūrų. HPH apdorotose kokultūrose stebėta papildoma ~27 kDa juosta, galimai indikuojanti bakterinę baltymų kontaminaciją, nors tam reikalingas biocheminis patvirtinimas.

Ginamieji teiginiai:

1. IEL sutrumpina chlorofilo fluorescencijos gyvavimo trukmę ties 685 nm *C. vulgaris*, priklausomai nuo impulso trukmės, nekeisdamas absorbcijos spektrų, indikuodamas, kad fotosintetinio aparato sutrikimas kyla dėl sustiprėjusios nespinduliuojančios energijos disipacijos, o ne dėl pigmentų degradacijos.
2. Nuoseklus plazmos išankstinis apdorojimas (250 V maitinimo šaltinis), po kurio taikomas IEL, atskiria membranos permeabilizaciją nuo makromolekulių išsiskyrimo, slopina kaspazės tipo aktyvumą ir sukelia neapoptotinį, nenekrotinį ląstelių mirties fenotipą, kuris skiriasi nuo klasikinės IEL sukeltos programuotos ląstelių mirties ir reikalauja tiesioginio plazmos poveikio.
3. IEL apdorojimas (40 kV/cm, 1 μs, 4-100 J/mL) sukelia stabilią *C. vulgaris* inaktyvaciją (>95 %), o *Delftia* sp. jautrumas priklauso nuo augimo fazės, kas leidžia selektyviai išskirti dumblių baltymus iš kokultūrų be papildomų baltymų juostų, stebimų mechaninio suardymo atveju.

CURRICULUM VITAE

Kamilė Jonynaitė

Education

2020-2026	PhD, Physics (N 002), State Research Institute Center for Physical Sciences and Technology (FTMC)/ Vilnius University
2018-2020	MSc, Microbiology and Biotechnology, Vilnius University
2017-2018	BSc, Biology (supplementary studies), Vilnius University
2014-2017	Professional BSc, Biomedical Diagnostics, Vilnius College

Research experience

May 2022-Dec 2024	**Co-Investigator, PLASMALGAE Project** | FTMC | Led all biological experimental work on *Chlorella vulgaris*, including cell viability assays, permeabilization analysis, and compound extraction. Contributed to three peer-reviewed publications (Papers I, II and V).
May 2023-Jul 2023 | Sep 2021-Jun 2022	**Principal Investigator**| Karlsruhe Institute of Technology, Germany | Independently designed and executed two research visits funded by the German Federal Environmental Foundation (DBU). Investigated *C. vulgaris* and *Delftia* sp. interactions and PEF effects in co-culture. Resulted in two peer-reviewed publications (Papers III and IV).
Feb 2021-Dec 2021	**Co-Investigator, ExtraIMTA Project** | FTMC | Investigated plasma treatment as an extraction method for recovery of valuable compounds from microalgal biomass following wastewater bioremediation. Provided the foundation for the subsequent PLASMALGAE project.
2018-2020	**Students' Research Practice**| FTMC | Independent experimental work on PEF effects on microalgal biomass under bacterial co-culture conditions. Formed the basis of master's thesis research.
2014-2017	**Laboratory Technician Internship** | National Centre of Pathology, Vilnius University Hospital | Clinical sample collection, body fluid analysis, and results documentation.

Awards

2022	Best presentation award, Food Technology category | 4th World Congress on Electroporation and Pulsed Electric Fields | Denmark
2020	Best presentation award | FizTech conference | Lithuania
2020	Professor Karolis Jankevičius nominal scholarship for academic achievement

Professional development

2022	International Summer School on Experimental Electrochemistry (e-SPARK) | Institute of Physical Chemistry, Warsaw, Poland | Hands-on training in electroanalytical techniques, voltammetry, biosensor construction, and scanning electrochemical microscopy.
2021	Electroporation-Based Technologies and Treatments – postgraduate course | International Scientific Workshop | Ljubljana University, Slovenia | Week-long intensive program combining lectures, laboratory practical, and hands-on training across multiple electroporation applications.
2021	7th School on Pulsed Electric Field Applications in Food and Biotechnology | University of Zaragoza, Spain | Application-based online course covering theoretical and applied aspects of PEF technology.
2020	Certificate in Laboratory Animal Science | Vilnius University.

ACKNOWLEDGEMENTS

I would like to express my sincere gratitude to my supervisor and mentor, Dr. Arūnas Stirkė, for his guidance and support during my doctoral studies. His suggestion that I pursue PhD studies, which was not initially part of my plans, opened new possibilities and helped me grow as an individual, for which I am deeply grateful. I also appreciate how he consistently encouraged me to step outside my comfort zone. Although this was sometimes challenging, it was essential to my development as a researcher.

I would also like to express my gratitude to Dr. Christian Gusbeth and Dr. Wolfgang Frey at the Institute for Pulsed Power and Microwave Technology (IHM), Karlsruhe Institute of Technology, Germany, for supervising my research stays funded by the German Federal Environmental Foundation (DBU), and to the IHM Bioelectrics team for their support throughout both visits. This experience broadened my perspective and strengthened my work through extensive scientific collaboration. I would also like to thank Dr. Henri Gerken at Arizona State University, USA, for his consultancy and support. His openness, expertise, and ability to approach problems from novel angles provided valuable input at critical moments in my research.

I would like to express my sincere gratitude to the Center for Physical Sciences and Technology and the Department of Functional Materials and Electronics, including the Head of Department, Prof. Dr. N. Žurauskienė, for providing an excellent research environment and institutional support. I am especially thankful to my departmental colleagues and lab mates in the Bioelectrics Laboratory for their collaboration and for generously sharing their knowledge. Their support with experiments, technical problem-solving, scientific discussions, and encouragement during challenging periods was invaluable to both the progress and the quality of this work.

I would also like to thank our project partners at the Lithuanian Energy Institute for their cooperation throughout a challenging research journey, particularly as the project evolved in ways that differed from what was initially anticipated. Special thanks go to my students Dominykas Daunys**,** Giedrė Bergerytė**,** and Gintarė Dalmantaitė for their dedication, hard work, and contributions to the implementation and advancement of parts of the research.

Finally, I would like to thank my family, including my partner Karolis, as well as my relatives and friends, for their love, patience, and unwavering support. A special place in my gratitude belongs to my daughter, Kotryna, who came into my life at exactly the right time, when I needed a pause. This helped me return to my work with greater clarity and a deeper understanding of my research.

PUBLICATIONS INCLUDED IN THE THESIS

I. Liutauras Marcinauskas, Zydrunas Kavaliauskas, **Kamile˙ Jonynaite**, Rolandas Uscila, Mindaugas Aikas, Skirmantas Kersulis, Antanas Straksys, Arunas Stirke, Voitech Stankevic; The Influence of Voltage on Gliding Arc Discharge Characteristics, the Composition of Air Plasma, and the Properties of BG-11 Medium; ***Applied Sciences*** 14 (2024): 2135; https://doi.org/10.3390/app14052135

II. Voitech Stankevic, **Kamile˙ Jonynaite**, Ahmed Taha, Skirmantas Kersulis, Aldas Dervinis, Sebastjanas Kurcevskis, Sonata Tolvaisiene, Arunas Stirke, Nerija Zurauskiene; The Advancement and Utilization of Marx Electric Field Generator for Protein Extraction and Inducing Structural Alterations; ***Applied Sciences*** 14 (2024): 3886; https://doi.org/10.3390/app14093886

III. **Kamile Jonynaite**, Arunas Stirke, Henri Gerken, Wolfgang Frey, Christian Gusbeth.; Influence of growth medium on the species-specific interactions between algae and bacteria; ***Environmental Microbiology Reports*** 16 (2024): e13321; https://doi.org/10.1111/1758-2229.13321

IV. **Kamile Jonynaite**, Arunas Stirke, Wolfgang Frey, Christian Gusbeth; Application of Pulsed Electric Fields in Algal and Bacterial Co-cultures: Investigating Bacterial Responses and Purity of Algal Protein Extract; **Bioelectricity** (2025); https://doi.org/10.1177/25763113251403451

V. **Kamile Jonynaite**, Raimonda Celiesiute-Germane, Rolandas Uscila, Zydrunas Kavaliauskas, Mindaugas Aikas, Henri Gerken, Liutauras Marcinauskas, Voitech Stankevic, Arunas Stirke; Plasma Discharge Intensity Modulates Cell Death Pathways in Pulsed Electric Field-Treated Chlorella vulgaris (submitted to **Bioelectrochemistry** (Manuscript Number: BIOELECHEM-D-26-00148)).

STATEMENT OF CONTRIBUTIONS

The publications included in this thesis are co-authored works. The specific contributions of the author and collaborators to each publication are described below.

Paper I. The author characterized plasma-induced physicochemical changes in BG-11 cultivation medium and contributed to manuscript preparation. The gliding arc discharge system design, plasma characterization, and electrical measurements were performed by L. Marcinauskas, Ž. Kavaliauskas, R. Uscila, M. Aikas, and S. Kersulis. A. Stirke and V. Stankevic provided scientific supervision.

Paper II. The author was responsible for biological experiments, cell viability assays, and protein concentration analysis, and contributed substantially to manuscript preparation. Further protein characterization and structural analysis were performed by A. Taha. The Marx generator design and electrical engineering aspects were performed by V. Stankevic, S. Kersulis, A. Dervinis, and S. Kurcevskis. A. Stirke and N. Žurauskienė provided scientific supervision.

Paper III. The author conceived and designed the study, performed all biological experiments at the Karlsruhe Institute of Technology (KIT), analyzed and interpreted the data, and wrote the manuscript. H. Gerken performed genetic analysis and constructed the phylogenetic tree and contributed to manuscript review. W. Frey and C. Gusbeth provided scientific consultation, contributed to study design, secured research funding, provided laboratory resources and reagents, administered the DBU fellowship project, and reviewed the manuscript.

Paper IV. The author conceived and designed the study, performed all biological experiments and data analysis at KIT, and wrote the manuscript. A. S. K. Müller assisted with protein concentration measurements and SDS-PAGE analysis. W. Frey and C. Gusbeth provided scientific consultation, contributed to study design, secured research funding, provided laboratory resources and reagents, administered the DBU fellowship project, and reviewed the manuscript.

Paper V. The author conceived and designed the study, performed the sequential plasma-PEF treatments, permeabilization assays, and protein release experiments, led data analysis and interpretation, and wrote the manuscript. R. Celiesiute-Germane performed caspase 3-like activity assays and amino acid determination, contributed to data analysis, and assisted with manuscript preparation. G. Bergeryte and G. Dalmantaite assisted with experimental work. The gliding arc discharge plasma system was operated by

L. Marcinauskas, Ž. Kavaliauskas, R. Uscila, and M. Aikas. S. Kersulis and V. Stankevic provided technical support with the PEF system. H. Gerken provided scientific consultation and contributed to manuscript review. A. Stirke provided scientific supervision.

NOTES

NOTES

NOTES

Vilniaus universiteto leidykla
Saulėtekio al. 9, III rūmai, LT-10222 Vilnius
El. p. info@leidykla.vu.lt, www.leidykla.vu.lt
bookshop.vu.lt, journals.vu.lt
Tiražas 13 egz.